A SEARCH FOR NATURAL SUPERSYMMETRY VIA ELECTROWEAK PROCESSES WITH HIGGS AND Z BOSONS IN THE FINAL STATE

By

PATRICK W. ZYWICKI

A dissertation submitted to the

Graduate School—New Brunswick

Rutgers, The State University of New Jersey

in partial fulfillment of the requirements

for the degree of

Doctor of Philosophy

Graduate Program in Physics and Astronomy

written under the direction of

Prof. Sunil Somalwar

and approved by

_____

_____

_____

_____

_____

New Brunswick, New Jersey

October, 2014

ABSTRACT OF THE DISSERTATION

A Search for Natural Supersymmetry via Electroweak Processes with Higgs and Z Bosons in the Final State

By PATRICK W. ZYWICKI

Dissertation Director:

Prof. Sunil Somalwar

We present the individual and combined results of several analyses that search for the next-to-lightest supersymmetric particle (NLSP) in the context of the Natural Higgsino NLSP model. The model posits that the NLSP is in a pure Higgsino energy eigenstate, and upon production mediated by electroweak processes, decays to either a Higgs or Z boson and the lightest supersymmetric particle (LSP), which is in a pure Bino energy eigenstate. The Higgs and Z bosons then decay in the Standard Model (SM) fashion, leading to a number of possible final states, all of which include missing transverse energy (MET) coming from the LSP. Six independent analyses search for the existence of the Higgsino-like NLSP by examining events that have the signature of a particular final state of the model. In addition to MET, these unique final states include multileptons, four b-jets, two photons and two b-jets, two photons and a lepton, two b-jets and two leptons, and two light-flavored jets and two leptons. The data used was collected during the 2012 run of the CMS experiment at $\sqrt{s} = 8$ TeV and $L_{int} = 19.5 fb^{-1}$. No physics beyond the Standard Model was discovered. We therefore set limits on the mass of the Higgsino and the branching fraction of the Higgsino decays to Higgs and Z bosons.

Acknowledgments

For as long as I can remember, I have always been captivated by what seem to be unexplainable phenomena. When I was a kid, my father used to take me to Tannen's Magic in Manhattan. It was a place where a real pro could stock up on the latest tricks of the trade. They had everything; anything from a fake thumb to a heavy duty trick the size of an armoir, from what I can recall. That was nearly 20 years ago. I recall great excitement at the idea of being dumbstruck with the seemingly impossible, and then setting out to try and figure out how it was done.

I'm sure this analogy has been used before, but it's the same child-like sense of wonder with magic that resurfaced for me in adulthood in the form of physics, and science to a larger extent. That seemingly imposible things have a simple and often elegant explanation behind the smoke and mirrors amazed me. As a teenager, I was a good student, but lacked a sense of direction. During my first foray into high school physics, I caught an inkling of that old sense of incredulity which had been lying dormant since visits to Tannen's and such.

I did my undergraduate at Cornell University in Engineering Physics, and after four years of hard work, my awe for the immutable laws of nature and mathematical beauty was firmly cemented in me. I found myself asking that ubiquitous question that I'm confident every recently bachelorized twenty-something asks himself. What now? Graduate school was, for me, the simultaneously obvious and daunting path. And certainly NOT the path of least resisitance!

The last six years I've spent at Rutgers have been the most intellectually challenging times of my adult life. I've met some extraordinary thinkers and consider myself fortunate to live in a time when particle physics has never been more interesting. I hope that I've lent some sort of forward momentum to the history of physics, however indelible that may be.

I'd like to thank the many people that came into and out of my path these past six years. I learned a ton of physics from everyone in the HEX group, including, but not limited to, and in no particular order, P. Thomassen, S. Panwalkar, C. Seitz, S. Arora, R. Patel, A. Barker, M. Walker, R.C. Gray, and of course, the many nights burning the midnight oil with the brothers Contreras! I wish to give special thanks to my advisor, Sunil Somalwar, for helping me through this tumultuous process. I'm not usually one to play favorites, so I'll just assign equal weight to all other faculty members in the department, (but more so on the HEX/HET side). I would also like to acknowledge

the hard work of all the HEX undergraduates. Everybody has done remarkable work. Kudos to you all!

I'd also like to thank my family for their endless supply of love and affection. I hope I haven't been a burden to you all during this insane pursuit of higher learning. I'd also like to thank all the great thinkers that came before my time. We are all eternally indebted to you.

Dedication

For Uncle Al

Table of Contents

List of Tables

List of Figures

Chapter 1
Introduction

1.1 Particle Classification

Of all of the surprising truths of nature, perhaps none surpass the intricacy and counter-intuitive ideas purported by particle physics. The pinnacle of particle theory is the so called Standard Model, a quantum field theory that describes the nature of interactions between sub-atomic particles. To date, physicists have been able to identify four unique forces: the gravitational force, the electromagnetic force, the strong force, and the weak force. The Standard Model, or SM, is able to accomodate the latter three of these forces. Gravity is accurately described in Einstein's Theory of General Relativity, and is not included in the SM because it is not renormalizable (22). In terms of its particle content, the SM can be divided into two classes distinguished by their spin: fermions and bosons. The fermions, or matter constituents, have spin value $\frac{1}{2}$, while the bosons, or force carriers, have spin 1. Discovered in 2012 at the Large Hadron Collider, the Higgs boson is the only known fundamental spin 0 particle in nature (1).[1] It is the completion of the SM in some sense, but does not address all of the problems that lie in the high energy regime.

The fermions can be further subdivided into leptons and quarks, and still further subdivided into three families, or generations. The first generation of leptons are the electron (e) and the electron-neutrino (ν_e). The former partakes in the weak and electromagnetic forces, and carries a weak isospin charge and an electromagnetic charge. The latter partakes only in the weak force and therefore only contains a weak isospin charge. The first generation of quarks are the up (u) and down (d) quarks. A combination of these quarks form the basis of the parton model for the proton and neutron, for instance. The up and down quarks partake in the strong, weak, and electromagnetic forces. They therefore carry color charge, weak isospin charge, and electromagnetic charge. The second generation of fermions are the muon (μ), the muon-neutrino (ν_μ), and the charm and strange quarks. One can think of these are heavier versions of the first generation. Finally, there is the 3rd generation of fermions, which includes the tau (τ), tau-neutrino (ν_τ), and the top and bottom quarks. Again, these can be considered heavier versions of the second generation.

[1] Other particles that exist in the spin 0 state are bound states of fundamental particles.

The bosons of the SM serve as the force carriers between the fermions of the theory. The strong force is mediated by eight gluons. The weak force is mediated by two charged bosons, W^+ and W^-, and one neutral boson, the Z. Finally, the electromagnetic force is mediated by the photon, γ. The Higgs is a boson, but is not a force carrier. We will touch upon its unique position in the SM in the next section. For a complete listing of all specifications of the fundamental particles, see the Particle Data Group review (4).

1.2 The Higgs Boson

It is very odd that nature should provide us with only one spin 0 fundamental particle. This fact alone makes it look incredibly out of place in the spectrum of known sub-atomic particles. One might fairly ask, what is the role of the Higgs boson in the SM? To answer this question, I turn to two puzzles of the SM that exist without the Higgs boson, and which can be solved by including the Higgs boson.

1.2.1 Puzzle No.1: Dirac Mass Terms

The SM uses fields to mathematically describe its particle content, and is therefore appropriately written in terms of Lagrangian densities. The correct Lagrangian density to describe the fermions is the Dirac Lagrangian density, which has a mass term $m\bar{\Psi}\Psi$. Here, m is the mass of the fermion, Ψ is a four component bi-spinor field[2], and $\bar{\Psi} = \Psi^\dagger\gamma^0$. We can also write Ψ in terms of its left and right-handed two component spinors respectively:

$$\Psi = \begin{pmatrix} \psi_L \\ \psi_R \end{pmatrix} \tag{1.1}$$

If we expand the mass term from the Dirac Lagrangian density using this left and right-handed notation, we have:

$$\mathcal{L}_{mass} = m \begin{pmatrix} \psi_R^\dagger & \psi_L^\dagger \end{pmatrix} \begin{pmatrix} \psi_L \\ \psi_R \end{pmatrix} = m\psi_R^\dagger\psi_L + m\psi_L^\dagger\psi_R \tag{1.2}$$

The SM, however, is a chiral theory. It treats the left and right-handed components of the fermion fields differently under $SU(2)_L$ transformations[3]. It is also gauge invariant under transformations of $SU(2)_L$[4] before electroweak symmetry breaking occurs. Putting the expanded mass term into

[2] Ψ is also a solution to the Dirac equation
[3] The gauge groups of the SM, like $SU(2)_L$, rotate components of fields into linear combinations of one another
[4] Before EWSB, the SM Lagrangian remains unchanged after an $SU(2)_L$ rotation of all the fields.

the SM would violate the $SU(2)_L$ gauge invariance of the theory, and is not allowed if we want this invariance preserved (11; 20). We cannot, therefore, use the mass term of the Dirac Lagrangian density in the SM. Nature, however, provides masses for the quarks and some of the leptons, and so there seems to be a conundrum.

1.2.2 Puzzle No.2: Electroweak Symmetry Breaking

If one writes down the full SM Lagrangian density with all the particle content except for the Higgs boson, it can be shown to be gauge invariant under $SU(2)_L \otimes U(1)_Y$. This particular gauge invariance is what gives rise to the weak and electromagnetic forces amongst the fermions. It can be shown that these two forces actually merge into a unified force called the electroweak force. This unification between the weak and electromagnetic forces, however, must be broken at some energy scale, because the weak and electromagnetic forces are distinct in current particle physics experiments. How is this electroweak symmetry broken? Also, at what energy scale does the breaking take place?

Again, it is theorized that the Higgs boson is responsible for this symmetry breaking. Mathematically, the Higgs boson is described by a two component complex scalar field, Φ. The Langrangian density for the Higgs field takes the form:

$$\mathcal{L}_{Higgs} = D_\mu \Phi^\dagger D^\mu \Phi - \mu^2 \Phi^\dagger \Phi - \lambda (\Phi^\dagger \Phi)^2 \tag{1.3}$$

Where $D_\mu = \partial_\mu + ig\frac{\sigma^i}{2}W_\mu^i + i\frac{Y}{2}B_\mu$, and λ is positive (17; 12).[5] The last two terms in the Higgs Lagriangian density serve as a potential energy density for the SM. If μ^2 is positive, then the minimum of the potential is zero. If μ^2 is negative, however, the minimum of the potential, denoted by ν, is $\sqrt{\frac{-\mu^2}{2\lambda}}$, and we have a non-zero minimum energy density of the SM. This is the crux of electroweak symmetry breaking. As one descends along the energy scale, at some point the value of μ^2 switches sign from positive to negative , yielding a non-zero energy density. We can expand the Higgs field in terms of this non-zero minimum[6] as

$$\Phi = \begin{pmatrix} \phi^+ \\ \phi^0 \end{pmatrix} \rightarrow \frac{1}{\sqrt{2}} \begin{pmatrix} 0 \\ \nu + H \end{pmatrix} \tag{1.4}$$

Expanding the first term in the Higgs Langrangian density then yields mass terms for the three W bosons and the B boson. If we then define the $W^\pm$, the Z, and γ as linear combinations of the three W's and the B, it can be shown that the $W^\pm$ and Z bosons are massive, while the photon remains

[5] The constants g and Y are weak-isospin and weak-hypercharge respectively, and the W and B are the three W bosons and the B bosons, which are the energy eigenstates of the $W^\pm$, Z, and photon.

[6] We work in the unitary gauge

massless. So, the non-zero minimum breaks the symmetry between the weak and electromagnetic forces. Additionally, the expansion of the potential also yields a mass term for the scalar field, H, of the form $m_H = \sqrt{2\lambda\nu^2}$. The Higgs boson mass is currently measured at roughly 126 GeV, and so experimental probes of λ help put the value of ν around 246 GeV. Thus, the electroweak symmetry breaking scale is O(100 GeV).

The Higgs boson also offers a solution to the Dirac mass term puzzle. To give mass to the fermions, one introduces Yukawa terms involving the Higgs field into the SM. For details on this, see (11; 20).

1.3 Higgs Caveats

The Higgs boson offers a beautiful solution to two problems simultaneously, as we have seen. One might be tempted to end the story there, and claim that this is the final missing piece of the SM. In one sense, it is, as all the particles of the SM predictions have been discovered, and finally, we have found the one particle that was missing from the theory for nearly 50 years. There is, however, a serious problem that needs to be addressed regarding the Higgs boson.

To see how this problem arises, one must understand how physicists use the SM to perform calculations. The common technique is to use perturbative methods to make predictions about interactions amongst the particles. In the SM, pertubative methods involve difficult, multi-dimensional integrals that can be foreboding, to say the least. Luckily, physicists use Feynman diagrams which have particular rules associated with each piece of the diagram. These diagrams and their rules effectively set up the integrals needed for the perturbative calculation, and dramatically simplify computing time as well.

The Higgs boson has its own set of Feynman rules which can be derived from the SM. One particular diagram of interest is the Higgs propagator. It roughly describes the probability of a Higgs being created at one point, and annihilated at another. Because of quantum mechanical effects, we get an interesting interaction that leads to a loop in the propagator diagram, and represents a next to leading order term in perturbative methods. The loop diagram involves the Higgs boson interacting with fermions, which is allowed via the Yukawa couplings. The diagram can be seen in figure 1.1.

Using the Feynman rules for the loop portion of the diagram, we get the following integral[7]:

$$\int d^4p \frac{(\not{p} + m)^2}{(p^2 + m^2)^2} \propto \int dp p^3 \frac{1}{p^2} = \Lambda^2 \tag{1.5}$$

[7]Assuming the momentum dwarfs the mass terms

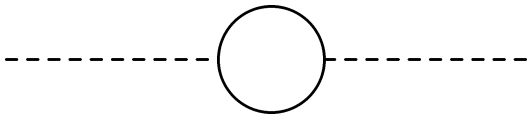

Figure 1.1: Virtual Fermion Loop in Higgs Propagator

Here, Λ is the cutoff for the theory, i.e. an energy scale where the SM might break down. One interprets this loop as a mass correction for the Higgs boson. As far as experiments have probed, this ultra-violet (UV) cutoff is unknown, but is at least O(100 GeV). This means the Higgs mass should at least be as large as 100 GeV, yet the value is measured to be 126 GeV. This is a fatal error of the theory. Why is the Higgs boson mass so apparently light compared to the cutoff scale? It is actually a larger problem for the SM in general, since the masses of each particle depend on its interaction with the Higgs boson. This is referred to as the hierarchy problem in particle physics. Without an explanation, it seems that there is nothing keeping all the masses of the SM particles from diverging towards this UV cutoff, Λ. If no explanation is found, physicists may have to be content with a possible fine-tuning of this sector of physics. Many candidate theories exist for resolving the hierarchy problem, and the one at the forefront of the pack is supersymmetry.

1.4 Supersymmetry

The idea of supersymmetry, or SUSY, is perhaps as old and as well known as the theory behind the Higgs boson. There are several varieties of supersymmetry, but I will concentrate on one that has the minimal amount of particle content. This is also an appropriate approach, because searches for new physics should not begin with the most complicated phenomenology. Incorporating minimal models of SUSY into the SM, one effectively doubles the particle content of the theory. Every particle in the SM would have a corresponding SUSY particle that carries the identical quantum numbers of its SM counterpart, with the exception that its spin would be $\frac{1}{2}$ less. For instance, the supersymmetric particles, or sparticles, would consist of supersymmetric leptons and quarks, or sleptons and squarks, that would be identical in every way to the leptons and quarks, but would be spin 0 particles. Similarly, the gauge bosons of the SM have their SUSY counterparts, the gauginos, that are all fermions with spin $\frac{1}{2}$. The Higgs boson is already a spin 0 particle, and its SUSY

counterpart is the spin $\frac{1}{2}$ fermion called the Higgsino.

Before getting too deep into SUSY phenomenology, I need to demonstrate how and why SUSY is a leading candidate for physics beyond the SM. If we go back to the divergent loop diagram for the Higgs progagator, we can construct a similar diagram if SUSY is included in the SM. Since the fermions interact with the Higgs, the sfermions would also interact with the Higgs boson in the following way:

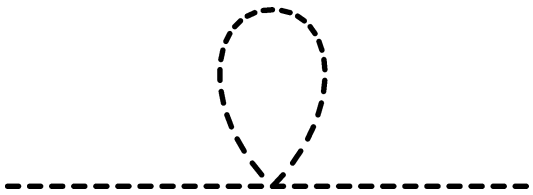

Figure 1.2: Virtual Sfermion Loop in Higgs Propagator

The Feynman rules for the loop portion of this diagram lead to an integral of the form

$$\int d^4p \frac{1}{(p^2+m^2)} \propto \int dpp^3 \frac{1}{p^2} = \Lambda^2 \tag{1.6}$$

This is exactly the form in which the fermion contribution to the Higgs propagator takes. In quantum field theory, loops of fermions have an extra factor of -1 assigned to them, so these two diagrams can thus cancel each other out, and rid the Higgs mass of the quadratic divergence. A logarithmic term of the form $ln(\frac{\Lambda_{UV}}{m_{sfermion}})$ is still present, but this is a well behaved divergence. One can see the idea of supersymmetry is very attractive for fixing the hierarchy problem. Of course, this cancellation requires that the masses of the fermions and sfermions are identical. This cannot be the case, however, as SUSY has not been discovered at any experiment in high energy physics. If SUSY does exist, it must be a broken symmetry, i.e. one in which the sfermions have masses higher than that of their fermionic superpartners. Otherwise, physicists would have detected them by now. Supersymmetry also cannot be broken too badly, because this would ruin the cancellation between the two loop diagrams (19).

As a bonus, supersymmetry also provides a possible answer concerning the nature of dark matter. Observations of dark matter show that it does not interact with the electromagnetic force (hence the term dark matter), and so cannot be electrically charged. It is also not baryonic in composition, meaning it is not made of SM particles. It does interact with the gravitation force and is massive.

SUSY theories that require their lightest supersymmetric particle, or LSP, to be stable can provide a nice candidate for the dark matter. In such versions of SUSY, the LSP is electrically neutral and non-baryonic by default, and can be massive as required of a dark matter particle candidate. Finally, SUSY allows for the unification of the strong, weak, and electromagnetic forces near or at the grand unified scale, which is $\propto 10^{16}$ GeV. At this scale, the electromagnetic force is already unified with the weak force, and SUSY would bring the color force together with the electroweak force to give one unified force. This is popular in many grand unified theories, or GUTs.

SUSY offers so many advantages that it would be a disappointment if it is not realized in nature. I have briefly illustrated the SM with all its particle content, and introduced SUSY as an extension of the SM. In the next section, I will describe a particular model of SUSY that solves the hierarchy problem, is a potential source of dark matter, and allows for unification of the three SM forces. It is also the sparticle content of this model that we search for in this thesis.

1.5 Natural SUSY Higgsino NLSP

As stated before, if SUSY exists in nature, it must be a broken symmetry. The only question is, what is the SUSY breaking scale? If we want the divergence of the fermion loop to cancel, SUSY had better not be broken too badly, otherwise we double the particle spectrum without solving the hierarchy problem. This would be just a more complicated version of the regular SM. Another way to put this is we would like our extension of the SM to have some degree of naturalness. Naturalness is a notion in which the physical parameters of the theory do not stray too far from some central value. Naturalness would be ideal, because it requires less explanation than a theory with parameters that are unrelated and cover a wide range of spectrum. As an example, take the top quark contribution to the fermion loop of the Higgs propagator. This is the most massive of all the quarks, and its mass is near the electroweak symmetry breaking scale. If the sfermions of SUSY have masses all around the electroweak symmetry breaking scale, i.e. $10^2 - 10^3$ GeV, then we could cancel the diverence of the fermion loop and could say that the electroweak and SUSY breaking scales are on par with one another. The theory would be natural in this sense.

For the subsequent analysis in this thesis, we consider a model of SUSY that is natural to some degree. It is called the Natural SUSY Higgsino NLSP model, or HiggsinoNLSP for short. Within its sparticle spectrum, all the sfermions decouple from the theory, except for the right handed top squark[8]. The gluinos, which are strong gauginos, are also decoupled. All the other gauginos, i.e. the electroweak gauginos, are light, around $\Lambda_{EWSB} \sim$O(100 GeV). These electroweak gauginos include

[8]The stop needs to be light to cancel the quadratic divergence of the top quark loop

the four Higgsinos, three Winos, and the Bino, all of which are SUSY counterparts to the SM Higgs, three W's, and the B boson respectively.

In the SM, the $W^{\pm}$, Z, and photon are just linear combinatinos of the three W's and the B boson. Similarly, in minimal SUSY extensions of the SM, we have four charginos, $\chi^{\pm}_{1,2}$, and four neutralinos, $\chi^{0}_{1,2,3,4}$, which are linear combinations of the electroweak gauginos. In the Higgsino NLSP model, we consider the charginos and neutralinos to be comprised purely of Higgsinos, except for the χ^{0}_{1}, which is comprised purely of the Bino sparticle (16). As a final caveat, the $\chi^{\pm}_{2}$ and χ^{0}_{4} are considered heavy and decoupled as well.

I summarize the sparticle spectrum in the following figure

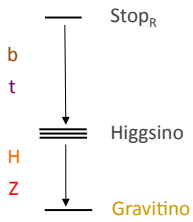

Figure 1.3: Natural SUSY Higgsino NLSP Mass Hierarchy for the Sparticles (7)

Notice the right-handed top squark is at the top of the spectrum of sparticles that are not decoupled. If we consider production of top squarks, then they are produced strongly. The model does, however, allow for direct Higgsino production as well, and we can bypass strong physics altogether. This is electroweak production of the Higgsinos. In SUS-13-002, we consider strong and electroweak production together as the model for new physics (7). For this thesis, I will only consider the electroweak production of Higgsinos.

In the HiggsinoNLSP scenario, the $\chi^{\pm}_{1}$ is at the center of the three lines in figure 1.3, and the χ^{0}_{3} and χ^{0}_{2} are $\pm$ 5 GeV above and below the chargino mass respectively. This leads to eight distinct electroweak production processes: $pp \rightarrow \chi^{0}_{3}\chi^{0}_{3}, \chi^{0}_{3}\chi^{\pm}_{1}, \chi^{0}_{3}\chi^{0}_{2}, \chi^{+}_{1}\chi^{-}_{1}, \chi^{\pm}_{1}\chi^{0}_{2}$, and $\chi^{0}_{2}\chi^{0}_{2}$. In the pure higgsino limit, and setting $\tan\beta$ to 30 and the value of μ >0, the kinematics turn out to be identical for each of the eight production processes[9]. To simplify the computation time, we therefore only use the $pp \rightarrow \chi^{0}_{3}\chi^{0}_{2}$ process, but use the production cross section for all eight processes. We also consider the gauginos to be mass degenerate. Thus, the χ^{0}_{3} and χ^{0}_{2} serve as our next to lightest supersymmetric particles, or NLSPs. Again, they are Higgsino-like (16)).

At the bottom of the sparticle spectrum is the Bino-like χ^{0}_{1}, which serves as our LSP. We consider the NLSPs to decay to a Higgs or Z boson, and the LSP. This leads to three distinct topologies: hh,

[9]In MSSM models, two Higgs fields are required to avoid anomalies in calculations. $\tan\beta$ is defined as the ratio of the vacuum expectation values of the two Higgs fields. The parameter μ is defined as the Higgsino mass parameter (19)

hZ, and ZZ + two LSP's.

1.5.1 Multilepton Final States

In the analysis for this thesis, we search for events in proton collision data that have 3 and ≥ 4 leptons. The HiggsinoNLSP model is an excellent signal for a multilepton search such as this. This is because the Higgs couples to all particles with mass, and so it naturally follows that the Higgs will lead to final states that have multileptons. Also, the Z boson decays to two leptons ~ 10 % of the time. The multilepton search strategy will be discussed at length in chapter 3. For now, it suffices to list the decays of the Higgs and Z boson within each of the three topologies mentioned above.

For the hh, or pure Higgs topology, we consider Higgs decaying to $W^{\pm}W^{\mp}$, ZZ, $\tau\bar{\tau}$, and $b\bar{b}$. Of the ten possible final states for hh decays, we consider the following in our analysis:

- $W^{\pm}W^{\mp}W^{\pm}W^{\mp}$
- $W^{\pm}W^{\mp}$ ZZ
- $W^{\pm}W^{\mp}$ $\tau\bar{\tau}$
- ZZ ZZ
- ZZ $\tau\bar{\tau}$
- ZZ $b\bar{b}$ (Z's decayed leptonically)
- $\tau\bar{\tau}$ $\tau\bar{\tau}$

For the hZ topology, we consider the Higgs decaying to $W^{\pm}W^{\mp}$, ZZ, $\tau\bar{\tau}$, while the Z is decayed leptonically. This leads to the following final states of hZ decay modes:

- $W^{\pm}W^{\mp}$ Z
- ZZ Z
- $\tau\bar{\tau}$ Z

Finally for the ZZ topology, we consider the Z's to decay leptonically. In the subsequent chapters, we also combine the results of the multilepton search with other analyses that search for hh $\rightarrow b\bar{b}b\bar{b}$, hh $\rightarrow \gamma\gamma b\bar{b}$, hh $\rightarrow \gamma\gamma\ell^{\ell} \pm l^{\mp}$, hh $\rightarrow \gamma\gamma + \ell^{\pm}$, hZ $\rightarrow b\bar{b}l^{\pm}l^{\mp}$, and ZZ $\rightarrow \ell^{\pm}\ell^{\mp}$ di-jet (light-flavored).

This concludes the theoretical section of this thesis. For more information on the HiggsinoNLSP model and it's motivation, see (16).

Chapter 2
The Large Hadron Collider

2.1 CMS Detector

The Compact Muon Solenoid (CMS) detector, is one of several detectors located along the Large Hadron Collider (LHC) at CERN. The LHC is a circular proton-proton collider that is capable of exploring the energy regime at and around the 1 TeV scale, which is the scale at which physicists predict new physics to arise. It is an impressively large machine with a circumference of 27 km. The protons used in the collisions are initially clustered together into bunches in the Proton Synchrotron (PS) and then injected into the Super Proton Synchrotron (SPS) of Figure 2.1. In the SPS, the protons are accelerated from 26 GeV to 450 GeV, and then injected into the main LHC ring. Each bunch has approximately 100 billion protons collectively, and there are 2808 bunches injected at a time, with a time delay of 25 ns between each bunch.

Around the turns of the LHC ring are a total of 1232 dipole magnets which serve to give the protons an extra 0.5 MeV in energy along each turn. The protons therefore accelerate to a center-of-mass energy of 8 TeV before they are collided. The full design center-of-mass energy is 14 TeV, which will be attempted in 2015. The full design luminosity is around 10^34 collisions per centimeter per second.

The CMS detector in Figure 2.1 is a cylindrical detector whose geometry is best described with polar coordinates. The origin of the coordinate system is located at the proton-proton collision point. The z-axis is defined as being along the direction of the interaction of the two proton beams. Because the energy in the plane transverse to the beam axis is a Lorentz invariant quantity, a variable called pseudorapidity is used to define the angle with respect to the z-axis.

$$\eta = -ln(\tan\frac{\theta}{2}) \tag{2.1}$$

The angle ϕ is the usual aximuthal angle in the transverse direction. Kinematic quantities of particles in the transverse direction are now more conveninient to use. Transverse momentum (p_T) and missing transverse energy (MET) are of utmost importance, the latter being used to detect if a particle has escaped detection. The total transverse 4-momentum of all the reconstructed particles

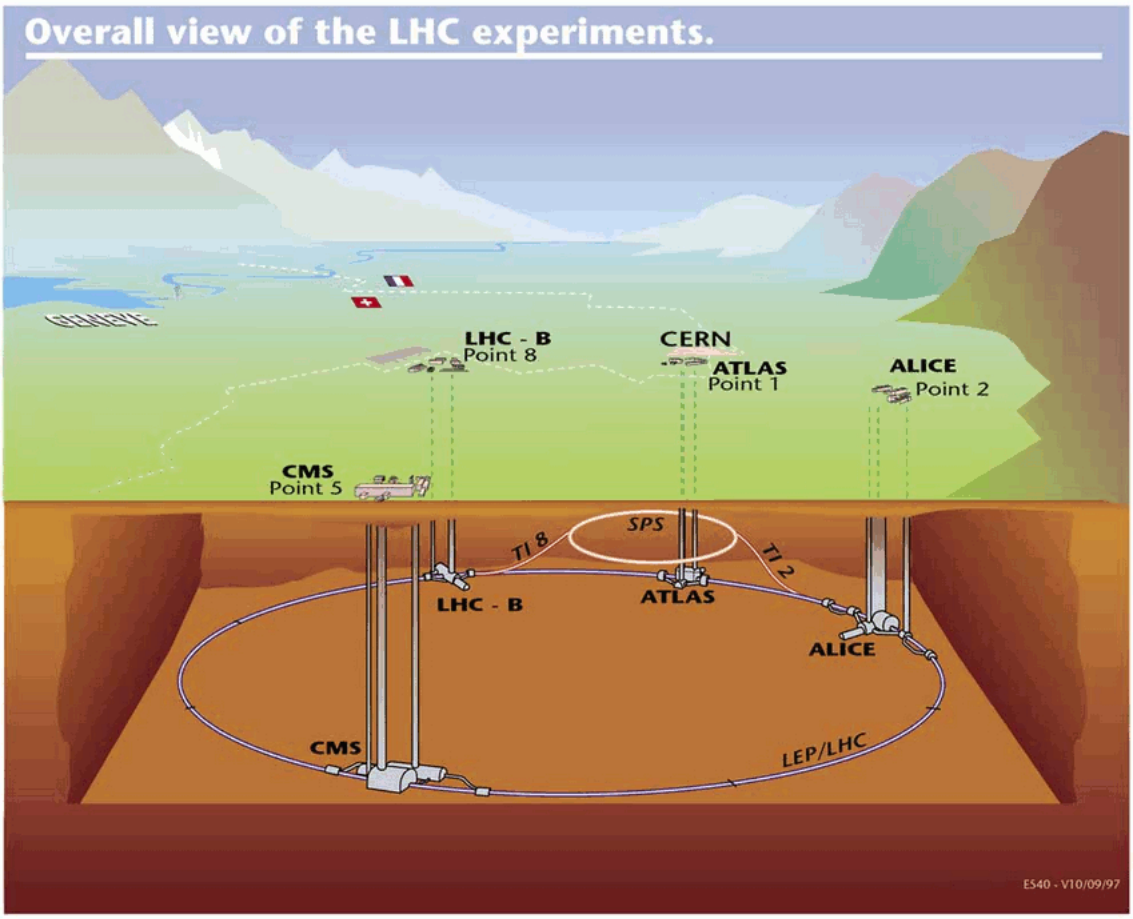

Figure 2.1: The LHC in its full form (13).

post proton collision should sum to zero since the collision occurs in the z-axis. A neutrino candidate, which escapes detection due to its weak interaction, can then be detected by a non-zero value of MET.

Working radially outward from the center of the CMS detector, we first encounter a superconducting solenoid capable of generating a 4T magnetic field. The strength of this field is capable of bending charged particles that emerge from the proton collisions. It is 13 meters in length and 5.9 meters in diameter. Beyond the solenoid is the tracker, which as the name suggests, reconstructs the tracks of charged particles back to their inception. Particles like photons and neutral pions leave no tracks since they are not electromagnetically charged. The electromagnetic calorimeter, or ECAL, is the next layer of CMS, and it was designed to stop and capture the energy of electrons and photons. Heavier particles like hadrons (quark bound states) pass through the ECAL and are stopped in the hadronic calorimeter. They deposit most of their energy here, but can leave some trace of their energy in the ECAL. The outer layers of CMS are devoted to muon capture. The

muon is a minimally ionizing particle, so it tends to punch through the ECAL and HCAL. It decays, but is still light enough to travel to the farthest layers of the detector (8).

2.1.1 Tracker

Using various software algorithms, the tracker's main function is to aid in the reconstruction of the paths which the electromagnetically charged particles take before being stopped in the calorimeters. There are three main regions within the tracking system that of are of importance. These regions are defined by the particle flux which passes through them. The first is the region closest to the interaction point, where the tracker is made up of pixel detectors with individual areas of approximately 100 by 150 square micrometers. These pixel layers are place at different radii below 20 cm. Over 66 million pixels are used, which covers a total area of approximately 1 square meter. The region beyond a radius of 20 cm is divided into an intermediate and outer region, where silicon based strip detectors are used in place of pixel detectors. Over 9.6 million silicon strips are used, which covers a total area of approximately 200 square meters and covers pseudorapidity $|\eta| < 2.4$ (8).

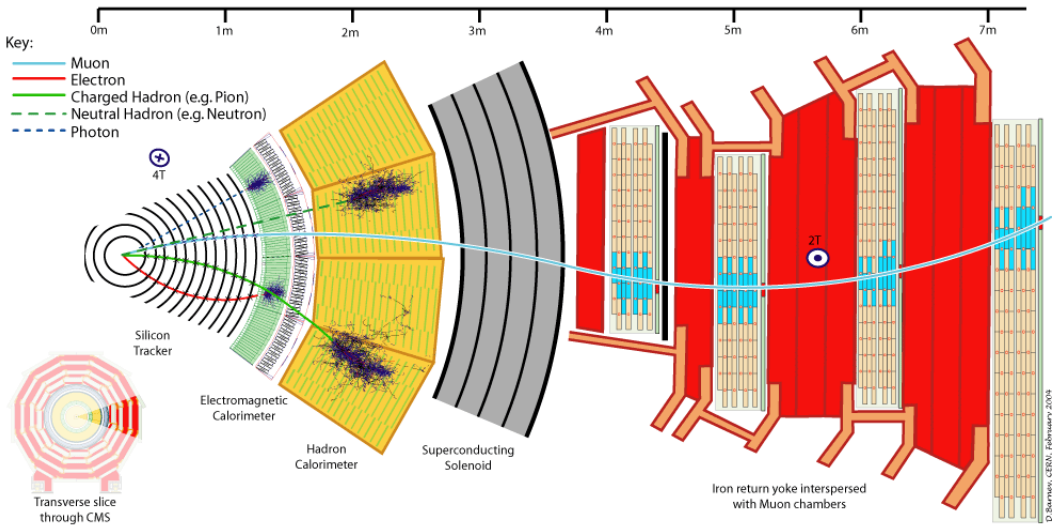

Figure 2.2: The CMS detector in a cross sectional view (6).

2.1.2 ECAL

Moving radially outward from the tracker is the electromagnetic calorimeter, or ECAL. As its name suggests, it is designed to capture the energy of electrons and photons that result from proton collisions. The ECAL can be described by splitting it into two parts: the barrel region, $0 < \eta < 1.479$, and the endcap region, $1.497 < \eta < 3.0$. In these regions are placed lead tungstate ($PbWO_4$) crytals, which provide fast read output and excellent resolution. The crystals are also radiation resisitant,

resulting in low loss of energy resolution. In the barrel region, there are 61,200 of these lead tungstate crystals, which have a volume of 22 x 22 x 230 cubic millimeters each (height, width, and length). These extend out to a radius of 129 cm from the interaction point. In the endcap region, there are 7,324 crystals with a volume of 28.6 x 28.6 x 220 cubic millimeters (height, width, and length). To cover very large range of pseudorapidity, a preshower device is fitted in front of the endcap crystals (8).

2.1.3 HCAL

Outside of the ECAL is the hadronic calorimeter, or HCAL. It is designed to capture the energy deposited by hadrons, which are bound states of quarks. When quarks or gluons are emitted in a collision, they undergo a complicated process known as hadronization. This process can loosely be described as quarks and gluons radiating other quarks and gluons until an low energy threshold known as the confinement scale is reached; at which point the quarks and gluons become bound together, forming mesons and baryons (collectively hadrons). In the collider, the final state of quark production and subsequent hadronization appears as a spray of hadrons, or a jet of heavy particles. Jets are notoriously difficult to reconstruct, and a mismeasurement can result in MET that is not genuine. To off-set this issue, the HCAL uses a combination of brass plates and plastic scintillator technology. Brass is chosen due to its short interaction length, and the fact that it is not a magentic materal. The scintillator plates have a thickness of 3.7 mm, and are placed between layers of brass (8).

2.1.4 Muon Detector

In the farthest radial region of the detector lies the muon chambers. This portion of the detector is unique in that it uses three different types of gases to detect muons. The muon will enter the gaseous material and knock the electrons out of the gas atoms. The electrons then move through a voltage difference, leaving tracks. In this way the detector can reconstruct the four momentum of the muon. A muon can be seen in figure 2.2, and its track switches direction because it is entering the return yoke of the magnetic field, which is pointing in the opposite direction with respect to the direction of the field within the tracker, ECAL, and HCAL. In the barrel region, $\eta < 1.2$, the muon flux and magnetic field strength are low, so a drift tube (DT) chamber is used. In the endcap region, the muon flux is high as is the magnetic field from the return yoke, and a cathode strip chamber (CSC) is employed. Finally, resistive plate chambers (RPC) are used in both barrel and endcap regions. They generally have a faster response time than both the DT and CSC technologies, and so allow for additional coverage (8).

Chapter 3
Searching for New Physics

3.1 Analysis Overview

Large sections of the thesis from this chapter and the next originate from the SUS-13-002 paper (7). Performing an analysis that searches for new physics in events with multileptons serves two purposes. The first is that the SM physics processes that lead to three and $\geq$ four leptons are rare, and so a lot of low energy QCD, which is difficult to estimate as a background to new physics, is not worrisome. Secondly, the new physics we are interested in is supersymmetry, in particular the Natural SUSY Higgsino NLSP spectrum, which has Higgs and Z boson final states. This type of signal is an excellent fit for a multilepton search, since the Higgs produces leptons through multiple processes, and the Z decays to leptons 10% of the time. With enough sample statistics, multileptons events are produce copiously in this model. All three topologies, hh, hZ, and ZZ, are rich in multilepton final states.

3.1.1 Lepton Triggers

The data we use in this analysis was collected during the $\sqrt{s} = 8$ TeV run of proton proton collisions in the CMS detector. Each proton has an energy of 4 TeV in every event. The total integrated luminosity on the data, L_{Data}, which is a measure of how many events occured per unit area, is 19.5 fb^{-1}. Since we are interested in events which have multiple leptons, we use data sets that contain at least two reconstructed leptons in every event. We also put in place what are known as event triggers which need to be passed. For instance, we use a dataset which contains at least two muons, labeled Double_Mu, and we use a double muon trigger that checks the p_T of each of the muons. The leading muon, or the muon with the largest p_T, must have a $p_T \geq 17$ GeV, and the next to leading muon must have $p_T \geq 8$ GeV to fire the double muon trigger. This is the minimum requirement to be a two muon candidate event for our analysis. Although this trigger is in place, we actually require 20 GeV and 10 GeV for the leading and next-to-leading p_T of our muons, and more generally, our leptons at the analysis level.

We use three datasets that total $L_{Data} = 19.5 fb^{-1}$: DoubleElectron, DoubleMuon, and MuEG.

The type of events in each set is reflected in the name. MuEG is obscurely named, but it is a dataset that has events with at least one muon, one electron, and one photon. We use several double electron, double muon, and muon electron triggers to select the events from the respective datasets for our analysis. In order to get an idea of how efficient the triggers are, we use a different type of dataset for testing purposes. This is to remain unbiased. For trigger efficiency tests, we use a dataset that has a significant amount of hadronic activity, or H_T (defined below). Using the triggers on this dataset, we have demonstrated that the maximum efficiency of each trigger is 95% for the double electron trigger, 90% for the double muon trigger, and 93% for the muon electron trigger. These values are used to scale simulated events to data (7).

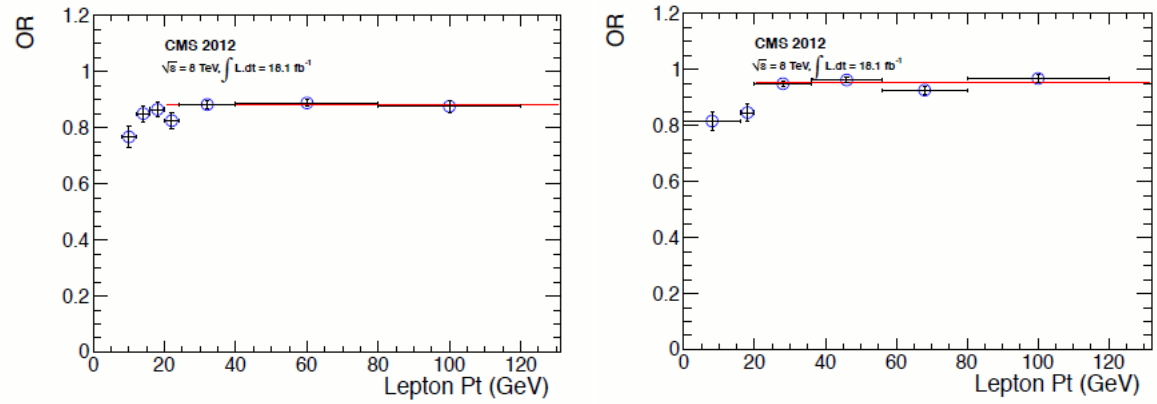

Figure 3.1: Trigger efficiency plots as a function of lepton p_T. The double muon (left) and electron (right) trigger efficiencies are depicted (3).

Of the triggers we use, we require that only one of them fires among the list, so we use the OR method of trigger firing (3).

3.1.2 Lepton Cuts and Efficiencies

We are interested in multiple leptons in an event, but ideally we want the leptons to be isolated with respect to other physics objects in the event. This is because SUSY and other physics beyond the SM often contains leptons that are high in transverse momentum, and therefore veer away from the cluttered low energy physics. To this end, we use the particle flow algorithm to reconstruct all electrons and muons, and define a variable called relative isolation, or I_{rel}. Relative isolation is defined as the sum of the transverse momentum from all particles in a cone of $\Delta R < 0.3$ around the lepton, divided by the transverse momentum of the lepton itself. Here, $\Delta R = \sqrt{\eta^2 + \phi^2}$. If $I_{rel} < 0.15$, we consider the electron or muon to be isolated. This way, if a jet radiates a muon or electron, it is less likely to be selected for our analysis. The taus are a little trickier. We widen the

cone to $\Delta R = 0.5$, and require that the energy around the leading track to be less than 2 GeV.

To further reject the possibility of fake leptons coming from jets, we require a d_{xy} cut of less than 0.02 cm from the primary vertex. d_{xy} is defined as the distance measured in the plane transverse to the beamline; it is also referred to as the impact parameter. Jets formed from heavy quarks, like bottom quarks for example, tend to have a large impact parameters, and therefore fake leptons coming from b-jets would also tend to have large impact parameters.

As in the case of the triggers, we also have measurements on how well our lepton isolation and identification cuts perform. To test these cuts, we use a well-known method called tag and probe. The basic idea behind tag and probe is to identify two leptons (electrons or muons) with a tight lepton cut and a loose lepton cut respectively. These cuts are applied before the isolation and ID cuts are made. The tighter the lepton cut, the more sure we are that the object that passes it is a real lepton. The lepton that passes this tight cut is the tag lepton, and the lepton that passes the looser cut but not the tight cut is the probe lepton. Then one takes the invariant mass of the tag and probe leptons. If it falls between the Z-mass window, 75 to 105 GeV, then one can be confident that the probe is most probably a real lepton. The novelty of this approach is that now one has a lepton (the probe) with very minimal cuts applied to it, and can use these probe leptons to test the efficiencies of other cuts without worrying about correlations amongst other cuts. The cuts required to be a probe electron/muon are, to zeroth order, that the p_T is > 5.0 GeV and the η is < 2.1. For more details on tag and probe cuts, see (3). To give an idea of what the efficiencies for isolation and identification cuts look like, see figures 3.2-3:

3.1.3 Binning Procedure

The general feature of doing this multilepton analysis is a binning in several kinematical variables. By bin, I mean a separate collective space for events that pass the thresholds required for a particular variable. For instance, we could simply look for events that have exactly three electrons, and events that have exactly three muons, and store the number of these events in different areas, ideally in histograms. More directly, we bin events by how many leptons are present (3 or ≥ 4 leptons, where lepton is an electron, muon, or hadronic tau). We also bin events by how many opposite sign same flavor pairs are present in the event, and whether or not they form an invariant mass on the Z boson peak. Again, as an example, suppose an event contains the following leptons: $e^-e^+\mu^-$. This event has one opposite sign, same flavor pair, namely, the two electrons. We call this variable DY (Drell-Yan), and since there is one pair, we label it DY1. Let's also assume that the invariant mass of the electrons is outside the 75 - 105 GeV window. We would call this an off-Z pair, or a Z-veoted (ZV) pair. It also has three total leptons, so the bin this event would be stored in would be the

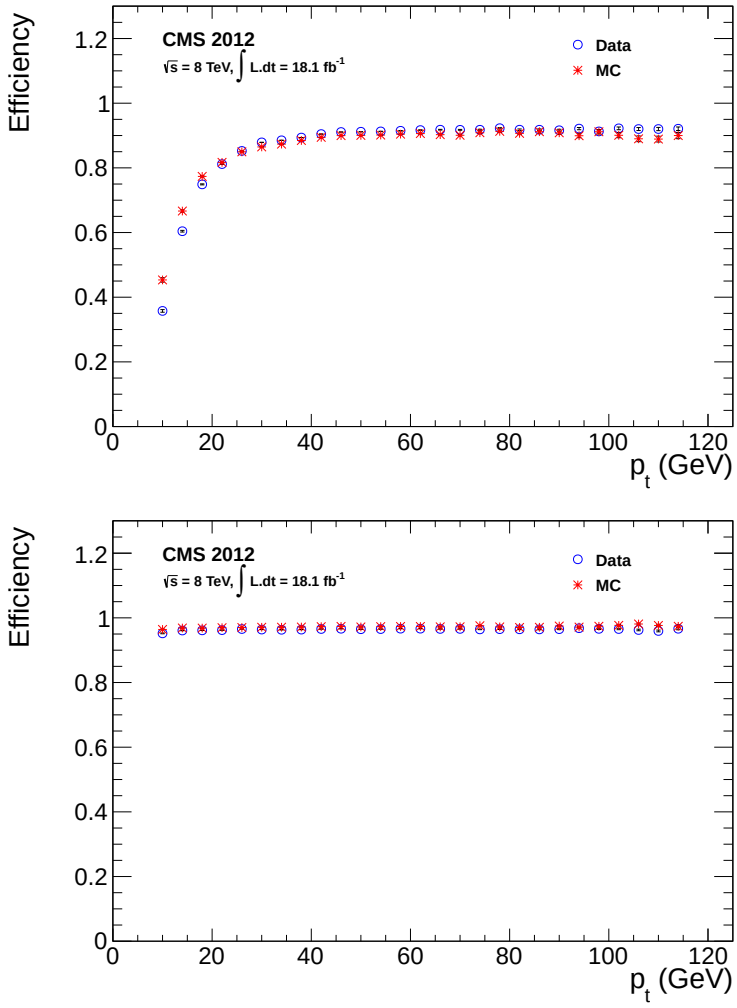

Figure 3.2: Lepton identification efficiency plots as a function of lepton p_T. The electron identification (top) and muon identification (bottom) efficiencies are depicted (3).

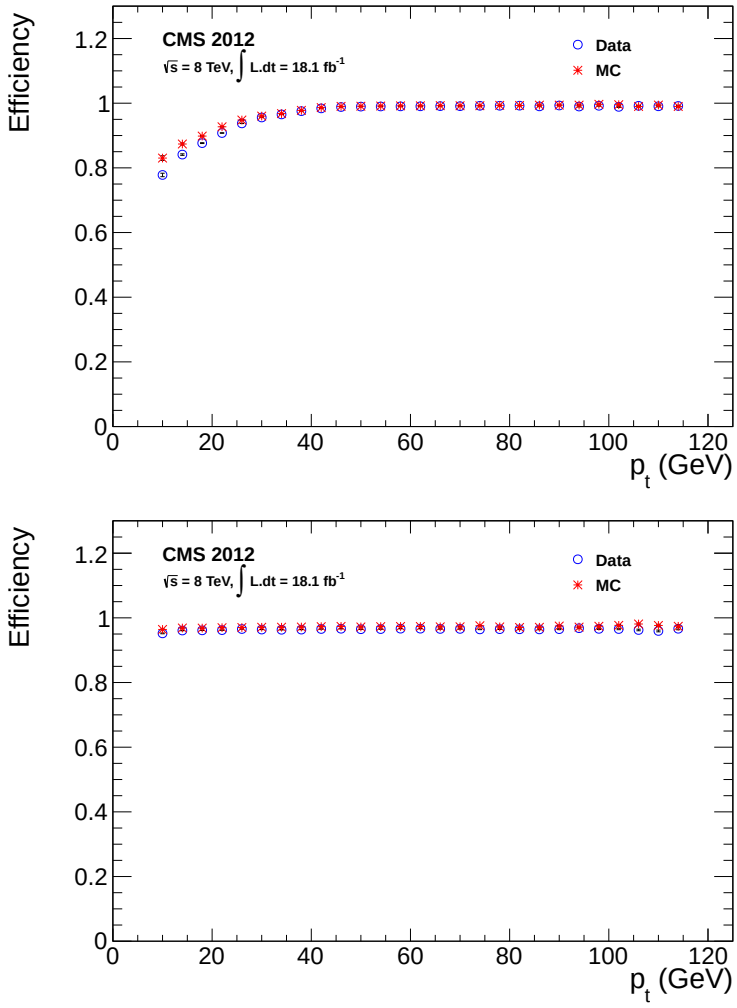

Figure 3.3: Lepton isolation efficiency plots as a functin of lepton p_T. The electron isolation (top) and muon isolation (bottom) efficiencies are depicted (3).

L3DY1ZV. Whether or not the muon is positively or negatively charged is irrelevant in our binning scheme, and both types of events would land in the same bin.

We also bin in the number of b-tagged jets and the number of hadronic taus that were reconstructed in the event. Specifically, we look for events with 0 or ≥ 1 b-tagged jet, and 0 or 1 hadronic tau, τ_h. Finally, we come to the kinematic variables that we bin in. We use two unique variables, the familiar quantity known as MET, or missing transverse energy, and H_T, which is the scalar sum of all hadronic activity in the event. MET is a particularly useful kinematic variable, because the LSP of the Natural SUSY Higgsino NLSP model is stable, and therefore if it exists, will only show up as MET. By binning in MET, we avoid being biased to the 1 GeV LSP of the model. The bins are 0 to 50, 50 to 100, and > 100 GeV. The H_T variable is also a good variable because it is orthogonal to the MET variable, and also allows for the model independent idea that new physics might appear with lots of jet activity. This variable is binned from 0 to 200 GeV (low H_T), and > 200 GeV (high H_T).

The combinatorics of all these bins is large, and as a result we have a wide search window for new physics. We also, however, open ourselves up to the look elsewhere effect (15), which is exactly what happens in our analysis.

Chapter 4
Standard Model Background

4.1 Multilepton Backgrounds

In order to notice new physics in an experiment such as this one, it is necessary to estimate the known physics processes from the SM that contribute to the observed events in the data. To accomplish this, we use both simulation and data-driven estimation methods.

4.1.1 Simulation

We use simulation to model three SM physics processes that produce multileptons. They are $t\bar{t}$, WZ, and ZZ production. The production of $t\bar{t}$ is important because top quarks decay approximately 99% of the time to a W boson and a bottom quark. The W boson can then decay leptonically approximately 30% of the time to a lepton, l, and the associated anti-neutrino, $\bar{\nu}_l$. The bottom quark hadronizes, and the jet that results can then radiate a lepton that is mistaken as an isolated and prompt lepton. Thus, we have multiple leptons, b-tagged jets, and $\not{E}_T$ from the neutrinos. The jet spectrum of $t\bar{t}$ tends to be higher in p_T, and is thus more trustworthy for simulation purposes.

WZ and ZZ events are similar. In the first case, one has three leptons and $\not{E}_T$, where two of the leptons come from fully leptonic decay of the Z boson, which occurs approximately 10% of the time. In the second case, ZZ events decay to four leptons with no MET. WZ is of special interest, however, because we use it to study the resolution of MET. In general, MET resolution is modeled using a series of gaussian distributions. The gaussians themselves are very sensitive to effects such as event pileup and the presence of jets. Pile up tends to make the gaussian distributions wider, and the diverse jet spectrum tends to make the tails of the gaussian distributions longer. Thus, if one wants to quantify the sensitivity of the gaussians to pileup and jet activity, it makes sense to use the number of vertices and H_T as variables (7).

We use a sample of dilepton data that has low missing transverse energy upon which to build the MET resolution model. The logic here is the more controllable the MET, the better our model's predictive power. The primary process that contributes to a dilepton data sample is an event that has a Z boson and a jet. The Z boson decays to neutrinos 20% of the time, and this has significantly

less MET than, for example, a sample that has mostly events coming from $W \pm W \mp$. We bin the data sample in the number of vertices and the H_T into two components in the transverse plane. Then, using the sum of the gaussians to model the MET, we go bin by bin to derive scale factors that are needed to match the model to the data. These scale factors vary by bin, and can be as low as 0 and as high as 25%.

The WZ simulation is then weighted by these scale factors based on what MET bins the MC events land in. It is also weighted with the lepton efficiencies ratios from chapter 3. Finally, for the WZ simulated events that land in bins that are both on the Z peak (i.e. the invariant mass of the OSSF pair is in the Z-window) and have low H_T, we scale these events to the data. This is our control region because it is a situation in which new physics is least likely to present itself, according to the BSM theories we are probing. In figure 4.1, one can see the WZ control region scaled accordingly (7).

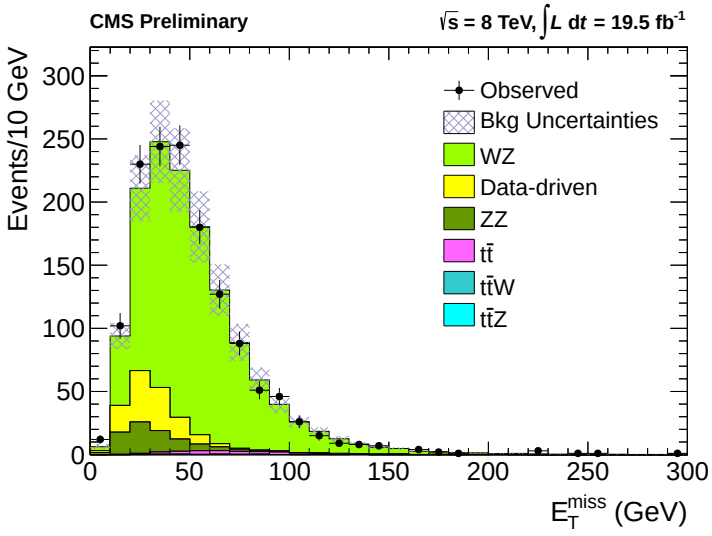

Figure 4.1: Control region plot using simulation enriched in WZ events and binned in MET. Scale factors derived from this are applied to WZ events in search regions (2).

The final most significant background for multileptons is the contribution from $t\bar{t}$ production. The top quark decays almost exclusively to a W boson and a bottom quark. From there, the W can decay semi-leptonically approximately 30% of the time. If one of the b-quark jets radiates a lepton, then there is potential for three leptons to come from this background: two from the W boson leptonic decay, and the third from the lepton coming from a b-jet. Obviously, this type of event is important for channels that have b-tags. We apply similar MET smearing to this sample as well, and lepton efficiencies. To see if the $t\bar{t}$ simulation is accurately describing data events, we select events in data that have dilepton pairs that are opposite in flavor (e μ) and have at least

one b-tagged jet. Then, we take the simulation and scale it up to the full luminosity, and compare distributions for the kinematic variable H_T, and MET. Below are the results of this test. As can be seen, data and simulation are in excellent agreement.

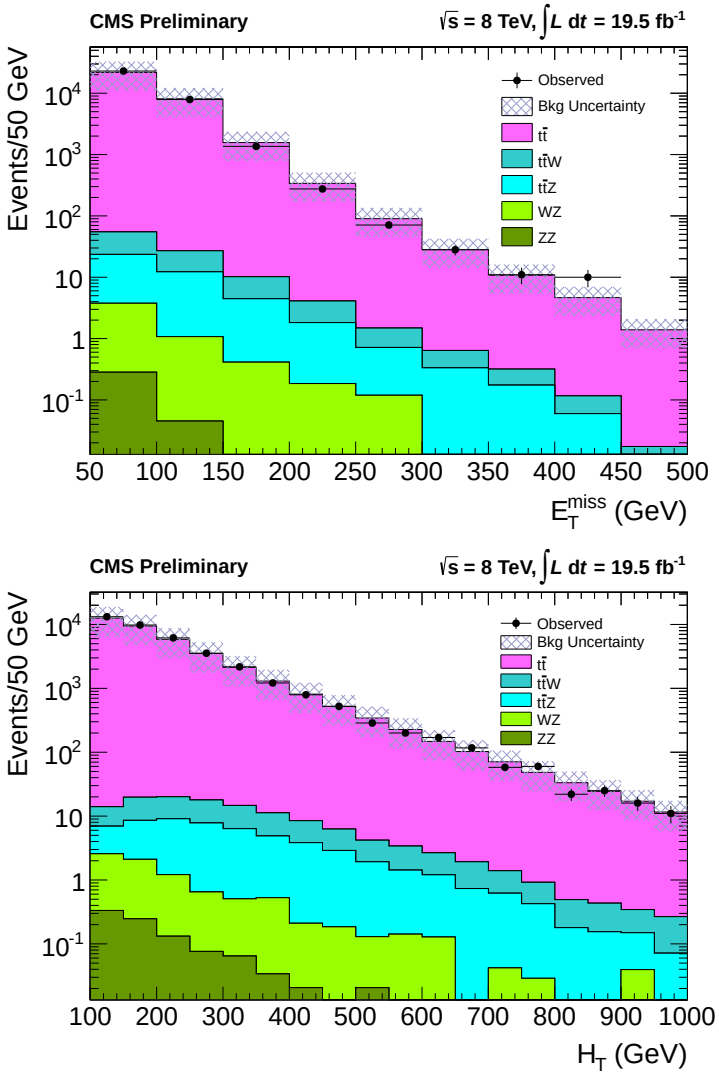

Figure 4.2: Control region plot using simulation enriched in $t\bar{t}$ events binned in MET (top) and H_T (bottom) (2).

We deal with rarer SM backgrounds, but di-boson and $t\bar{t}$ are the backgrounds with the highest cross section that we consider using simulation for.

4.1.2 Data Driven

There are some backgrounds that one cannot rely on simulation for. Take perhaps the largest background for multileptons, Z + jets. Simulation does not accurately depict the tail of a MET

distribution for such a background. Additionally, any background heavy in jets is going to be better dealt with using data driven methods. A data driven method is one in which simulation is not relied upon, and one uses clever cuts in data samples to derive some kind of scale factor applicable for another data sample, roughly speaking. These methods can get quite complicated as we shall see. The backgrounds that must be taken account in this way are the number of jets faking hadronic taus, the number of fake leptons coming from light-flavored jets, and the number of internal photon conversions that produce opposite sign same flavor pairs. A unique method is derived for each of these background processes and is described below in turn.

ft vs fsb

We begin with a method known as f_T vs f_{SB}. Since the multilepton analysis bins in the number of hadronic taus, one must be careful to distinguish between a real hadronic tau, and a jet that looks like a hadronic tau. Their resemblance is due to the fact that taus can decay to charged pions (1-prong and 3-pronged for this analysis), which can have products that form a cone in the hadronic calorimeter, mimicking a jet. The way we account for this is to take a data sample enriched with jets and make a distribution of the relative isolation. Recall that relative isolation, or I_{rel} is defined as:

$$I_{rel} = \frac{\Sigma p_{T_{objects in cone of \Delta R=0.3}}}{p_{T_{object}}} \tag{4.1}$$

Now the more isolated something is, the less likely that it is surrounded by clusters of objects. That is to say, as I_{rel} decreases, the more likely we are dealing with real hadronic taus, and not objects such as jets which deposit a lot of energy in and around the cone of the primary track. We define three regions in such a distribution. $I_{rel} < 0.15$ is considered the region in which there is the lowest number of fakes. $0.15 < I_{rel} < 2.0$ is considered the side-band region. A relative isolation above 2.0 is almost certainly a fake hadronic tau. A naive method of deriving some kind of scale factor would be to take the ratio of the number of events in the data sample that pass the $I_{rel} < 0.15$ criteria to the number of events that fall in the side-band. This would be the fake rate of jets to fake hadronic taus, or f_T.

There is a problem with defining a fixed flat fake rate, however. The f_T depends heavily on the data sample that one uses. One might get an f_T for a particularly soft jet spectra that differs from one might get for a harder jet spectra. See figure 4.4 below.

The solution to this is to find another parameter in which to parameterize the data set being used. In essence, we convert f_T from a flat rate to a function that depends on the new parameter.

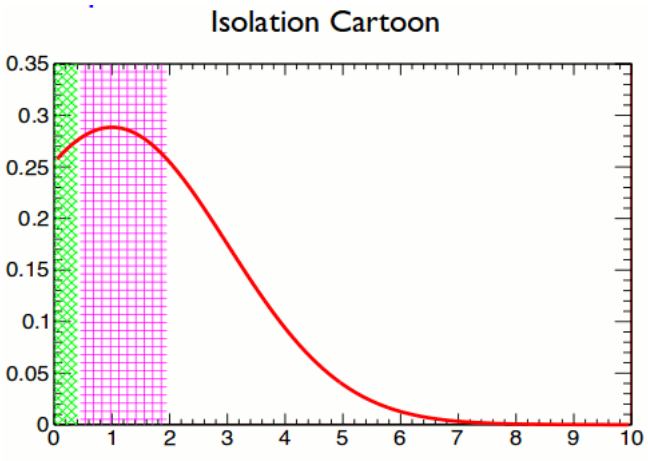

Figure 4.3: An illustration demonstrating the isolation distribution of hadronic tau fakes. The x-axis is I_{rel} and the y-axis is the fake rate (14).

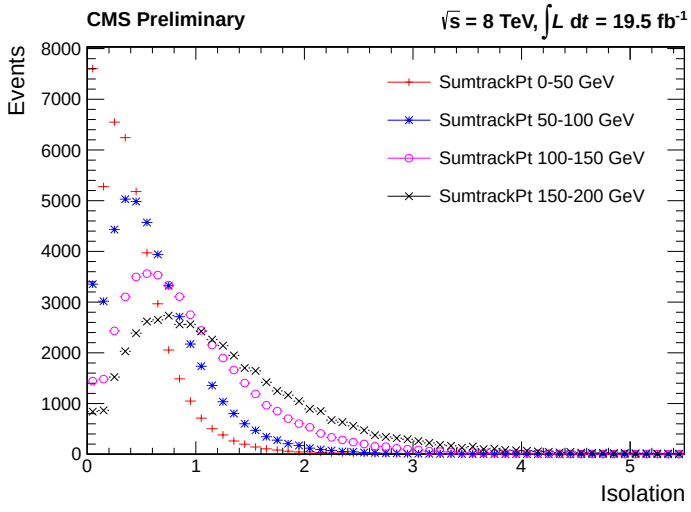

Figure 4.4: An illustration demonstrating how the isolation distribution changes based on jet spectra (2).

The parameter we choose is called f_{SB}. It is definied as the ratio of events that land in the side-band to the events that have $I_{rel} > 2.0$. For a given dataset, one can calculate the f_{SB} and determine the corresponding f_T. Applying this to the number of jets in the data sample will give an estimate as to the number of fake hadronic taus, and is added to the background for each channel.

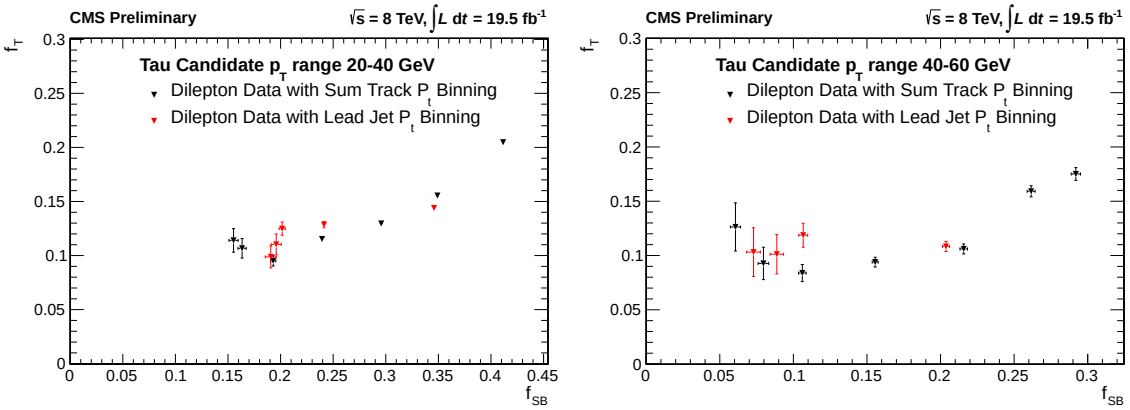

Figure 4.5: f_T vs f_{sb} using two datasets for p_T 20-40 GeV (left) and p_T 40-60 GeV (right) (2).

Rdxy

The second data driven method that we use is the calculation of a fake rate of jets to radiate isolated leptons (electrons and muons). These are not the leptons we are interested in in the analysis because they do not come from the primary vertex, or interaction point. Using a data set that is primarily jet enriched, we take the ratio of the number of isolated tracks that pass the lepton criteria to the ratio of total number of isolated tracks. Mathematically it is written as:

$$f_l = \frac{N_l^{iso}}{N_T^{iso}} \tag{4.2}$$

Similar to the fake rate for hadronic taus, the fake rate here is sensitive to the flavor of jet spectra being used. We therefore need a tuning parameter, similar to f_{SB} as in the previous section. First, we break the fake rate equation in the following way:

$$f_l = \frac{N_l^{iso}}{N_T^{iso}} = \frac{N_l}{N_T} \frac{\epsilon_{iso}^l}{\epsilon_{iso}^T} \tag{4.3}$$

The first ratio is measured in a di-lepton data seed to reduce the dependence on control data and uses all non-isolated leptons and tracks. The second ratio is now dependent on the jet flavor, since the first ratio has now factored out and it does not use isolation in its measurement. Each of the efficiencies in the second ratio can be parameterized by a variable called $R_{d_{xy}}$, where $R_{d_{xy}}$ is

defined as the ratio of tracks that have a dxy $>$ 0.02 cm to the number of events with dxy $<$ 0.02 cm. Since b-jets are much heavier than the u,d, and s quarks, it tends to have a secondary vertex farther than 0.02 cm in the transverse plane of the detector. Consequently, a large value of $R_{d_{xy}}$ would indicate more b-jet activity, whereas a small value of $R_{d_{xy}}$ indicates activity of the lighter jet flavor. One can use a Z+jets data sample to make the distribution of isolation efficiency versus $R_{d_{xy}}$ for isolated leptons and isolated tracks. With this in hand, the $R_{d_{xy}}$ can be measured on an event by event level, and a corresponding fake rate f_l can be used to multiply by the number of raw trilepton events in the search channel, and added to the background.

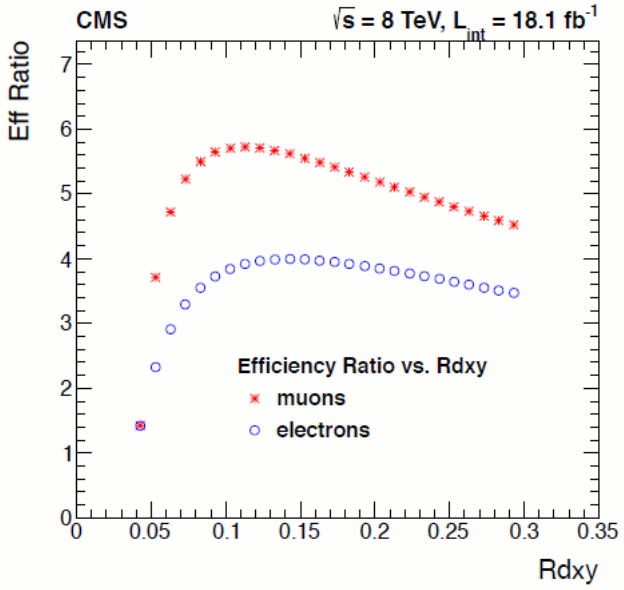

Figure 4.6: Efficiency ratio $\frac{\epsilon^l_{iso}}{\epsilon^T_{iso}}$ as a function of impact parameter (3).

Asymmetric Photon Conversion

This is the final data driven method used for the multilepton analysis for background estimation. Suppose one had a trilepton event with an invariant mass on the Z-mass window. Is this new physics? It might be a bit puzzling at first, but it is completely understandable in terms of asymmetric photon conversion.

The idea is simple. Consider the following Feynman diagram in figure 4.8. First, the Z boson decays to two leptons. One of these leptons now radiates a hard, off-shell photon, leaving itself with very low pT. Then the off-shell photon decays into two leptons. Since the lepton with very low pT probably will not be reconstructed by the detector, we are left with what appears to be a trilepton event with an invariant mass on the Z-peak. Such trilepton events not sufficiently accounted for in

simulation.

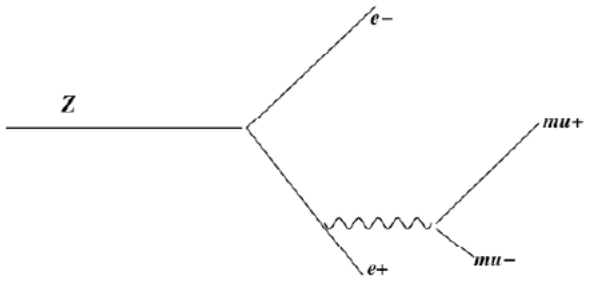

Figure 4.7: Feynman diagram for the background leading to a three lepton invariant mass in the Z mass window (3).

We estimate a fake rate in the following way. We take the number of trilepton events ($l^+l^-l^{'\pm}$ and $l^+l^-l^\pm$) that are within 15 GeV of the Z mass (7), and divide by the number of $l^+l^-\gamma$ events in a Z+jets sample. This ratio roughly fits the value of the fake rate. We apply the fake rate in the trilepton search channels and add this to the background. A 50% systematic uncertainty is applied based on the assumption that the rate of real photons is of the same rate as off-shell photons.

Chapter 5
Additional Analyses

5.1 hh Topology

Large portions of this chapter and subsequent chapters originate from the public analysis summary (PAS) SUS-14-002 (9) and the as yet unpublished paper version of the PAS, of which I am an author. Since the Natural SUSY Higgsino NLSP model has such a variety of final state signatures, many different analyses can be optimized for a particular final state. We mention these analyses in turn, because the parameter space that can be excluded with the added contribution of these analyses to the multilepton analysis can be greatly extended. There are five additional analyses that we consider in the combination. The analyses for the hh topology are four b-jets (4b), two photons and two leptons (2γ2b), and two photons and a lepton ($2\gamma+\ell$) final states. For the hZ topology, we consider an analysis that looks at the Higgs decaying to b-jets and the Z decaying leptonically, and also the two photons and a lepton ($2\gamma+\ell$) analysis. The fifth and final analysis considers the ZZ topology, where one Z decays to light-flavored jets (u,c,s,d), and the other leptonically. I describe each analysis in turn below.

5.1.1 hh $\rightarrow$ bbbb

This search channel is a promising one because the Higgs branching ratio to two b-jets is large, approximately 58%. The analysis is summarized in SUS-13-022, in which we optimize the search appropriately for four b-tagged jets. The object selection is similar to the multilepton search for b-tagged jets: a cut of pT $>$ 20 GeV and $\eta < 2.4$ is required for all the b-tagged jets. Additionally, we require exactly four or five jets in total, where a threshold of of at least 50 GeV must be met by at least two of the jets. A cut on the significant MET, or S_{MET} of greater than 30 is also required. This is because of the models LSP, the bino-like neutralino, which is 1 GeV in mass, is expected to carry away a lot of transverse momentum. The 4b channel in the model is not accompanied by isolated electrons and muons, and so events with isolated e's and μ's or charged objects with pT $>$ 10 GeV and $\eta < 2.4$ are rejected. Events with hadronic taus are also rejected with the same pT and η requirements as the b-jets.

The last of the object selection cuts is a variable we define as $\Delta\phi_{min}$ which is the minimum polar angle amongst the MET vector and the jets in the event. The largest background for this analysis is semi-leptonically decaying $t\bar{t}$, where one of the W's decays hadronically, and the other leptonically. This is a background with four jets, a lepton, and MET from the neutrino. The S_{MET} for this background is not expected to be large, and when the lepton is not reconstructed properly, the background looks like four jets with small MET. The angle between the b-jet that comes from the leptonically decaying W and the neutrino's momentum will be large, and the MET vector might be close to one of the other 3 jets from the other top quark decay. Therefore, for $30 < S_{MET} < 50$, a requirement of $\Delta\phi_{min} > 0.5$ is made to reject such backgrounds. For $S_{MET} > 50$, the requirement is relaxed slightly to $\Delta\phi_{min} > 0.3$.

2b, 3b, and 4b samples

Having defined the object selection, we can now talk about how the analysis defines the samples. We define three different samples by the following criteria:

- 2b sample : exactly two tight b-tagged jets, and no medium b-tagged jets
- 3b sample : exactly two tight b-tagged jets, a third tight or medium b-tagged jet, and no other jets
- 4b sample : exactly two tight b-tagged jets, a third tight or medium b-tagged jet, and a fourth tight, medium, or loose b-tagged jet

The signal hh $\rightarrow$ 4b will obviously most often land, after the cuts applied described above, in the 4b sample. The 3b sample is included in the analysis to improve signal efficiency. The 2b sample will not have much signal landing within it, but we will see that it helps determine the background in the 4b sample.

With these samples defined, we now set up a signal region, or SIG, based on three additional variables, and is used within each sample. It is most easily explained via the 4b sample. In a 4b sample, we have four b-tagged jets, and if one forms pairs amongst the four b-jets, one gets three possible unique combinations of di-jet pairs. For each of the 3 combinations, we form the invariant mass of each of the di-jet pairs, and subtract them. Mathematically, it looks like:

$$\Delta|m_{bb}| = |m_{bb,1} - m_{bb,2}| \tag{5.1}$$

Taking the smallest value for $|m_{bb}|$ of the three combinations will give the closest set of di-jet pairs that come from a Higgs boson. The second variable we define for the SIG is ΔR, which is the

distance in the η vs ϕ plane between the b-jets of $m_{bb,1,2}$ that minimizes $|m_{bb}|$. Because of the boost of the Higgs, the b-jets will tend to land in a tight cone in the HCAL, and so using smaller values of the ΔR will pick out events that are more Higgs-like. Finally, we define a third variable, which is simply the average of the invariant masses of $m_{bb,1,2}$ that minimize $|m_{bb}|$. The figures 5.1 and 5.2 show the distribution in the three SIG variables for the data and simulation in the 4b sample.

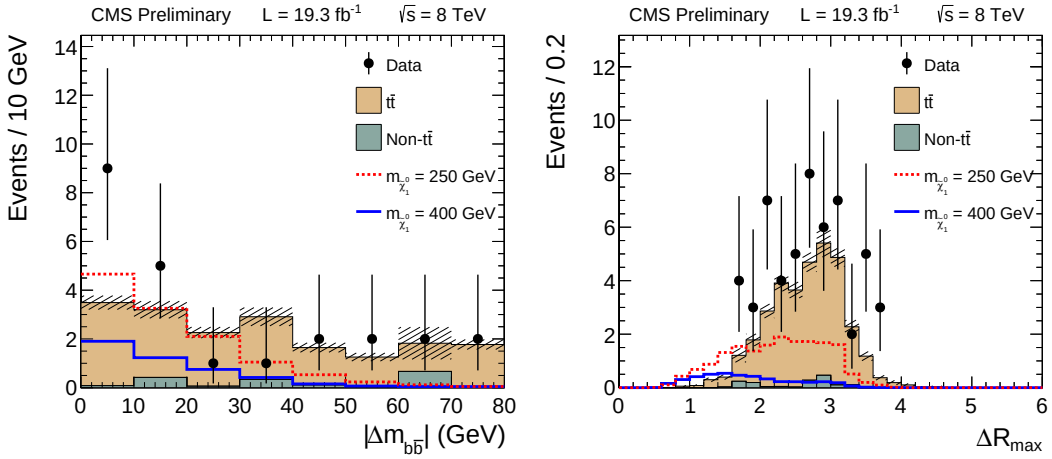

Figure 5.1: The m_{jj} (left) and ΔR variable plotted with Higgsino signal 250 GeV (red) and 400 GeV (brown) superimposed (9).

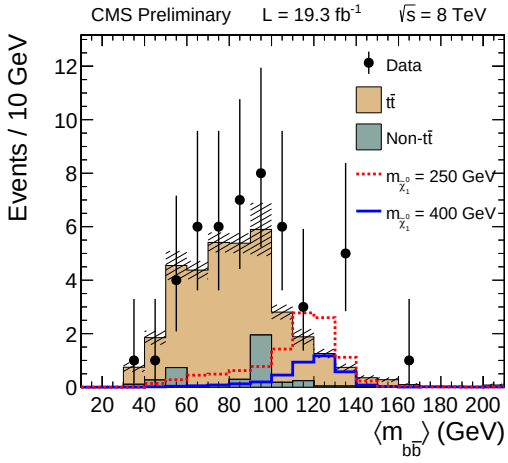

Figure 5.2: The average di-jet mass plotted with Higgsino signal 250 GeV (red) and 400 GeV (brown) superimposed (9).

Using these variables, we define the SIG by requiring $|m_{jj}| < 20$GeV, $\Delta R < 2.2$, and $< m_{jj} >$ between 100 and 140 GeV.

A side-band region is also defined as SB, which focuses on the parameter space outside the boundaries $|m_{jj}| < 30$GeV, and $< m_{jj} >$ between 90 and 150 GeV. To determine the background in the 4b sample, we use the ABCD method, where A,B,C, and D individually represent the following:

- A is the number of background events in the 4b signal region
- B is the number of background events in the 4b side-band region
- C is the number of background events in the 2b signal region
- D is the number of background events in the 2b side-band region

If we look at figure 5.3, we can see that the 4b and 2b samples have similar SIG and SB regions, and assuming the 2b sample is mostly dominated by the background, then the number of background events in the 4b signal region, A, is:

$$A = \frac{C}{D} * B \tag{5.2}$$

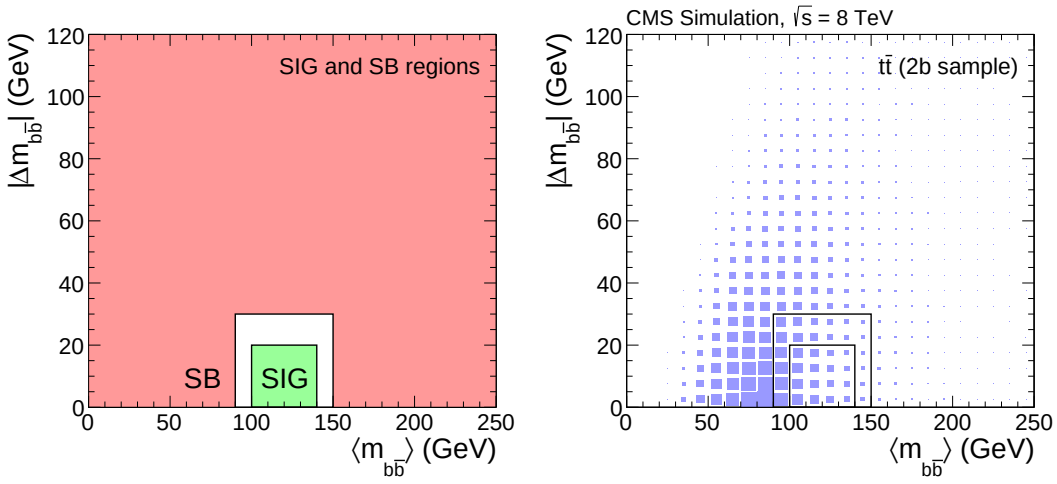

Figure 5.3: The signal (SIG) and sideband regions (SB) defined visually (left) and event density plot for the signal (SIG) and sideband regions (SB) the 2b sample (right) (9).

With the SIG and SB regions defined and determined for each sample, we can further subdivide the events in the 2b, 3b, and 4b samples into bins of S_{MET}: 30-50, 50-100, 100-150, and > 150. A likelihood function is determined for the background in each S_{MET} bin. The results of the experiment for the 3b and 4b sample are shown in figure 5.4. The results show a slight excess in the 3rd bin of the 4b sample. Plotted against the background is the signal for higgsino mass 250 and 400 GeV respectively. This is the expected mass region of sensitivity that the analysis can exclude. As expected, the signal populates the 50-100 S_{MET} bin mostly due to the significant MET carried away by the LSP (10).

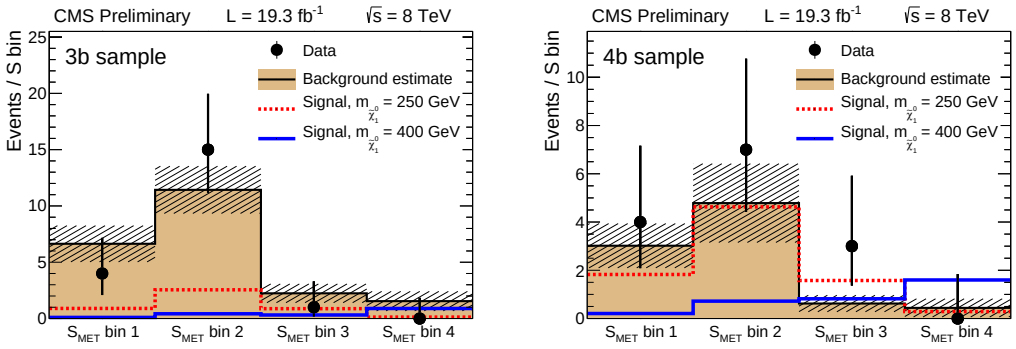

Figure 5.4: Results of analysis of the 3b sample (left) and results of analysis of the 4b sample (right). A slight excess can be seen in the third S_{MET} bin (9).

5.1.2 hh $\rightarrow \gamma\gamma$bb

The $\gamma\gamma$bb search channel is a difficult one to probe at the current luminosity and center-of-mass energy of the data we use. This is because the Higgs branching fraction to di-photons is approximately 0.2%. The background in these channels, however, is very small and clean, so it is an excellent discovery channel with enough data. To optimize the search for this signal, we require the following:

- Two photons with at least $p_T > 40$ and $p_T > 25$ respectively, and $\eta < 1.4442$
- $120 < m_{\gamma\gamma} < 131$GeV, where the invariant mass is of photons with the highest p_T values in the event
- Exactly two b-tagged jets with $p_T > 30$GeV and $\eta < 2.4$ using the CSV medium criteria
- $95 < m_{bb} < 155$GeV
- No identified nor isolated leptons with $p_T > 50$GeV and $\eta < 2.4$, where the isolation requirement is $I_{rel} < 0.15, 0.12$ for electrons and muons respectively

That takes care of the optimization. To estimate the background in the search channel, three regions of the $m_{\gamma\gamma}$ distribution are selected: two sideband regions and a signal region. The lower side band region is from 103 to 118 GeV, and the upper side-band region is from 133 to 163 GeV. The signal region is 118 to 133 GeV, where we expect the Higgs boson from higgsinos to land. A power law is used to fit the lower and upper sideband regions simultaneously. The function is continued through the signal region, but not fit for the signal region itself. Scale factors are then derived from the fit. The ratio of the number of events in the signal region to the sideband regions individually yields two separate scale factors that are used as I will describe in a moment.

We now choose a variable called Higgs S_T, or S_T^H for short. It is defined as the scalar sum of the transverse moment of the Higgs boson candidates, or the scalar sum of the two photon p_T's and the two b-jet p_T's. This distribution is plotted for both of the side-band regions. Using the scale factors from the power law fit, the two distributions are then scaled by their respective factors, and give an estimate of how many background events one would get in the signal region of an S_T^H distribution. Taking the average of the two distributions then yields the final result for the background in this variable. The SM Higgs background is incorporated using simulation and is added in after this procedure. In figures 5.5 and 5.6, you can see the power law fit for the di-photon invariant mass distribution and the results of the experiment respectively. The analysis is most sensitive to a low higgsino mass, but there is no deviation from the SM background.

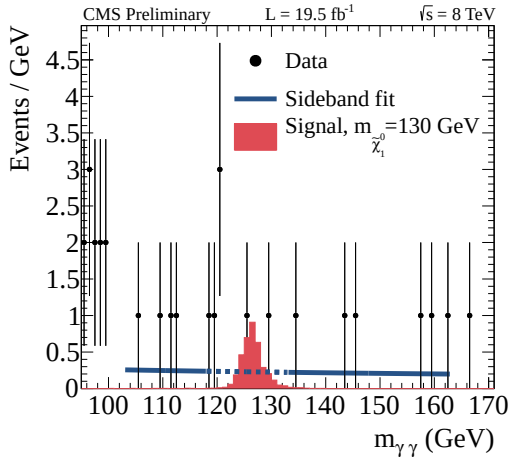

Figure 5.5: Result of the power law fit for the events in the side-band of the $m_{\gamma\gamma}$ window (9).

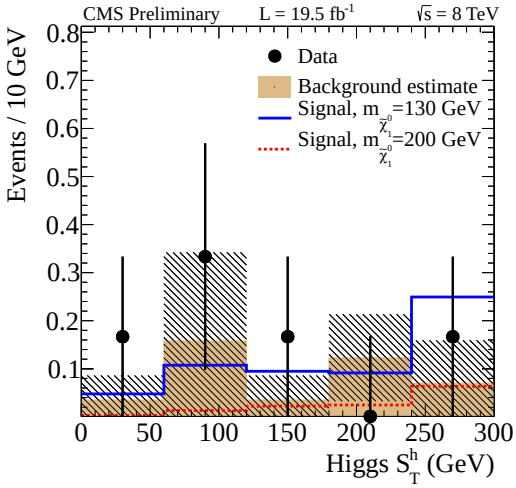

Figure 5.6: Experimental results of the $\gamma\gamma$bb search as a function of S_T^H. Data is in good agreement with the SM background (9).

5.1.3 hh $\rightarrow \gamma\gamma + l$

This analysis is very similar to the search for $\gamma\gamma$bb, in that the requirements for the photon are identical. The main difference is that we require there to be at least one electron or muon candidate in each event. But the isolation and id requirements are inverted since now we look for events with leptons in them. The b-tagged enforcement is relaxed for obvious reasons, but at most one b-tagged jet is allowed so as to not overlap with other analyses in the combination.

The one additional requirement is that the ΔR cut between an electron or muon and each of the photon candidates be larger than 0.3. Beyond that, the background estimation method is similar, only instead of using S_T^H, we use m_T which is defined as:

$$m_T = 2 * MET * p_{T_l} * [1 - \cos(\Delta\Phi_{l,MET})] \tag{5.3}$$

Here, p_{T_l} is the transverse momentum of the lepton, and $\Delta\Phi_{l,MET}$ is the cross sectional angle between the p_{T_l} and MET vectors. The main background in this channel is from $\gamma + Z \rightarrow \gamma l^+ l^-$ events, where one of the leptons is misidentified as a photon. To reduce this background, the invariant mass of one of the photons and the lepton is formed, and if it falls within the Z-peak, it is thrown away. The rest of the background comes from SM Higgs processes, which are small in cross section.

The method of estimating the non-Higgs SM background is exactly the same as defined in subsection 5.1.2, except the m_T variable is used. One can see the fit to the invariant mass of the $m_{\gamma\gamma}$ and the corresponding distributions in m_T in which the side-band backgrounds have been scaled to the functional fit that passes through the signal region in figure 5.7.

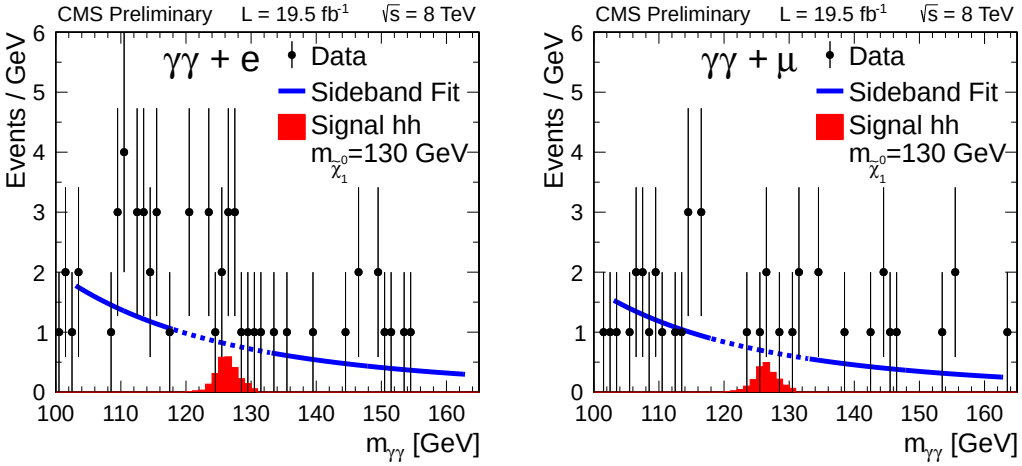

Figure 5.7: Result of the power law fit for the events in the side-band of the $m_{\gamma\gamma}$ window for events with one electron (left) and one muon (right) (9).

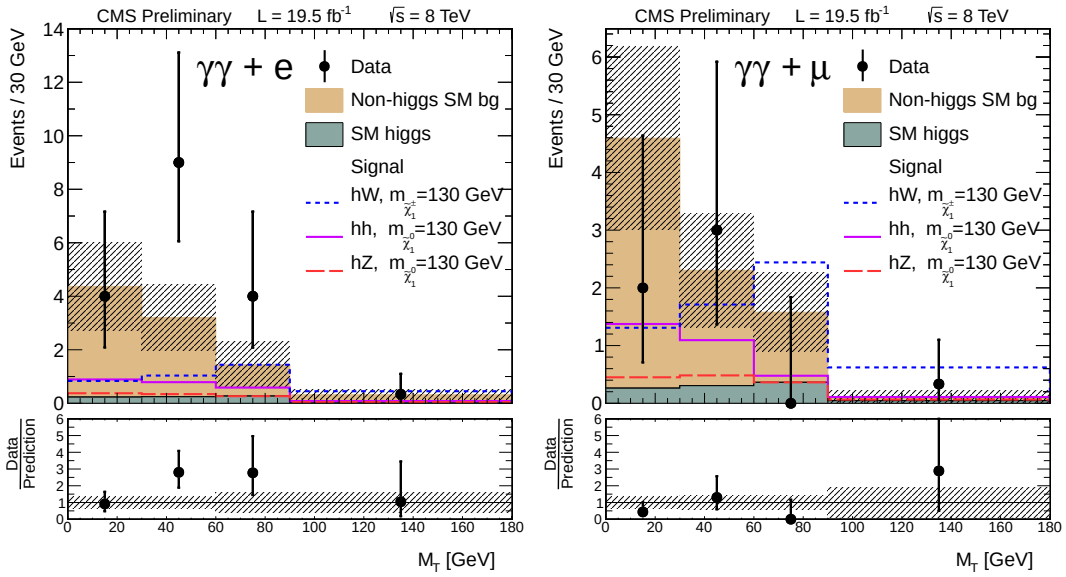

Figure 5.8: Experimental results of the $\gamma\gamma$+e (left) and $\gamma\gamma + \mu$ search as a function of M_T. A slight excess in 30< M_T <60 is observed in the elctron search. (9)

5.2 hZ Topology

We now turn the focus on to the mixed topology of hZ events, which, by themselves are unphysical. Two analyses other than multileptons focus their efforts in this topology.

5.2.1 hZ → 2b2l

This analysis optimizes for the Higgs boson decaying to two b-jets, and the Z boson decaying leptonically. The requirements for these final state objects are:

- electrons and muons must have $p_T > 20$ GeV, $\eta < 2.4$, and an I_{rel} <0.15 for a cone size of 0.3.
- one OSSF lepton pair on the Z-mass peak between 81 and 101 GeV
- no additional leptons as defined by the first bullet, but using $p_T > 10$ GeV as the cut-off
- jets must have $p_T > 30GeV, \eta < 2.5$, and a minimum $\Delta R = 0.4$ between the jet and lepton candidates
- at least 2 b-jets, where the invariant mass of the most b-like jet is between 100 and 150 GeV
- no hadronic taus with $p_T > 20GeV$

The no additional lepton requirement is so that the search does not overap with the multilepton search in the hZ topology. Electron candidates with η between 1.4442 and 1.566 are rejected due to

detector reconstruction efficiencies being low in the region. All b-tagged jets use the CSV medium criteria.

Once these cuts are in place, a significant background comes from semi-leptonic $t\bar{t}$ decay. To this end, the analysts invent a variable called M_{T2}^{j}, which is defined as the vector sum of the b-tagged jet p_T, the lepton p_T, and the MET from the neutrino, all of which are coming from the leptonic top quark decay. If the detector were ideal, the M_{T2}^{j} variable would have a cutoff at the top quark mass of 175 GeV. Because of detector misreconstruction, we put the cutoff at 200 GeV. Taking events above this threshold significantly reduces the semi-leptonic $t\bar{t}$ background. An additional cut of MET $> 60, 80, or 100$ GeV is used depending on which gives the greatest signal yield for each mass point.

Once the cut is made on M_{T2}^{j}, the main backgrounds that play a role are Z+jets, $t\bar{t}$ (fully leptonic), WW, and di-tau. Data driven methods are used for these background estimations. Since a MET cut is used in the analysis, Z+jets simulation faces a problem in that often the MET is not reconstructed correctly in the tails. To estimate the Z+jets background, then, the analysts use a γ+jets data sample. The idea is to use this background as a template for the Z+jets. One makes distributions of H_T and boson p_T, and reweights the γ+jets sample to match that of the Z+jets sample. Then, one makes the MET distribution of the γ+jets sample, and normalizes it to unity. One further sub-divides this distribution into a portion that contains events with exactly two b-tagged jets, and another that contains events with more than two b-tagged jets. The same sub-division is done for the Z+jets MET distribution. Finally, one weighs each of the γ+jets templates by the corresponding number of events in the Z+jets MET distribution.

The second main source of background comes from $t\bar{t}$ (fully leptonic), WW, and di-tau events. These processes can yield both OSSF and OSOF pairs. For instance, WW can yield an $e^{-}e^{+}$ or an $e^{-}\mu^{+}$ event. The rate of production for these types of events is identical once electron and muon reconstruction efficiencies are applied. Since the events are treated equally amongst flavor, the analysts refer to it as flavor symmetric background, or FS. To estimate the FS background, we use data sample triggered on one electron and one muon, and apply all the same leptonic cuts in the list above, but removing the Z-mass peak for the invariant mass. Instead, we use a scale factor from simulation that gives the probability for an $e\mu$ event to have an invariant mass on the Z. This scale factor is then applied to the number of events that pass the cuts.

Rarer processes like ZW, ZZ, ttV, and VVV are also included, and simulation is used for these. In figures 5.9 and 5.10, one can see the effect of the Z+jets and the FS background estimation methods respectively. In the left plots, a requirement that there be no b-tagged jets is present to reduce $t\bar{t}$ and have Z+jets dominate. The right plot enforces the $M_{T2}^{j} < 200$ GeV, so that $t\bar{t}$ events

prevail, and thus the FS background dominate.

Of course, these are control region plots. To see the results within the scope of the signal, see figure 5.11 and the table below.

5.3 ZZ Topology

We add further sensitivity to our searches by adding an analysis that searches in the ZZ final state of the Higgsino NLSP cascade (18). This analysis focuses on a leptonic and hadronic final state of ZZ decays, i.e. $Z \to l^+l^-$ and $Z \to jj$. The analysis selects events with exactly one e^+e^- or $\mu^+\mu^-$ pair, and no other leptons in the event. We also require the presence of at least two jets, none of which can be tagged as coming from a b-quark. The invariant mass of the lepton pair and the jet pair with the highest p_T must be on the Z-mass window.

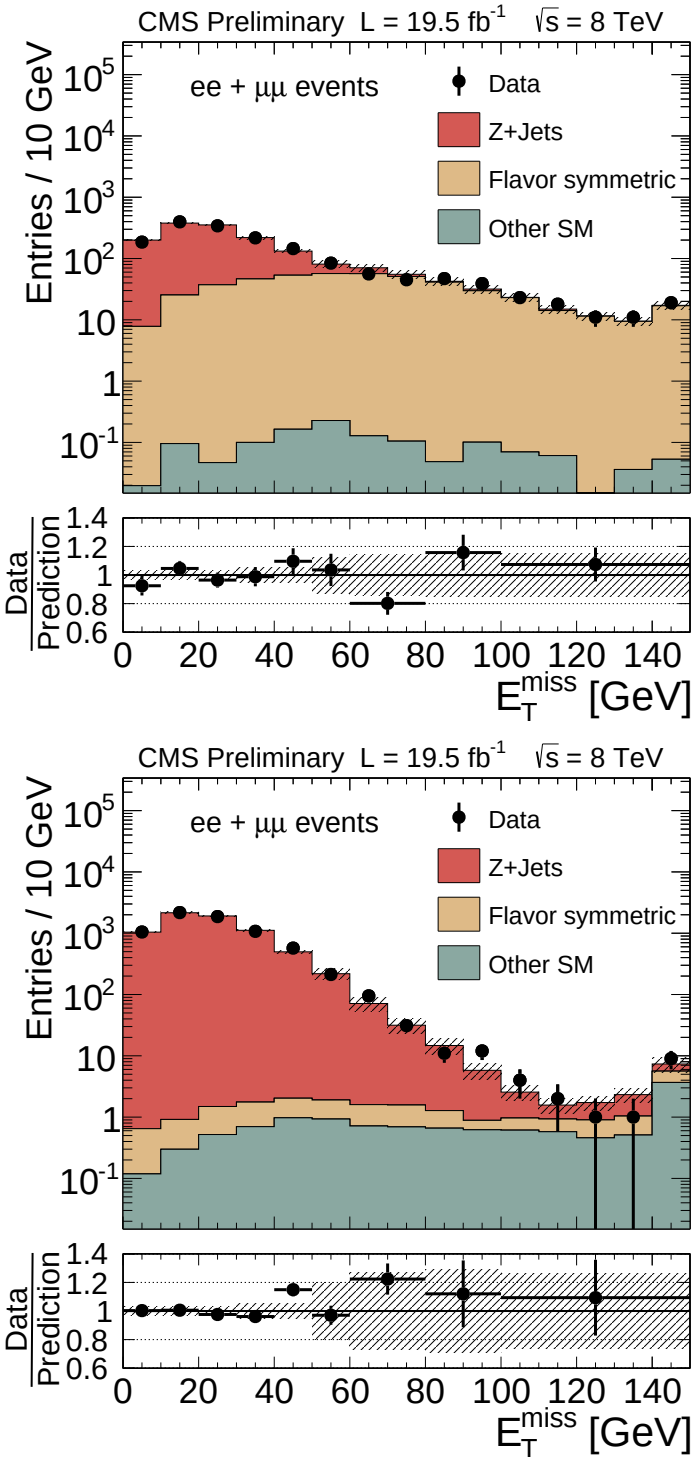

Figure 5.9: Control region plot for Z+jets dominated background in the 2b2l analysis (top) and control region plot for flavor symmetric dominated background in the 2b2l analysis (bottom) (9).

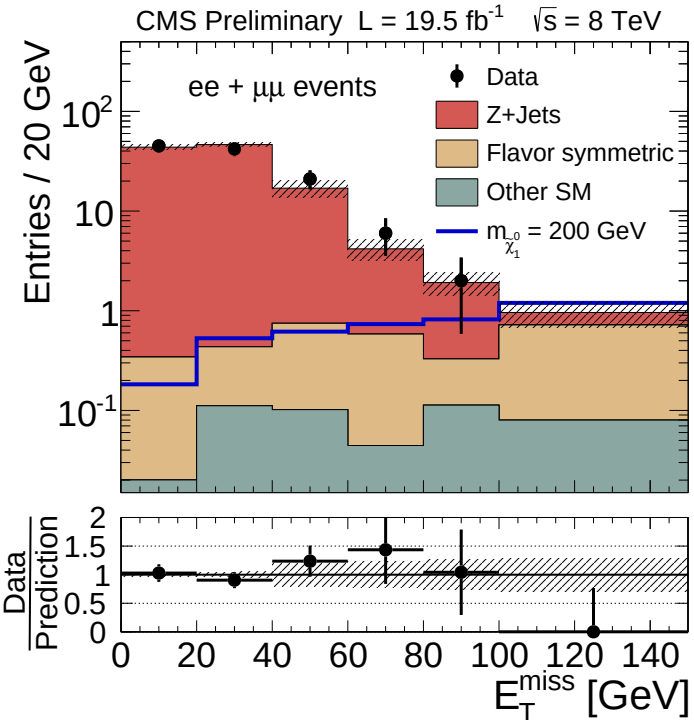

Figure 5.10: Experimental results of the 2b2l analysis with Higgsino 200 GeV overlayed (9).

	$E_{\mathrm{T}}^{\mathrm{miss}} < 25\,\mathrm{GeV}$	$25 < E_{\mathrm{T}}^{\mathrm{miss}} < 50\,\mathrm{GeV}$	$50 < E_{\mathrm{T}}^{\mathrm{miss}} < 60\,\mathrm{GeV}$
Z+jets bkg	56.7 ± 1.9	43.3 ± 2.3	5.7 ± 1.2
Flavor symmetric	0.4 ± 0.3	0.4 ± 0.3	0.4 ± 0.3
Other SM bkg	< 0.1	0.1 ± 0.1	0.1 ± 0.1
Total SM bkg	57.2 ± 1.9	43.8 ± 2.3	6.2 ± 1.2
Data	54	47	7
	$E_{\mathrm{T}}^{\mathrm{miss}} > 60\,\mathrm{GeV}$	$E_{\mathrm{T}}^{\mathrm{miss}} > 80\,\mathrm{GeV}$	$E_{\mathrm{T}}^{\mathrm{miss}} > 100\,\mathrm{GeV}$
Z+jets bkg	5.7 ± 1.8	2.2 ± 0.9	0.6 ± 0.3
Flavor symmetric	2.4 ± 0.9	1.8 ± 0.7	1.6 ± 0.6
Other SM bkg	0.3 ± 0.2	0.3 ± 0.2	0.2 ± 0.1
Total SM bkg	8.5 ± 2.0	4.3 ± 1.2	2.4 ± 0.7
Data	8	2	0
hZ events			
$m_{\tilde{\chi}_1^0} = 130\,\mathrm{GeV}$	5.4 ± 0.1	3.1 ± 0.1	1.7 ± 0.1
$m_{\tilde{\chi}_1^0} = 150\,\mathrm{GeV}$	5.3 ± 0.1	3.3 ± 0.1	2.0 ± 0.1
$m_{\tilde{\chi}_1^0} = 200\,\mathrm{GeV}$	4.7 ± 0.1	4.2 ± 0.1	3.3 ± 0.1
$m_{\tilde{\chi}_1^0} = 250\,\mathrm{GeV}$	3.5 ± 0.1	3.2 ± 0.1	2.8 ± 0.1

Figure 5.11: Results of the 2b2l analysis in table format. At each mass point, we choose the channel with the greatest sensitivity (9).

Chapter 6
Statistical Methods

6.1 Limit Setting

The results of each analysis is that there is no significant deviation from the SM. We therefore turn to what can be done in such a case, and that is setting limits on the parameter space of the Higgsino NLSP model. For this, we must understand how to expound on the idea of a confidence limit and an r-value.

6.1.1 A Simple Example

The simplest way to explain how to statistically quantify the results of our analysis is to present an example. Suppose in the multilepton analysis, a particular channel has 10 observed events, 9 background events, and 1 signal event. For this example, I will disregard the statistical and systematic uncertainties that are usually tacked on to such numbers. One could ask the following question: what is the probability that 9 background events could fluctuate up to 10 events? In other words, how significant is the fact that we observed 10 events, and predicted 9? If we do a back of the envelope calculation, we will take the square root of the background, and allow that to serve as a 1 sigma deviation away from the mean, i.e. 9. We will use this naive measure as a zeroth order approximation of the statistical significance of the result:

$$\sigma = \frac{Observed - Expected}{\sqrt{Expected}} \tag{6.1}$$

In our crude formula, the value of σ is 0.33. This does not even correspond to being outside the width of a gaussian that is centered at 9 and has a width of 3. This is not a very significant deviation from the norm. A better approximation can be made by using the standard Poisson distribution. Mathematically, the Poisson distribution is:

$$P(n) = \frac{e^{-\lambda}\lambda^n}{n!} \tag{6.2}$$

where n is the observed value, and λ is the expected value. Therefore, P(n) is the likelihood of

observing 10 events in a channel where we expect 9 events. Plugging in the value, P(10) = 11.8%. The value is, again, not very significant, as a value less than around 5% would cause some bells to go off.

We can input the signal, and ask, how significant is a measurement of 10 when considering the SM background and the signal together? Our naive approximation gives a value of $\sigma = 0$. From the Poisson distribution, we obtain a value of 12.5%, i.e. it is not very significant. But from the σ value and Poisson calculation, we can see that it's at least a little more likely that a signal of 1 event rather than 0 events appear in the channel.

Let's reverse the situation and consider a channel in which we observe 10 events, predict 1 from the SM, and 9 signal events. How significant is this finding? Neglecting the signal for a moment, we get from the crude approximation $\sigma = 9$. That is certainly a rare channel! In terms of Poisson, we would expect to get these numbers 0.00001% of the time. That is incredibly unlikely, and is 5 orders of magnitude smaller than the 5% that would be cause for discovery. If we take into account the signal, we get $\sigma = 0$, and from the Poisson distribution, 12.5%, just as in the reverse case! What is this telling us?

What the statistics is saying is that, without a signal, it is incredibly unlikely that one would observe 10 events when the prediction is 1. However, if we include the signal, we can see that it would be very ordinary to get a value of 9 events. The interpretation is to say, that this signal, or model, is what is explaining the discrepancy between the observed and the expected values. A channel such as this one is truly a discovery channel.

In general, an experiment will not always have only one channel. The multileptons analysis has 196 channels, for instance. As we will see, the Poisson distribution is integral in understanding the statistical significance of analyses with much more complicated results.

6.1.2 CLs and CLsb

To compute statistical significance for analyses of CMS data, the usual format is to use CLs limits. We can begin by describing the method for a single channel, and move to analyses that have multiple, independent channels. The Poisson equation we used before needs to be slightly modified so we can build up a Poisson distribution to get probabilities for any number of observed events given a particular background and signal prediction. This is done by simply taking a summation in the following way:

$$\frac{\sum_{n=0}^{n_{obs}} \frac{e^{-(b+s)}(b+s)^n}{n!}}{\sum_{n=0}^{n_{obs}} \frac{e^{-b}b^n}{n!}} \tag{6.3}$$

This ratio is known as CL_s (21), which is the total probability of observing all values of $n \leq n_{obs}$ with a signal, divided by the total probability of observing all values of of $n \leq n_{obs}$ without signal. This ratio is a little difficult to understand, so I will talk about the numerator and denominator separately, and make analogies to the so called p-value. This will help elucidate this equation.

The denominator of the equation is known as CL_b, because it has only the background included in the summation. If one imagines a probability distribution like the one pictured in figure 6.1, we can safely say that the peak of the distribution is the most likely value to be observed in an experiment. It serves as the mean of the distribution, and if there were no new physics to be observed, then getting an observation that is very close to the mean would be very normal. In statistics terminology, this is known as support for the null hypothesis, meaning nothing new. Now, imagine obtaining an observed value that is far from the mean of the distribution, i.e. very unlikely. If we take the area under the distribution from that observed value to infinity, the answer would be very small indeed. This is known as a p-value. Assuming the distribution is normalized to unity, as it needs to be for a probability function, a p-value close to 1 would be evidence in favor of the null hypothesis, and a p-value closer to zero would be evidence against the null hypothesis. In other words, a p-value closer to 1 is telling one that we should assume we were correct in what our prediction was, and a p-value closer to 0 tells us that we have an observation that is very unexpected.

The numerator of the equation is known as CL_{s+b} because it has background and signal included. Again, we can imagine an analogous distribution that has a mean value equal to the sum of the background and signal events. And again, we could compute p-values for the observation based on this distribution. But because the central value of the distribution has now been shifted due to the addition of signal, the p-values will not be the same for the two distributions.

In fact, if the observed number of events is far in the tail of both distributions, it is clearly evidence against the null hypothesis, but the p-value for the background distribution will be smaller than that of the background plus signal distribution. We can imagine a ratio:

$$\frac{p_{s+b}}{p_b} > 1 \tag{6.4}$$

The fact that the p-values are small for both distributions is strong evidence against the null, but because p_b is smaller than p_{s+b}, it is more likely that the observation would come from the signal AND background distribution, rather than the background distribution alone. So we cannot say that the signal is incorrectly modeling the observation above the background.

On the other hand, if the ratio were less than 1, this would be the reverse situation. Imagine the observation falling somewhere in between the central values of the two distributions. The p-values

are now closer to 1, so neither value is very good evidence against the null hypothesis for their respective distributions. However, the p-value for the background will be larger than p_{s+b}, which means it is more likely that the observation will come from the background distribution alone. In these cases, the ratio is smaller than 1, and we can exclude the signal.

This is roughly what an r-value is. One can loosely define it as the ratio of p_{s+b} to p_b. The reason this analogy to the hardcore definition in equation 6.3 is important is twofold. First, the equation is not very illuminating on its own and requires some explaining. Second, the definition of confidence limit is not actually equation 6.4, but:

$$CL = 1 - \frac{\sum_{n=0}^{n_{obs}} \frac{e^{-(b+s)}(b+s)^n}{n!}}{\sum_{n=0}^{n_{obs}} \frac{e^{-b}b^n}{n!}} \tag{6.5}$$

which, at first glance, is incredibly confusing. The reason for subtracting from one is because the are not summing from n_{obs} to infinity as I have in my analogy. The sum is from 0 to n_{obs}. The second term in equation 6.5 is CL_s, but it is CL that is used in setting statistical significance, and is closer to what I have loosely defined as an r-value[1].

For experiments with more than 1 channel, the technique is extended to what is known as a log likelihood ratio, or log Q. Q is essentially the same formula as equation 6.5, only with a product instead of summation sign, and now the n values are channel by channel observations. There is also a complicated weighting function attached to the Poisson distribution. For details on this procedure, see [23].

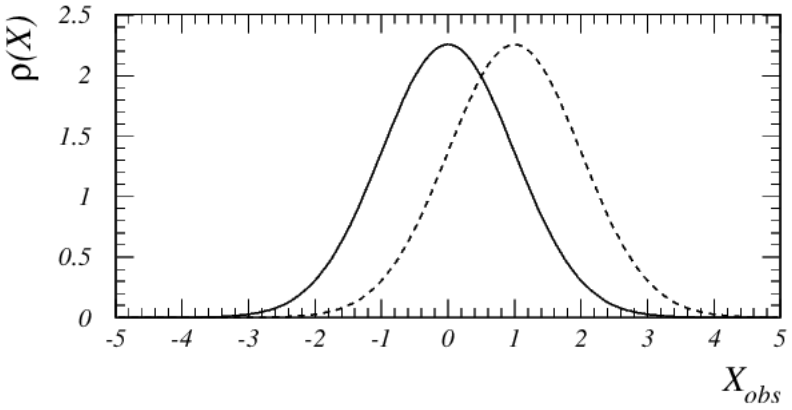

Figure 6.1: A typical Poisson distribution built from pseudoexperiments (21).

[1] r-values are NOT defined as in equation 6.5

Chapter 7
1d Results

7.1 LandS and 1d Curves

For the results of our analysis and that of the combination, we use a tool called LandS. It is a confidence level calculator that uses the distributions from the last chapter and outputs what is known as an r-value. In LandS terminology, the r-value is defined as the ratio of upper limit on the observed cross section to the theoretical cross section for a given mass point. LandS basically takes in the results of the experiment, whether they be single channel or multiple channel experiments, and then builds up a Poisson distributions using CL_s methods. The output of the software is then interpreted as the cross section ratio rather than a CL value. The idea of the r-value is still the same, however. An r-value > 1 indicates one cannot say exclude the signal point from the model, whereas an r-value < 1 indicates that the signal point cannot be describing new physics. This is all done at the 95% confidence level. I will now describe how to go from a collection of channels, to an exclusion plot, and how to interpret the plot in terms of the channels.

7.1.1 Results of the hh Topology

The hh topology of the HiggsinoNLSP model proves to be the most difficult topology to probe. The reason for this is simple. Four analyses out of the six probe this topology, two of which focus on the $\gamma\gamma$ search channel, which has an incredibly small branching fraction. The multilepton analysis suffers from Higgs branching fractions to vector bosons, and further BF's to leptons, significantly decreasing the number of signal events available. The 4b analysis has the greatest sensitivity in this topology, but it is still a tricky analysis and has low number of events in the channels.

multilepton

As described in chapter three, the multilepton search concentrates on seven possible hh decay modes. They are two Higgs bosons decaying to four W's, four Z's, two W and Z bosons, four τ's, two Z and τ's, two W and τ's, and two Z and b-jets. Because we have seven processes in our signal results, it is important to weigh each decay mode properly. One cannot simply take the raw events from the

signal model and add them together. Just as with the background simulation, we weigh the number of raw signal events by the cross section, luminosity, branching fractions, and all lepton efficiencies. The formula used is:

$$Signal_X = \frac{\sigma * L * BF(\tilde{H} \rightarrow H + LSP)^2 * BF(h \rightarrow X) * \epsilon_{Total}}{Signal_{TOTAL}} * (Signal_{X_{RAW}}) \qquad (7.1)$$

where X represents one of the seven Higgs decays. The multilepton search results are not optimized for a hh topology, as this is strictly a re-interpretation of the results published in 2013 (7). Once this scaling procedure is done, we can add the results into a signal bin.

Since SUS-13-002 was an inclusive search (model independent), I present here the results of the experiment in tables 7.1 and 7.2.

$\geq$4 leptons	$m_{\ell^+\ell^-}$	MET	$N_{\tau_h}=0$, $N_b=0$		$N_{\tau_h}=1$, $N_b=0$		$N_{\tau_h}=0$, $N_b\geq 1$		$N_{\tau_h}=1$, $N_b\geq 1$	
$H_T > 200GeV$			Obs.	Exp.	Obs.	Exp.	Obs.	Exp.	Obs.	Exp.
OSSF0	NA	(100, ∞)	0	$0.01^{+0.03}_{-0.01}$	0	$0.01^{+0.06}_{-0.01}$	0	$0.02^{+0.04}_{-0.02}$	0	0.11 ± 0.08
OSSF0	NA	(50, 100)	0	$0.00^{+0.02}_{-0.00}$	0	$0.01^{+0.06}_{-0.01}$	0	$0.00^{+0.03}_{-0.00}$	0	0.12 ± 0.07
OSSF0	NA	(0, 50)	0	$0.00^{+0.02}_{-0.00}$	0	$0.07^{+0.10}_{-0.07}$	0	$0.00^{+0.02}_{-0.00}$	0	0.02 ± 0.02
OSSF1	Off-Z	(100, ∞)	0	$0.01^{+0.02}_{-0.01}$	1	0.25 ± 0.11	0	0.13 ± 0.08	0	0.12 ± 0.12
OSSF1	On-Z	(100, ∞)	1	0.10 ± 0.06	0	0.50 ± 0.27	0	0.42 ± 0.22	0	0.42 ± 0.19
OSSF1	Off-Z	(50, 100)	0	0.07 ± 0.06	1	0.29 ± 0.13	0	0.04 ± 0.04	0	0.23 ± 0.13
OSSF1	On-Z	(50, 100)	0	0.23 ± 0.11	1	0.70 ± 0.31	0	0.23 ± 0.13	1	0.34 ± 0.16
OSSF1	Off-Z	(0, 50)	0	$0.02^{+0.03}_{-0.02}$	0	0.27 ± 0.12	0	$0.03^{+0.04}_{-0.03}$	0	0.31 ± 0.15
OSSF1	On-Z	(0, 50)	0	0.20 ± 0.08	0	1.3 ± 0.5	0	0.06 ± 0.04	1	0.49 ± 0.19
OSSF2	Off-Z	(100, ∞)	0	$0.01^{+0.02}_{-0.01}$	NA	NA	0	$0.01^{+0.06}_{-0.01}$	NA	NA
OSSF2	On-Z	(100, ∞)	1	$0.15^{+0.16}_{-0.15}$	NA	NA	0	0.34 ± 0.18	NA	NA
OSSF2	Off-Z	(50, 100)	0	0.03 ± 0.02	NA	NA	0	0.13 ± 0.09	NA	NA
OSSF2	On-Z	(50, 100)	0	0.80 ± 0.40	NA	NA	0	0.36 ± 0.19	NA	NA
OSSF2	Off-Z	(0, 50)	1	0.27 ± 0.13	NA	NA	0	0.08 ± 0.05	NA	NA
OSSF2	On-Z	(0, 50)	5	7.4 ± 3.5	NA	NA	2	0.80 ± 0.40	NA	NA

Figure 7.1: Results of the multilepton search binning in 4 or more leptons and high H_T (7).

$\geq$4 leptons	$m_{\ell^+\ell^-}$	MET	$N_{\tau_h}=0$, $N_b=0$		$N_{\tau_h}=1$, $N_b=0$		$N_{\tau_h}=0$, $N_b\geq 1$		$N_{\tau_h}=1$, $N_b\geq 1$	
$H_T < 200GeV$		(what)	Obs.	Exp.	Obs.	Exp.	Obs.	Exp.	Obs.	Exp.
OSSF0	NA	(100, ∞)	0	0.11 ± 0.08	0	0.17 ± 0.10	0	$0.03^{+0.04}_{-0.03}$	0	0.04 ± 0.04
OSSF0	NA	(50, 100)	0	$0.01^{+0.03}_{-0.01}$	2	0.70 ± 0.33	0	$0.00^{+0.02}_{-0.00}$	0	0.28 ± 0.16
OSSF0	NA	(0, 50)	0	$0.01^{+0.02}_{-0.01}$	1	0.7 ± 0.3	0	$0.00^{+0.02}_{-0.00}$	0	0.13 ± 0.08
OSSF1	Off-Z	(100, ∞)	0	0.06 ± 0.04	3	0.60 ± 0.24	0	$0.02^{+0.04}_{-0.02}$	0	0.32 ± 0.20
OSSF1	On-Z	(100, ∞)	1	0.50 ± 0.18	2	2.5 ± 0.5	1	0.38 ± 0.20	0	0.21 ± 0.10
OSSF1	Off-Z	(50, 100)	0	0.18 ± 0.06	4	2.1 ± 0.5	0	0.16 ± 0.08	1	0.45 ± 0.24
OSSF1	On-Z	(50, 100)	2	1.2 ± 0.3	9	9.6 ± 1.6	2	0.42 ± 0.23	0	0.50 ± 0.16
OSSF1	Off-Z	(0, 50)	2	0.46 ± 0.18	15	7.5 ± 2.0	0	0.09 ± 0.06	0	0.70 ± 0.31
OSSF1	On-Z	(0, 50)	4	3.0 ± 0.8	41	40 ± 10	1	0.31 ± 0.15	2	1.50 ± 0.47
OSSF2	Off-Z	(100, ∞)	0	0.04 ± 0.03	NA	NA	0	0.05 ± 0.04	NA	NA
OSSF2	On-Z	(100, ∞)	0	0.34 ± 0.15	NA	NA	0	0.46 ± 0.25	NA	NA
OSSF2	Off-Z	(50, 100)	2	0.18 ± 0.13	NA	NA	0	$0.02^{+0.03}_{-0.02}$	NA	NA
OSSF2	On-Z	(50, 100)	4	3.9 ± 2.5	NA	NA	0	0.50 ± 0.21	NA	NA
OSSF2	Off-Z	(0, 50)	7	8.9 ± 2.4	NA	NA	1	0.23 ± 0.09	NA	NA
OSSF2	On-Z	(0, 50)	*156	160 ± 34	NA	NA	4	2.9 ± 0.8	NA	NA

Figure 7.2: Results of the multilepton search binning in 4 or more leptons and low H_T (7).

For the most part, the data is in good agreement with the SM background hypothesis. This includes the SM Higgs boson background with a mass of 126 GeV. Because there are a total of 196 search channels, the so-called look elsewhere effect can and does play a role here (15). The effect boils down to saying that because there are so many search channels, then the odds are in favor of a few of them having deviations from the SM background that are understandable from a pure statistical

3 leptons $H_T > 200GeV$	$m_{\ell^+\ell^-}$	MET	$N_{\tau_h}=0$, $N_b=0$ Obs.	Exp.	$N_{\tau_h}=1$, $N_b=0$ Obs.	Exp.	$N_{\tau_h}=0$, $N_b\geq 1$ Obs.	Exp.	$N_{\tau_h}=1$, $N_b\geq 1$ Obs.	Exp.
OSSF0	NA	(100, ∞)	5	3.7 ± 1.6	35	33 ± 14	1	5.5 ± 2.2	47	61 ± 30
OSSF0	NA	(50, 100)	3	3.5 ± 1.4	34	36 ± 16	8	7.7 ± 2.7	82	91 ± 46
OSSF0	NA	(0, 50)	4	2.1 ± 0.8	25	25 ± 10	1	3.6 ± 1.5	52	59 ± 29
OSSF1	Above-Z	(100, ∞)	5	3.6 ± 1.2	2	10.0 ± 4.8	3	4.7 ± 1.6	19	22 ± 11
OSSF1	Below-Z	(100, ∞)	7	9.7 ± 3.3	18	14.0 ± 6.4	8	9.1 ± 3.4	21	23 ± 11
OSSF1	On-Z	(100, ∞)	39	61 ± 23	17	15.0 ± 4.9	9	14.0 ± 4.4	10	12.0 ± 5.8
OSSF1	Above-Z	(50, 100)	4	5.0 ± 1.6	14	11.0 ± 5.2	6	6.8 ± 2.4	32	30 ± 15
OSSF1	Below-Z	(50, 100)	10	11.0 ± 3.8	24	19.0 ± 6.4	10	9.9 ± 3.7	25	32 ± 16
OSSF1	On-Z	(50, 100)	78	80 ± 32	70	50 ± 11	22	22.0 ± 6.3	36	24.0 ± 9.8
OSSF1	Above-Z	(0, 50)	3	7.3 ± 2.0	41	33.0 ± 8.7	4	5.3 ± 1.5	15	23 ± 11
OSSF1	Below-Z	(0, 50)	26	25.0 ± 6.8	110	86 ± 23	5	10.0 ± 2.5	24	26 ± 11
OSSF1	On-Z	(0, 50)	*135	130 ± 41	542	540 ± 160	31	32.0 ± 6.5	86	75 ± 19

Figure 7.3: Results of the multilepton search binning in 3 leptons and high H_T (7).

3 leptons $H_T < 200GeV$	$m_{\ell^+\ell^-}$	MET	$N_{\tau_h}=0$, $N_b=0$ Obs.	Exp.	$N_{\tau_h}=1$, $N_b=0$ Obs.	Exp.	$N_{\tau_h}=0$, $N_b\geq 1$ Obs.	Exp.	$N_{\tau_h}=1$, $N_b\geq 1$ Obs.	Exp.
OSSF0	NA	(100, ∞)	7	11.0 ± 4.9	101	111 ± 54	13	10.0 ± 5.3	87	119 ± 61
OSSF0	NA	(50, 100)	35	38 ± 15	406	402 ± 152	29	26 ± 13	269	298 ± 151
OSSF0	NA	(0, 50)	53	51 ± 11	910	1035 ± 255	29	23 ± 10	237	240 ± 113
OSSF1	Above-Z	(100, ∞)	18	13.0 ± 3.5	25	38 ± 18	10	6.5 ± 2.9	24	35 ± 18
OSSF1	Below-Z	(100, ∞)	21	24 ± 9	41	50 ± 25	14	20 ± 10	42	54 ± 28
OSSF1	On-Z	(100, ∞)	150	150 ± 26	39	48 ± 13	15	14.0 ± 4.8	19	23 ± 11
OSSF1	Above-Z	(50, 100)	50	46.0 ± 9.7	169	140 ± 48	20	18 ± 8	85	93 ± 47
OSSF1	Below-Z	(50, 100)	142	130 ± 27	353	360 ± 92	48	48 ± 23	140	133 ± 68
OSSF1	On-Z	(50, 100)	*773	780 ± 120	1276	1200 ± 310	56	47 ± 13	81	75 ± 32
OSSF1	Above-Z	(0, 50)	178	200 ± 35	1676	1900 ± 540	17	18.0 ± 6.7	115	94 ± 42
OSSF1	Below-Z	(0, 50)	510	560 ± 87	9939	9000 ± 2700	34	42 ± 11	226	228 ± 63
OSSF1	On-Z	(0, 50)	*3869	4100 ± 670	*50188	50000 ± 15000	*148	156 ± 24	906	925 ± 263

Figure 7.4: Results of the multilepton search binning in 3 leptons and low H_T (7).

fluctations point of view. In a search with 54 channels, one can expect that roughly $\frac{1}{100}$ channels will produce a deviation like this. A channel that falls into this category is the 4 lepton channel, with 2 OSSF pairs that have invariant mass outside the Z-window, low H_T, $50 < MET < 100$GeV, no hadronic taus, and no b-jets. The observed is 2, and the SM background is expected to be 0.18. This is by far the largest discrepancy in the experiment. However, much work has been done to show that it is in fact a statistical fluctuation, and not evidence of new physics. We do not remove this channel however, and other channels like it. As a result, these channels will produce some interesting effects in limit curves that are presented here.

Let's begin with the limit we place on the hh topology using these multileptons results. The procedure is to take our signal simulation, the HiggsinoNLSP model, and put it through the same framework as the data and SM simulation, including all the quality cuts, and bin it according to the kinematic variables already described and seen in the 4 tables. The signal is re-weighted according to equation 7.1 above. One could imagine just extending the tables by adding a signal column, for instance. The next step is to take the channels that hold 90% of the signal efficiency. The 10% remaining has such small signal that it is negligible, and processing time is sped up. The channels are then ranked according to the signal sensitivity, and organized in a text file, or datacard. This datacard is what is the input for LandS to calculate the r-value for the given mass point. The output of LandS is, as explained before, a ratio of the observed cross section to the theoretical cross section

for the given mass point, calculated to the 95% confidence level. LandS computes two r-values, one based on the actual observation, and one as if the observed was equal to the SM background. These are observed and expected r-values respectively. It also computes confidence bands. Multiplying these r-values by the theoretical cross section yields the upper limit on cross section for the mass point. Performing this procedure for all the signal mass points, we get the following plot:

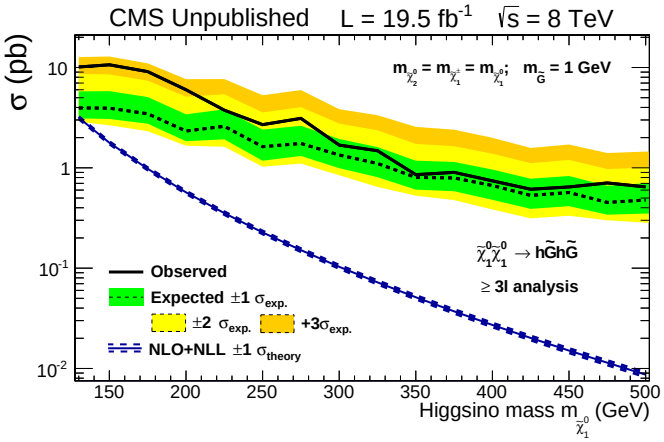

Figure 7.5: 95% C.L. Exclusion on Higgsino mass in the hh topology using the multilepton analysis. An excess is observed at low Higgsino mass (10).

Let's break this plot down piece by piece. We can start with the theoretical line, which is the easiest to understand. This is the prediction from theory to NLO+NLL. It is the cross section that would exist up to one loop, with an uncertainty placed on it at each mass point based on the uncertainty in the parton distribution functions. Nothing spectacularly difficult about this line. Next, we look at the dashed black line, which is the expected limit. Recall that an r-value is roughly like the ratio of p-values. Now, instead of using the observed value for a given channel, use the SM background for the value of n_{obs} in the analogy I made for p-values. Since now the number of observed events is equivalent to the prediction, the p-value will be larger for the background distribution than for the signal + background distribution. The larger the value of the signal, the farther the s+b distribution will shift, and the lower the ratio will be. Thus, if there is no new physics (which is equivalent to setting the observed to the background) for this mass point, the r-value will tend to be smaller and smaller as the signal gets larger and larger. Channels where the signal is very large will contribute to driving the r-value smaller. Now, since LandS outputs an r-value in terms of $\frac{\sigma_{obs}}{\sigma_{theory}}$, one simply multiplies by the theory cross section to get the expected cross section, i.e. the dashed black line. The lower the line, the more confident we are that the signal can be excluded based on expectations that there is NO new physics. When the expected line crosses the blue line and goes below it, the r-value has has now plunged below 1, and we can say that we expect that

this point can be excluded.

So in figure 7.5, we can see the multileptons analysis is most sensitive at the low end of the higgsino mass spectrum, since this is where the expected almost crosses the theory line for the first time. But because it never crosses in this range, we should not expect to exclude any of the mass points using this analysis for this topology. The other reason that the line gets so close to the theory line for low mass, is because this is where the theoretical cross section is largest. It is easier to create a low energy state than a high energy state, since the Feynman rule for intermediate higgsino production goes as $\frac{1}{E}$.

The observed line is then, just an extension of the logic used to describe the expected line. When you calculate the r-values for this line, you use the actual number of observed events in the channel. But the interpretation is the same: an r-value < 1 indicates the experiment favors no new physics beyond the SM background, and the point can be ruled out if it crosses the theory line. An r-value > 1 indicates that there might be new physics here, and that the signal hypothesis is more likely, and cannot be ruled out.

For low values of the higgsino mass, it is clear that the observed line is farther from the theory line than the expected line. This is where the colored bands become useful. Take mass point 150 GeV, for instance. It is clear that the experiment for this mass point has some channels in which the observed number of events is significantly different from the background, and that there is not enough signal to rule out the model. How significant is it? From the bands, one can see that the 150 GeV point has an observed cross section that is statistically almost +3 sigma above the expected value. Is this evidence for new physics? What about the signal? Does this mean that the model is correct, and explaining the divergence from what we would consider no new physics, i.e. the expected line?

The answer to both questions is, not necessarily. First, particle physics is very conservative in what it calls a discovery. It is certainly noteworthy, but falls short of the 5 sigma excess that is needed. Even a 5 sigma excess, however, would not be cause to claim victory. Recall the look else-where effect. One would have to see this type of excess happening in more than a few channels, and probably would have to be verified in more than one experiment.

Still, we need to examine why the observation is far enough into the 2 sigma territory. It is not the first time that an excess has appeared in an interpretation of a model using the multilepton analysis. In SUS-13-002, we set a limit on a model called stauNLSP. In the exclusion plot of the stau vs smuon mass plane, an excess of +3.1 σ presented itself at the point (150,50) GeV. This is the largest excess in that exclusion plot. The paper goes into depth about the excess and concludes that it is the result of statistical fluctuations. In table 7.1, I have listed the top 10 most sensitive

channels of the analysis using the (150,50) GeV point of the stauNLSP scenario.

N_ℓ	Selection	$m_{\ell\ell}$	E_T^{miss} [GeV]	N_τ	data	background	signal
4	OSSF1 $H_T < 200$	Off-Z	(50,100)	1	4	2.1 ± 0.5	4.56 ± 0.99
4	OSSF1 $H_T < 200$	Off-Z	(0,50)	0	2	0.46 ± 0.18	2.46 ± 0.60
4	OSSF1 $H_T < 200$	Off-Z	(50,100)	0	0	0.18 ± 0.06	1.99 ± 0.60
4	OSSF1 $H_T < 200$	Off-Z	(0,50)	1	15	7.5 ± 2.0	3.96 ± 0.97
3	OSSF1 $H_T < 200$	Above-Z	(50,100)	0	50	46.0 ± 9.7	4.87 ± 1.00
4	OSSF1 $H_T < 200$	On-Z	(50,100)	0	2	1.2 ± 0.3	1.00 ± 0.30
4	OSSF2 $H_T < 200$	Off-Z	(50,100)	0	2	0.18 ± 0.13	0.74 ± 0.28
3	OSSF1 $H_T < 200$	Below-Z	(50,100)	0	142	130 ± 27	6.1 ± 1.2
4	OSSF1 $H_T < 200$	On-Z	(50,100)	1	9	9.6 ± 1.6	1.53 ± 0.41
3	OSSF1 $H_T < 200$	Above-Z	(50,100)	1	169	140 ± 48	4.91 ± 0.88

Table 7.1: The ten most sensitive channels for the (150,50) GeV (smuon,stau) point in the stauNLSP in decreasing order of sensitivity. All channels have 0 b-tagged jets (9).

The channels that are the most discrepant in this top 10 list are the channels with (data,bkg) : (4,2.1), (2,0.46), (15,7.5), and (2,0.18). When we look at the top 10 most sensitive channels of the re-interpretation of the paper using the hh topology of the HiggsinoNLSP model, we have the following:

N_ℓ	Selection	$m_{\ell\ell}$	E_T^{miss} [GeV]	N_τ	data	background	signal
3	OSSF1 $H_T < 200$	Below-Z	(50,100)	0	142	130 ± 27	7.4 ± 1.6
3	OSSF0 $H_T < 200$	NA	(50,100)	0	35	38 ± 15	2.68 ± 0.60
3	OSSF0 $H_T < 200$	NA	(0,50)	0	53	51 ± 11	3.05 ± 0.64
4	OSSF1 $H_T < 200$	Off-Z	(50,100)	0	0	0.18 ± 0.06	0.45 ± 0.17
4	OSSF1 $H_T < 200$	Off-Z	(50,100)	1	4	2.1 ± 0.5	0.69 ± 0.19
3	OSSF0 $H_T < 200$	NA	(50,100)	1	406	402 ± 152	8.0 ± 1.4
4	OSSF1 $H_T < 200$	Off-Z	(0,50)	1	15	7.5 ± 2.0	0.85 ± 0.20
4	OSSF0 $H_T < 200$	NA	(0,50)	1	1	0.7 ± 0.3	0.30 ± 0.11
4	OSSF2 $H_T < 200$	Off-Z	(50,100)	0	2	0.18 ± 0.13	0.23 ± 0.12
3	OSSF1 $H_T < 200$	Above-Z	(50,100)	0	50	46.0 ± 9.7	1.10 ± 0.24

Table 7.2: The ten most sensitive channels for a 150 GeV higgsino and BF($NLSP \to h + LSP = 1.0$) in decreasing order of sensitivity. All channels have 0 b-tagged jets (9).

The three most discrepant channels in this table are (data,bkg) : (4,2.1), (15,7.5), and (2,0.18). These same three channels are a subset of the four most discrepant channels in the stauNLSP scenario. The fact that the excess for the 150 GeV higgsino is less than the stauNLSP excess is clear now. The channels driving the excess in the HiggsinoNLSP scenario are the same channels (minus one) driving the stauNLSP scenario. These discrepant channels also appear further down the list in table 7.2 as they do in table 7.1. To drive the point home, we include a figure mapping the most discrepant channels from one top 10 sensitivity table (HiggsinoNLSP) to another (stauNLSP).

So, we can see that this is not sufficient evidence of new physics afterall, but additionally, there is not enough signal to rule out the mass point from the multilepton analysis. Recall that a good

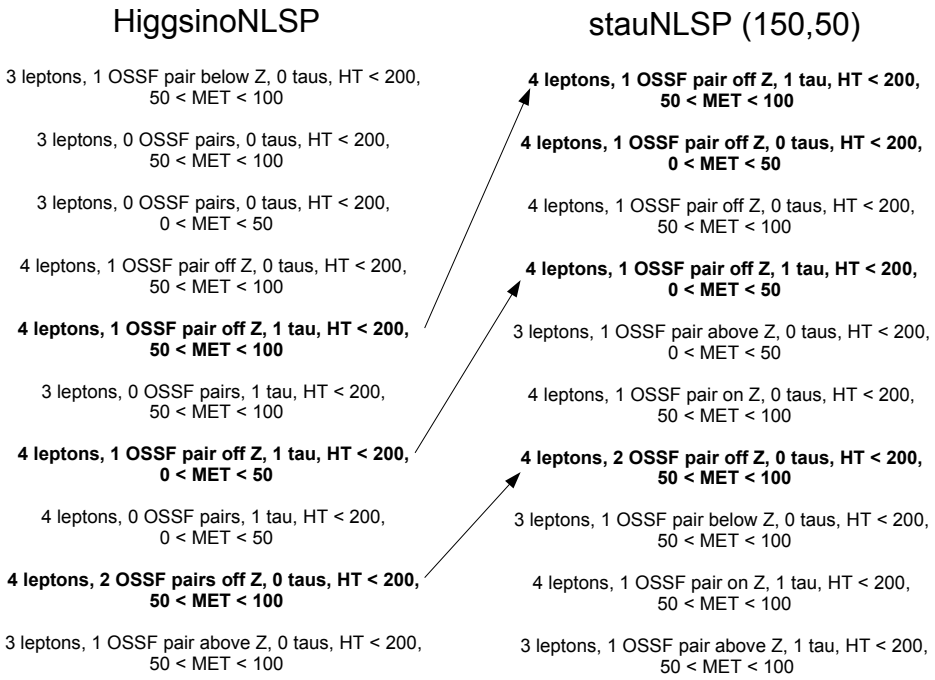

Figure 7.6: A mapping of discrepant channels from the HiggsinoNLSP 150 GeV top 10 sensitivity list to the stauNLSP (150,50) GeV top 10 sensitivity list (10).

indicator would be if there was a large discrepancy (as we see) AND that the signal is large, large enough to fill the gap between observed and expected without going over.

Another feature of the plot is the apparent jaggedness. This is present simply because the mass points are discrete, and the cross section can vary as the channels that are sensitive can be re-arranged from point to point. The trend of the plot makes sense overall though, decreasing sensitivity as higgsino mass rises due to smaller and smaller cross sections, while the observed and expected lines remain roughly flat because the r-value is increasing monotonically due to lack of signal sensitivity.

4b, and Combined

Next, I present the results of the 4b analysis for the entire higgsino mass spectrum. The analysis is not sensitive to higgsino masses below 175 GeV, so we do not plot the limits as they diverge and are superfluous based on the context of the plot for higher masses.

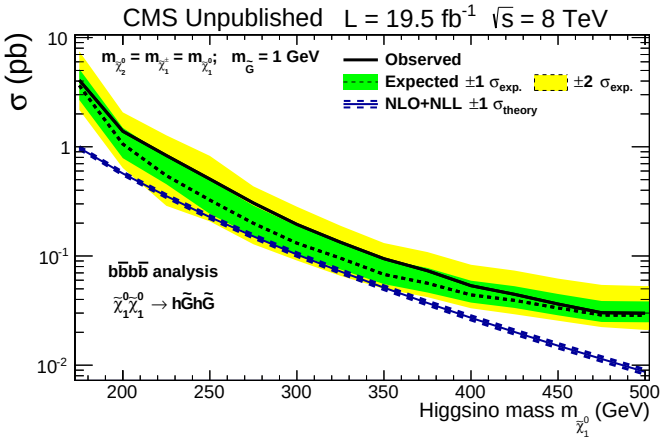

Figure 7.7: 95% C.L. Exclusion on Higgsino mass in the hh topology using the 4b analysis (10).

From figure 5.6, we can see there is a slight excess in the third S_{MET} bin, but not enough to cause large discrepancies in the observed and expected curves. The analysis' most sensitive region is between 250 and 350 GeV. It picks up most of the signal at 250 GeV, and then as the higgsino mass rises, the MET of the LSP gets larger, which gets picked up in the fourth S_{MET} bin. This explains the sort of bowed shape in the limit. The observed is in good agreement, however. Outside this region, the limits begin to diverge because of lack of sensitivity to the model due to the cuts of the analysis.

A reasonable thing to do, at this point, is to ask if we combine both analyses, can any additional limit setting power be gained? The answer is not always clear, since there is slight excess in both analyses. In general, if the two analyses are othogonal, i.e. no overlapping cuts, channels, etc., then

the expected limits MUST get better. One can think of adding r-values like one adds resistors in parallel. Since there are no discrepancies when doing expected limits, this is roughly the case, and a combined expected limit will be better. For observed limits, the answer is not as clear cut. If there is discrepancy in only one of the analyses, then yes, the r-value for observed will be better, but if there is excess in both experiments, then it could get worse. Knowing when to add an analysis can be tricky in this sense. Since the 4b analysis in general has a better sensitivity to the model, it makes sense to add their analysis with multileptons. This can be seen below:

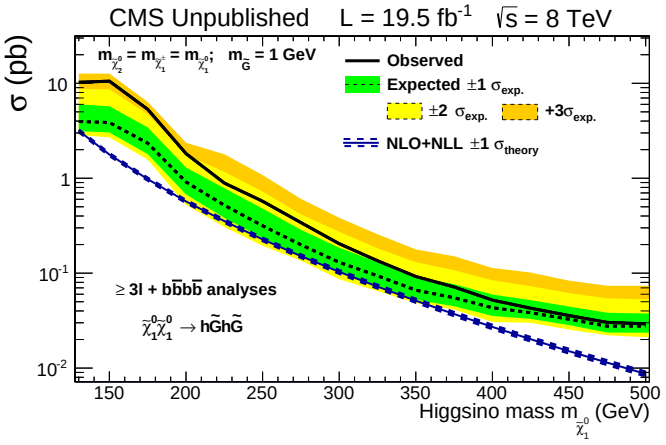

Figure 7.8: 95% C.L. Exclusion on Higgsino mass in the hh topology using the combination of the multilepton and 4b analyses (10).

As you can see, the expected curve between 250 and 350 GeV does get slightly better. The low end of the higgsino mass is still dominated by the multileptons, since we do not have sensitivity below 175 GeV for 4b. This means the excess at 150 GeV is still purely coming from multileptons. Above the 175 GeV mass threshold, the limit is set mostly from the 4b analysis. The combination comes very close to setting an expected limit. The hh topology is truly a difficult one to probe, as two analyses together are still just shy of setting a limit. We shall see if adding the other analyses that probe hh can add anything further.

One aspect of the combination that must be addressed is how to correlate the systematic uncertainties amongst the various experiments. We choose to correlate the luminosity, jet energy scale, and initial state radiation systematic uncertainties amongst the analyses. All other systematics are treated independently. The way to do this is to simply have a common name for the systematic throughout the datacards. For these three variables, we use LUMI, JES, and ISR.

$\gamma\gamma$bb

The results of the $\gamma\gamma$ bb experiment were that no deviations above the standard model were seen in the observations. Thus, we expect a limit where the observed limit is tightly bound near the expected limit. It is also treated slightly differently by LandS, because of the use of a fit function to predict the SM background beneath the Higgs peak. Feeding a datacard with channels into LandS gives a set of results, but using the fit information can actually improve the limits. This is exactly what we do in this case. Using the fit functions is also relatively easy, and only requires an additional line in the datacard to include the information. The resulting limit is seen in figure 7.9:

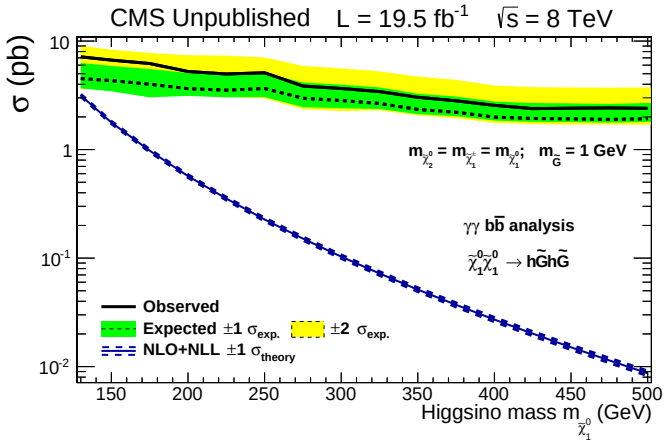

Figure 7.9: 95% C.L. Exclusion on Higgsino mass in the hh topology using the 2a2b analysis (10).

The greatest sensitivity is at the lowest higgsino mass value of 130 GeV. In this sense it is much like the multilepton result, only without the excess. The plot is also almost completely flat as a function of higgsino mass. This is, again, because the theoretical cross section drops proportionally to the rise in r-value, and the S_T^H variable does not pick up any additional signal at some large higgsino mass value. The experiment is one channel only. The Higgs becomes more boosted for larger values of higgsino mass, which will in general lead to larger values of S_T^H, but because the efficacy of the background method is independent of the value, the r-value and theory cross section increase/decreate monotonically, more so than for the multilepton case.

Combining the results of the $\gamma\gamma$bb analysis with multileptons and 4b will improve the expected limit of the combination. However, because the observed limit is slightly above the expected line, the combined observed limit will not improve for this topology. It is marginally different because the discrepancy between observed and expected is within the upper 1 σ band. The result of the combination of all three analysis is shown in figure 7.10:

Since the $\gamma\gamma$4b analysis probes the 130-150 GeV higgsino mass, we get an expected exclusion for

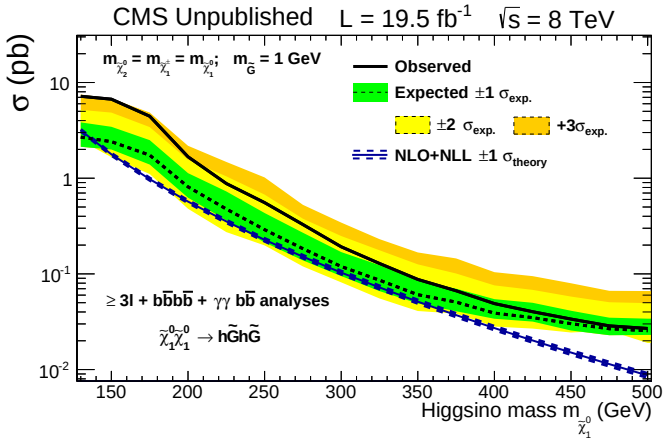

Figure 7.10: 95% C.L. Exclusion on Higgsino mass in the HH topology using the combination of the multilepton, 4b, and 2a2b analyses (10).

the point at 140 GeV, meaning all points below this mass are expected to be excluded. The observed limit tells another story. The point at 150 GeV is now almost beyond the upper 2 σ band, and the regions beyond 150 GeV where 4b is most sensitive is also pushed higher in the observed regime. Again, this is understandable within the context of the small excess in the di-photon channel and the 4b channel. The observed upper limit on cross section is still better than with multileptons alone for higher masses of the higgsino.

$\gamma\gamma$+ l

As described in section 5.1.3, this analysis has cuts that are identical on the photons as that of the $\gamma\gamma$bb analysis. Instead of selecting on b-jets, we select on a lepton, and require at most one b-tagged jet. The search also uses a slightly different variable, m_T, which relies by its definition on the MET and vector pT of the lepton. The results of figure 5.8 go into the datacard, and the search is divided amongst two final states, one with an electron and one with a muon. The individual limits can be seen in figure 7.11 (left and right) for the electron and muon channels respectively.

Muons are much cleaner objects than electrons. Electrons shower photons through interaction with the detector, and internal photons convert to electrons. They are more complicated objects, so we should expect that a limit with a muon object selection will be slightly better than one with electrons, and that is exactly the case. The background in an electron selected channel will be more difficult to predict, so the observed line is not as close to the expected as in the case of muon channels. The limits look similar to that of the di-photon channel. This is because the branching fraction of Higgs to leptons is also incredibly small.

We are now ready to combine all of the results of the analyses for the hh topology into one limit.

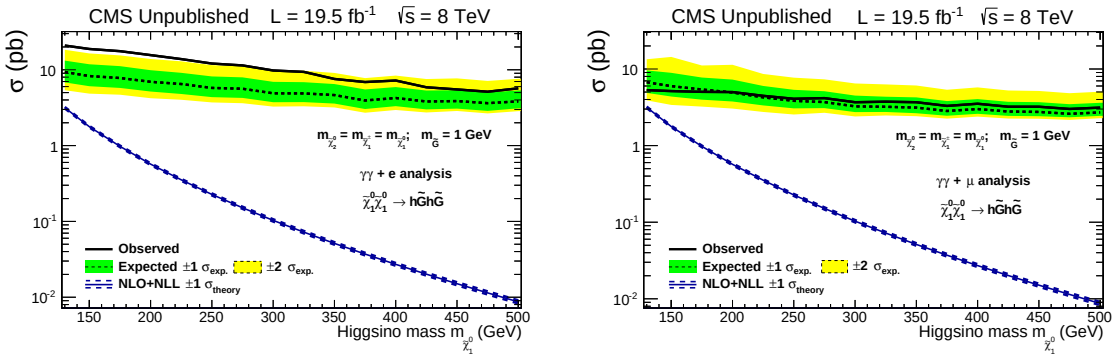

Figure 7.11: 95% C.L. Exclusion on Higgsino mass in the hh topology using the 2a+e analysis (left) and using the 2a+mu analysis (right) (10).

That is, the results of multileptons, 4b, $\gamma\gamma$bb, and $\gamma\gamma$ + lepton analyses. The full result can be seen below in figure 7.12. Because of the small deviation in the $\gamma\gamma$ + lepton analysis, the observed contour is slightly worse than in figure 7.10. This is the full power of the hh searches. The excess in the observed limit is and has been from the beginning, largely due to the multilepton discrepant channels, which are merely statistical fluctuations. The two di-photon analyses also contribute to this excess as well. The 150 GeV point, which is the most divergent mass point from the expected curve, is approximately +3.15 σ away from the expected curve. Meanwhile, the expected limit has been pushed to below 150 GeV as well. In the next section, I will discuss the searches in the hZ topology.

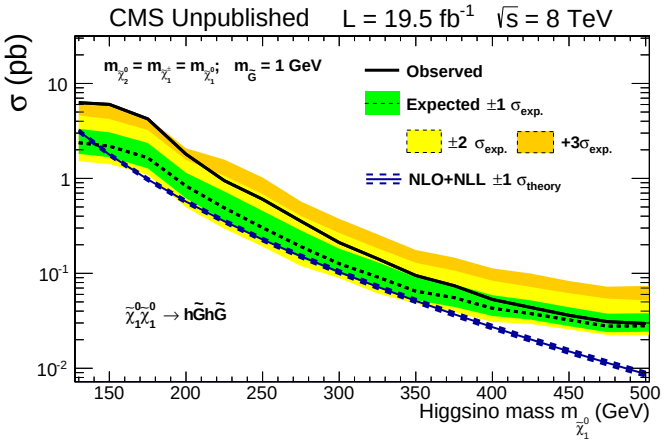

Figure 7.12: 95% C.L. Exclusion on Higgsino mass in the hh topology using all analyses (10).

7.1.2 Results of the hZ Topology

In this section, we concentrate on the mixed topological final state where the NLSP decays to a Higgs boson and a Z boson and two LSPs. The multilepton analysis, as we will see, does a better

job in this topology as it doesn't suffer as badly from the Higgs branching fraction. An important feature of searches in this final state is that, by themselves, the searches are unphysical. This is because if the HiggsinoNLSP model is correct, then hZ events occur, but cannot be a pure state. We can, however, put the searches in a wider context where hh and ZZ, pure states, also occur, and the limit becomes physical. This will be elaborated on in section 8.1. For now, it is a useful exercise to see what kind of limit one can set if this were indeed, a pure topology.

multilepton

The hZ topology is one where multileptons can potentially set a better limit. This is because the branching fraction of higgs to final state decays is not longer squared as in the case of pure hh topology. As described in section 1.5.1, in this topology, multileptons utilizes the Higgs to ZZ, WW, and $\tau\tau$ final state signal events, where the associated Z is decayed democratically. Similary to the hh topology, the signal events need to be weighted according to the NLSP $\rightarrow$ h/Z + LSP branching fraction. In this case, the weight is $2 * BF * (1 - BF)$ where BF is the branching fraction of the higgsino to Higgs. The factor of two is because the Higgs and Z are distinguisable. Thus, the signal events from each decay mode are weighted by their proper decay branching fractions as well as the additional branching fraction mentioned above. For the purpose of presentation, I assume a higgsino to Higgs branching fraction of 50%. This is the optimal branching fraction for the search, as the rate $2 * BF * (1 - BF)$ has a maximum at BF = 0.5. The multilepton limit is seen in figure 7.13.

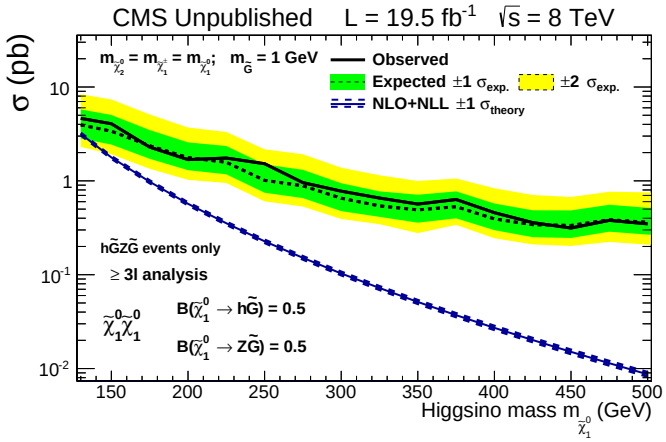

Figure 7.13: 95% C.L. Exclusion on Higgsino mass in the hZ topology using the multilepton analysis. Plot is unphysical (10).

As expected, the search for anomalous hZ events leads to a better limit. The fact that there is not significant excess means that the channels that drove the excess for the hZ topology are not part of the 90% signal sensitivity in this topology. The analysis is still not sensitive enough to produce

a limit on its own for this branching fraction. The features remain roughly flat as a function of higgsino mass, with the best sensitivity at low higgsino mass. The observed limit oscillates around the expected line, which just means that the channels that are in the datacards are fluctuating their order from mass point to mass point, but that there is not a significant discrepancy in any of the channels. No evidence of physics beyond the SM background is present, yet the model is still not excluded.

2b2l

The table of results for the 2b2l analysis seen in figure 7.15, shows now significant excess beyond the SM background. We can therefore expect that, by combining with the multilepton analysis, that a significant portion of phase space can be carved out by expected and observed contours. Again, I have assumed a 50% branching fraction of higgsino decay, and the efficiencies of the datacards from this analysis have been scaled appropriately to reflect this. The result is seen below.

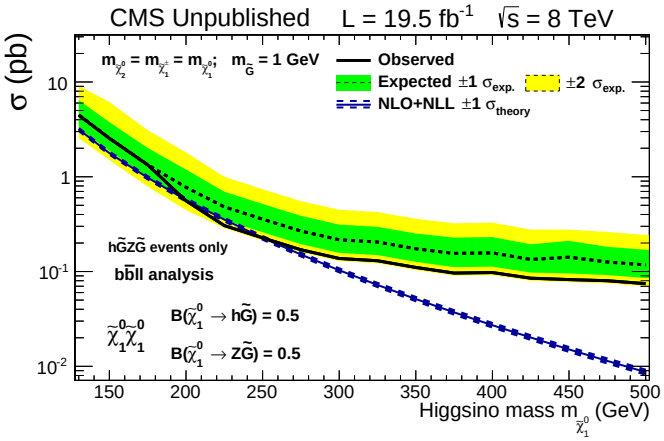

Figure 7.14: 95% C.L. Exclusion on Higgsino mass in the hZ topology using the 2b2l analysis. Plot is unphysical (10).

This plot has some interesting features that demand attention. First, the expected contour does not reach below the theoretical contour, which by itself is not terribly surprising given the features in the plots we've seen thus far. The observed contour, however, follows the expected contour almost exactly, until about the point 175 GeV, where it takes a dive below the expected, and crosses the higgsino range 200 to 250 GeV. What do we take away from this? The fact that the observation yields a better limit than expected could mean that the background in the 2b2l analysis is being overestimated. A second possibility, is that the data is statistically fluctuating downward to put the observed curve slightly outside the -1 σ band. The latter possibility is less likely, as we see the observed contour do this for almost all mass point above 200 GeV. Still, this is the best this analysis

can do, since at any other branching fraction, the higgsino branching ratio will be smaller, and the number of signal events will dip, causing both contours to rise farther above the theory line for all mass points. We can tentatively make the claim that we can exclude higgsino mass points between 200-250 GeV for a BF of 0.5, however.

Let's see what happens in the combination with multileptons. The combination can be seen in figure 7.16.

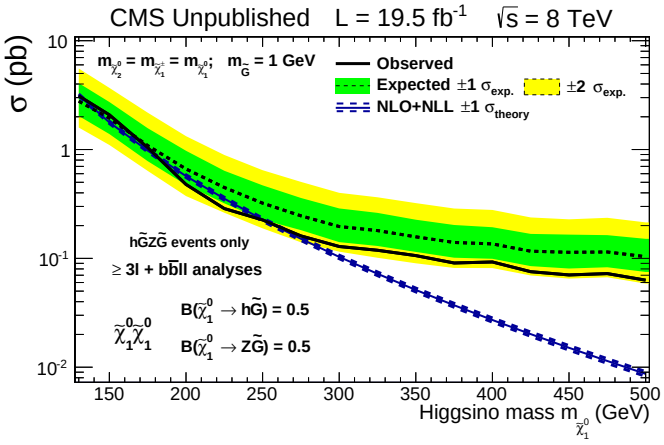

Figure 7.15: 95% C.L. Exclusion on Higgsino mass in the hZ topology using the combination of multilepton and 2b2l analyses. Plot is unphysical (10).

As with the case of the hh topology, we see we can start to expect to exclude below about 150 GeV. The observed limit also get slightly better, as now we observe an excluded region from about 190 to 250 GeV. This is some marginal improvement. The bands are also much smoother, and the observed contour is a little closer to the expected line, since multileptons alone had an observed contour slightly above the expected line.

$\gamma\gamma$ + l round 2

The $\gamma\gamma$ + lepton analysis also lends itself to the hZ topology, because of the fact that it does not optimize for any particular topology. We expect the limits to be marginally better for both muon and electron channels, because the Z boson to leptons branching fraction is much larger than the Higgs to lepton branching fraction. The limits can be seen in figure 7.16 and the cuts were described in section 5.1.3.

At first glance, one might think the limits contradict what I just said about the decay branching fractions. But, recall that this is an hZ topology, with an ADDITIONAL branching fraction of $2 * BR * (1 - BR)$ applied to the signal events. So, with a BR of 0.5, the limits are twice as poor as they could be if this were a pure topology, such as hh, or ZZ. Even with this factor of 2, it seems the

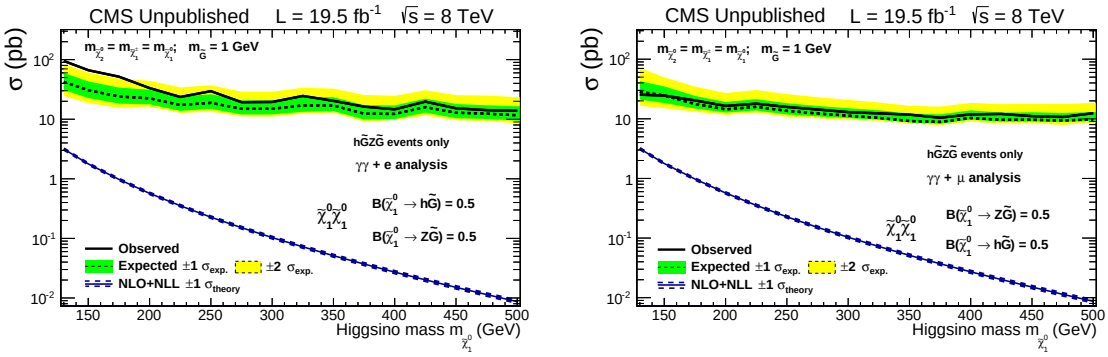

Figure 7.16: 95% C.L. Exclusion on Higgsino mass in the hZ topology using the 2a+e analysis (left) and the 2a+mu analysis (right). Plots are unphysical (10).

hh topology is a better fit for this analysis. We will come back to this in a moment. The features are similar across lepton type, however. The electrons do worse than the muon channels, precisely for the reason I described before.

As a final, educational plot, let's put the four analyses together, and see what we get. The result is in figure 7.17.

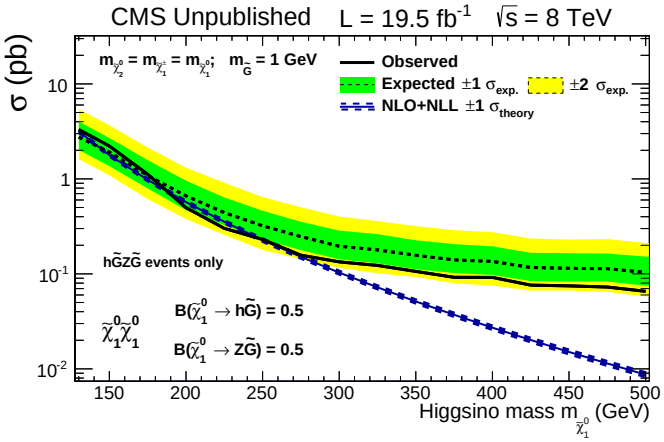

Figure 7.17: 95% C.L. Exclusion on Higgsino mass in the hZ topology using the combination of multileptons, 2b2l, and the 2a+l analyses. Plot is unphysical (10).

Because the limits on σ are so large for the $\gamma\gamma$ + l analysis, not much in the plot has changed from the combination with just multileptons and 2b2l.

7.1.3 ZZ topology

The final presentation of the 1d plots are for the pure ZZ topology, where no Higgs bosons are present in the NLSP decays. The analyes that are optimal for this signal are the multileptons and 2l2j analysis (SUS-13-006).

multileptons part 3

This is the strongest topology that multileptons can probe. The signal is larger than the other two topologies, due to the lack of small Higgs branching fractions. Recall that the events in this signal have Z's decaying purely to leptons. So the four lepton channels that are on Z should dominate here. The resulting limit can be seen in figure 7.18:

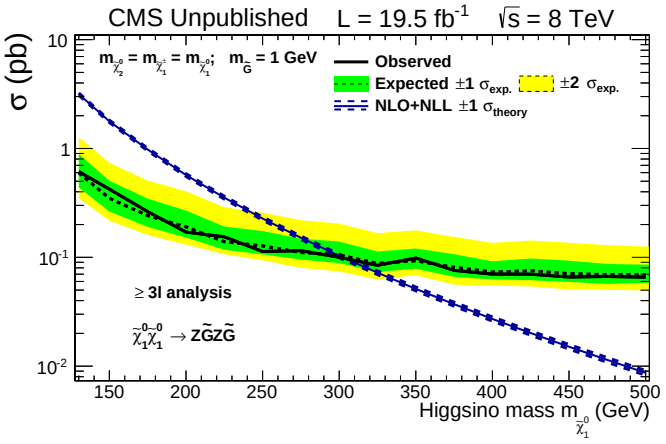

Figure 7.18: 95% C.L. Exclusion on Higgsino mass in the ZZ topology using the multilepton analysis (10).

The observed and expected contours are consistent with one another. The limit extends out to about 320 in higgsino mass. This means, for this model, the best multileptons can say is that there are no higgsinos with mass less than 320 GeV for the ZZ topology.

2l2j

The final analysis we consider is that described in SUS-13-006, where SUSY is searched for in a channel with exactly 2 leptons and 2 jets. The limit this analysis places is very similar. It can be seen in figure 7.19:

The reach of the limit is slightly better than the multilepton limit, about 340 GeV. Notice, however, at the low end of the higgsino mass range, this analysis comes close but does not exclude masses below 150 GeV. The lower one goes in higgsino mass, the more difficult it is to produce a boosted Z-boson. The less boosted the Z, the less energetic the jets it decays to, and consequently it might be more difficult to pick up signal events with lower pT jets at low higgsino masses. However, the combination of the two analysis gives the most powerful limit for all of the topologies. The combination is seen below:

The two analyses together probe all lepton numbers in events, and the exclusion is set out to around 400 GeV.

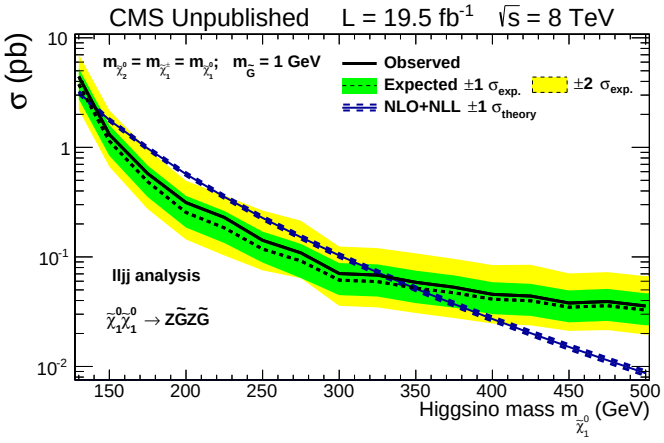

Figure 7.19: 95% C.L. Exclusion on Higgsino mass in the ZZ topology using the 2l2j analysis (10).

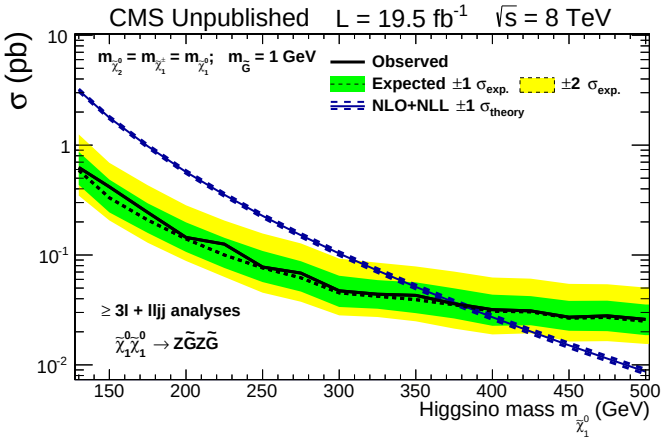

Figure 7.20: 95% C.L. Exclusion on Higgsino mass in the ZZ topology using the combinatio of multilepton and 2l2j analyses (10).

Chapter 8

2d Results

8.1 2d Contours

With all of the results of the last chapter in hand, we can now combine the information we gathered into an even more inclusive type of plot. One that does not favor any particular topology individually. For this, I introduce the sliding branching ratio plot. As for the 1d case, we have the higgsino mass on the horizontal axis. On the vertical axis, however, we have the branching ratio of the higgsino to higgs plus LSP, from 0 to 1.0. The interpretation of these plots are slightly different as a result. In the 1d case, the vertical was the upper limit on the observed cross section. What will go into a 2d version of the same plot, and how do we interpret it?

To explain the power of this type of plot, I will present it first for the multilepton case only. The multilepton sliding BR plot can be seen in figure 8.1.

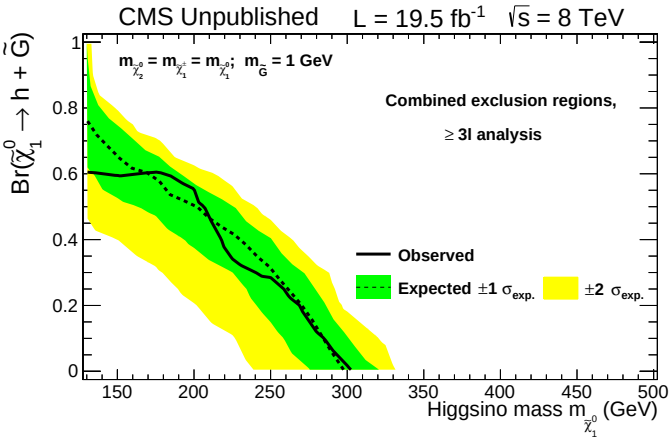

Figure 8.1: 95% C.L. Exclusion of the Higgsino Mass Range and variable branching fraction using the multilepton analysis. The x-axis is the Higgsino mass and the y-axis is the branching fraction of Higgsino to decay to a Higgs boson (10).

Let's start at the bottom of vertical axis of the figure. Since the vertical is the branching ratio of the NLSP to decay to the Higgs boson, the 0.0 would correspond to no higgsinos decaying to Higgs. Thus, taking a horizontal slice of the plane at y = 0.0 corresponds to the ZZ topology of the multilepton analysis. Recall in chapter 7, that the limit set by multileptons was at 320 GeV in the

higgsino mass range. In figure 8.1, we see this point plotted. At (320,0.0), we have a point plotted for the observed contour. In the 1d version, the mass point 320 GeV corresponded to a turning point in r-value, where we go from values smaller than 1 to values larger than 1. It is this turning point that is being plotted in the 2d plot at (320,0.0). The horizontal slice at y = 0.0 is correlated with the multilepton result for the ZZ-topology in exactly this way. In going from the 1d to 2d version, we lose the information on how the contours look for the rest of the higgsino mass plane, but we keep the point where the r-value has this shift.

In fact, every point on a contour in the 2d plane corresponds to an r-value of 1. Everything below the observed contour is considered excluded, while everything above it is yet to be determined. Perhaps new physics lies out there, and perhaps it does not. We cannot say.

So what's the advantage of such a plot if we lose all the information of all the jumps and wiggles from the 1d case? Well, for one thing, now we can change the branching ratio freely, and see what the excluded region is immediately instead of making plot after plot. Also, when we combine analyses, we will start to see what areas of the parameter space are being affected the most by each analysis. So in some sense, we do lose information, but some additional features are gained in the process.

One might ask, if you take the horizontal slice at y = 1.0, for instance, why is there no value? For this horizontal slice, which corresponds to the pure hh topology, we truly miss some information. The plot is merely telling us that there is no exclusion set from multileptons for this branching ratio. One would have to go to the 1d version to see the excess as presented in figure 7.5. The fact that we have both plots is a very powerful tool, and excellent for cross checking results.

Another question one might ask is what's going on at the slice y = 0.5? If the slice is supposed to correspond to the 1d versions, then why is there a limit set for (215,0.5), but there is no corresponding limit in figure 7.13? This is because the 2d plot for anything in between the pure topologies, i.e. for $0.0 < BR < 1.0$, there are hh and ZZ events in ADDITION to the mixed topology hZ state. This is to be expected of course. If we consider the NLSP decaying to a Higgs and the LSP 50% of the time, then we should expect hh events 25% of the time, ZZ events 25% of the time, and the mixed state of hZ events 50% of the time, exactly in accordance with the following weights:

- hh : $BR^2 * (\tilde{H} \rightarrow$H + LSP)
- hZ : 2 * BR * (1 - BR) ($\tilde{H} \rightarrow$H + LSP)
- ZZ : $(1 - BR)^2 * (\tilde{H} \rightarrow$H + LSP)

In other words, the point (215,0.5) has more information than the unphysical plot in figure 7.13. When combining events of different topologies, we simply use the branching fraction formula from

the list above. For instance, if the BR is 0.5, then an hh signal event gets a weight of $0.5^2 = 0.25$, in addition to its decay mode for the Higgs boson. An hZ type event would get a weight of $2*0.5*0.5 = 0.5$, and a ZZ type event would get an additional weight of $(1-0.5)^2 = 0.25$, in addition to the 1% applied due to it being a purely leptonic Z decaying sample.

Can we interpret the differences between observed and expected contours the same way as in the 1d case? The answer is yes and no. For instance, the observed contour for left of the mass point 175 GeV flattens out, while the expected contour keeps rising. Because any region bounded by the observed contour is considered excluded, we have to think the opposite way we did for the 1d case. The higher, or more farther reaching the curve, the more we are excluding, whereas for the 1d case, we wanted the contours to lie as low as possible to reach the theory line. Also, the fact that the observed contour is below the expected contour is different in the same way. In the 1d case, when the observed was above the expected, we knew that there was a discrepancy between the data and SM prediction, usually with the data being higher than what was predicted. In the 2d plot, when the observed contour is below the expected, we must think the other way around. We are excluding less than what is expected in the 2d plot, so we know that the data must be larger than the SM background for this region.

This is what you see, for example, at the point (130,0.6). We know as we move towards the pure hh topology for this mass point, the analysis becomes more sensitive to signal that lands in the discrepant channels I described in section 7.1.1. So we should expect this sort of trend, where the expected line moves above the observed line as we approach 1.0 alone the vertical line x = 130.

One final question might be, where is the blue theory line from the 1d cases? The theory line here is inappropriate, since we are plotting r-value of 1.0. The theory line crosses a contour if and only if the contour appears in the 2d plot. In this sense, the theory curve is indirectly plotted.

As we add analyses, little idiosyncracies will begin to pop up, and will be explained as we go along.

8.1.1 ml + 4b

A sliding BR plot with the results of the 4b analysis should not change much of figure 8.1 below the y = 1.0 line. The combination plot can be seen in figure 8.2:

The interesting feature is the yellow island that is at the top of the plot. At the y = 1.0 line, the islands range is from 200 to 360 GeV. Where does this strange feature come from, and what does it mean? To explain this, we must appeal to the 1d version in figure 7.9. On this plot, we can see that the theory curve cuts the lower -2 sigma band between this range. The range then appears in

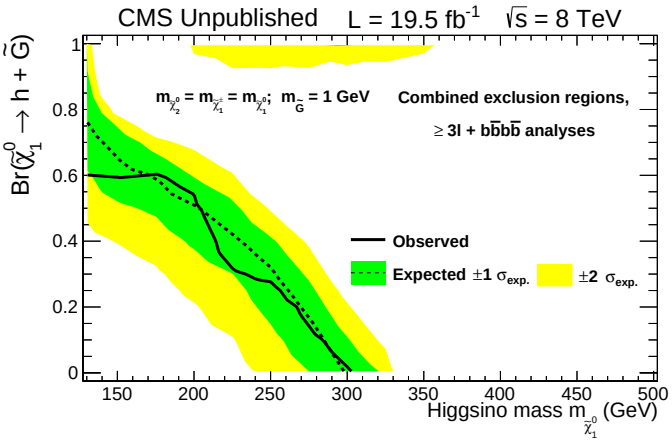

Figure 8.2: 95% C.L. Exclusion of the Higgsino Mass Range and variable branching fraction using the combination of multilepton and 4b analyses (10).

the 2d version as a result. We can see that the 4b analysis loses all of its sensitivity below the BR = 0.95 line. Again, as in the 1d case, the systematics that are correlated are the luminosity, jet energy scale, and initial state radiation.

8.1.2 ml + 4b + 2b2l

For chronological reasons, I have added the results of the 2b2l analysis next to the sliding BR combination. We do not expect this analysis to have any significant contribution near the y = 0.0 or 1.0 ends of the plot, since the weight factor of $2 * BR * (1 - BR)$ has non-zero minima at y = 0.1 and 0.9.

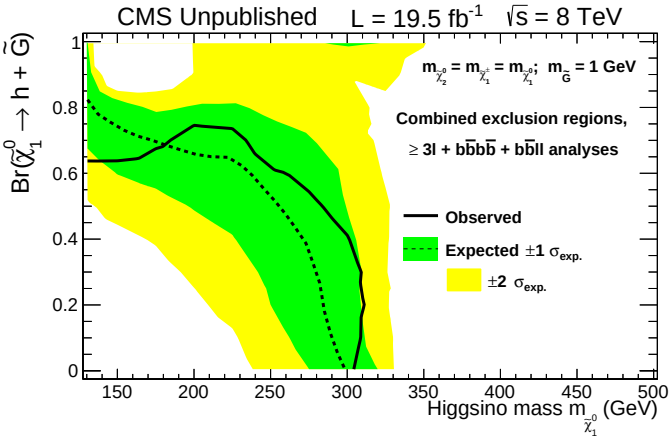

Figure 8.3: 95% C.L. Exclusion of the Higgsino Mass Range and variable branching fraction using the combination of multilepton, 4b, and 2b2l analyses (10).

Here we notice a dramatic shift in the observed and expected contours. For higgsino masses

higher than about 175 GeV, the observed line is above the expected line, which is consistent with what we saw in the 1d version of the 2b2l limit. Both contours are pushed higher for low higgsino masses as well. Another interesting feature is the green island has been extended downwards slightly, and the yellow island has merged with the upper 2 σ band from the multilepton result. Although small, the 2b2l analysis does contribute to the downward fluctuation in the -2 sigma expected line in that area. Overall, the excluded region is covering about twice more area than with only multilepton and 4b contributions. The number of pseudo-experiments, or toys, that we throw at LandS also affects the smoothness of the contours. We use 50K and 25K for the CL_{sb} and CL_b distributions respectively.

8.1.3 ml + 4b + 2b2l + 2a2b

Adding in the effect of the $\gamma\gamma$bb analysis, we arrive at the following 2d contour.

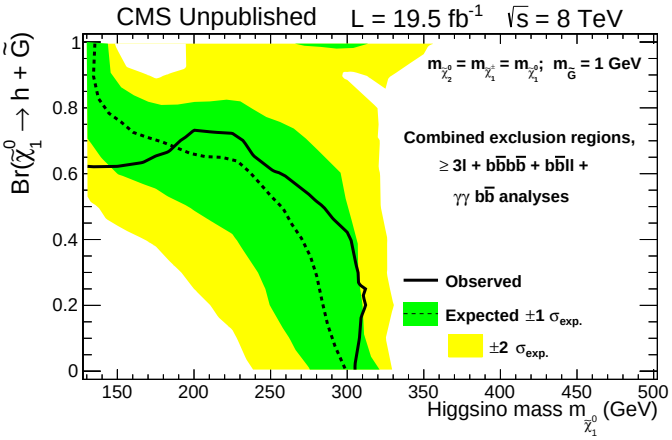

Figure 8.4: 95% C.L. Exclusion of the Higgsino Mass Range and variable branching fraction using the combination of multilepton, 4b, 2b2l, and 2a2b analyses (10).

The feature that differs here from the previous plot is that the expected contour is now pushed all the up to the y = 1.0 line at the mass point 140 GeV. Referring back to figure 7.12, we can understand that the expected contour is crossing the theory line at 140 GeV, so the two plots are consistent. Additionally, the green island seems to have changed its width, approaching a range of 40 GeV along the lower edge. Again, this could have to do with systematic uncertainties, or just a fluctuation due to the number of toys.

8.1.4 ml + 4b + 2b2l + 2a2b + 2l2j

Again, for chronological purposes, I add in the results of the 2l2j analysis. We expect this to really affect the 2d plot nearest the ZZ topology, or y = 0.0 line. One can see this in figure 8.5:

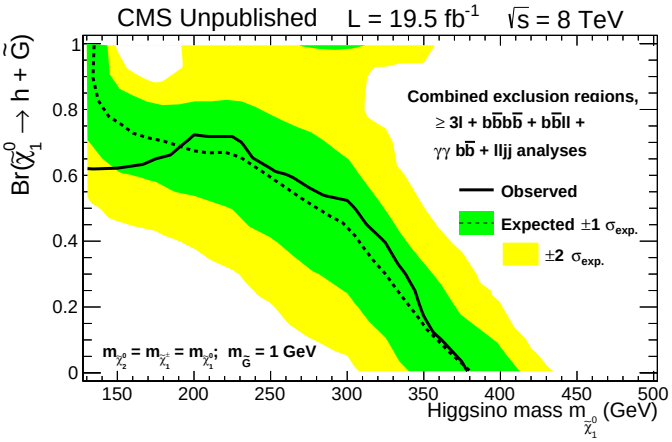

Figure 8.5: 95% C.L. Exclusion of the Higgsino Mass Range and variable branching fraction using the combination of multilepton, 4b, 2b2l, 2a2b and 2l2j analyses (10).

This is also a dramatic improvement in the limit. It is also consistent with the result of figure 7.20 in that the limit has been extended out to 390 GeV. One can almost think of dragging the line from 300 GeV and pulling it out to that mass point. The yellow island has smoothed out quite a bit with the combination of these five analyses.

Without further ado, let's add in the results of the $\gamma\gamma + l$ analysis, both for hh and hZ topologies. The coup de grace, money plot, can be seen in figure 8.6.

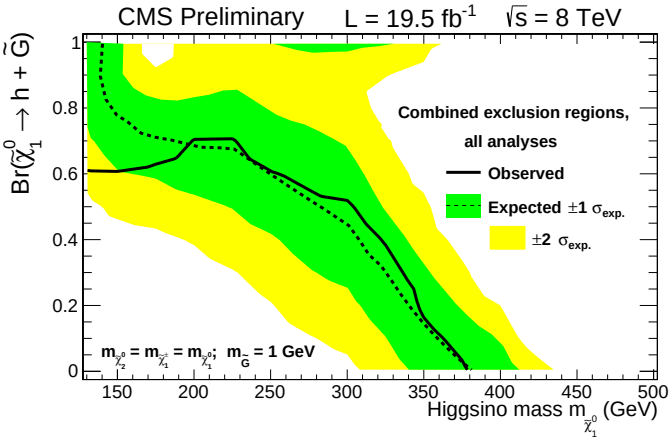

Figure 8.6: 95% C.L. Exclusion of the Higgsino Mass Range and variable branching fraction using the combination of all six analyses (9).

The expected lines improve marginally as we could have predicted from the 1d complete limit for the hh topology. The hZ improvement from this analysis is almost negligible. The green island has also been stretched to a range of nearly 100 GeV. Overall, the power of all of these analyses combined carves out almost a third of the parameter space for the electroweak production of the Natural SUSY Higgsino NLSP model.

Chapter 9
Conclusion

9.1 Conclusion

We have searched for hints of supersymmetry in the context of electroweak production in all of these analyses. We used 2012 data collected from the CMS detector with $\sqrt{s} = 8$ TeV and luminosity of $19.5 fb^{-1}$. With the Natural SUSY Higgsino NLSP model in mind, each analysis catered to particular decays of the Higgs boson, increasing the chances of catching new physics. The results are such that no new physics beyond the Standard Model has been observed. We are able to put excellent limits on the higgsino mass range, and the branching fraction of the NLSP decays. It will be interesting to see what will come in 2015 when the LHC turns on to its full energy and design luminosity, and to see how much further we can push the limits of SUSY models such as this, barring new physics.

Bibliography

[1] Georges Aad et al. Evidence for the spin-0 nature of the Higgs boson using ATLAS data. *Phys.Lett.*, B726:120–144, 2013.

[2] Arora, S et al. A search for anomalous production of events with three or more leptons using 19.5 fb^{-1} of $\sqrt(s) = 8$ TeV LHC data. CMS Analysis Note AN-12-343_v32, 2013.

[3] Arora, S et al. Background and Efficiency Determination Methods for Multilepton Analyses. CMS Analysis Note AN-12-257-v11, 2013.

[4] Beringer, J. et al. Review of Particle Physics. *Phys. Rev. D*, 86:010001, 2012.

[5] Campagnari, C. et al. Search for beyond-the-standard model physics in events with a Z boson, a Higgs boson, and missing transverse energy. CMS Analysis Note AN-13-217_v6, 2013.

[6] CERN-CMS. CMS Slice. `http://cmsinfo.cern.ch/Welcome.html/CMSdocuments/DetectorDrawings/Slice/CMS_Slice.gif`, 2014.

[7] Serguei Chatrchyan et al. Search for anomalous production of events with three or more leptons in pp collisions at sqrt(s) = 8 TeV. *Phys.Rev.*, D90:032006, 2014.

[8] CMS Collaboration. *CMS Physics : Technical Design Report Volume 1: Detector Performance and Software*. Technical Design Report CMS. CERN, Geneva, 2006.

[9] CMS Collaboration. Search for electroweak neutralino and chargino production in channels with Higgs, Z, and W bosons in pp collisions at 8 TeV. CMS Public Analysis Summary CMS-PAS-SUS-14-002, 2014.

[10] CMS Collaboration. SUS-14-002 TWIKI. `https://twiki.cern.ch/twiki/bin/view/CMSPublic/PhysicsResultsSUS14002`, 2014.

[11] S. Dawson. Introduction to Electroweak Symmetry Breaking. `http://arxiv.org/abs/hep-ph/9901280`, 1999.

[12] Abdelhak Djouadi. The Anatomy of Electro-Weak Symmetry Breaking. `http://arxiv.org/abs/hep-ph/0503172`, 2005.

[13] ATLAS Experiment. Overall view of the LHC experiments. http://www.atlas.ch/photos/atlas_photos/selected-photos/detector-site/surface/9906026-A4-at-144-dpi.jpg, CERN 2014.

[14] Richard C. Gray. Isolation Cartoon. https://indico.cern.ch/event/252532/contribution/3/material/slides/0.pdf, 2013.

[15] Eilam Gross and Ofer Vitells. Trial factors for the look elsewhere effect in high energy physics. http://arxiv.org/abs/1005.1891, 2010.

[16] Rutgers Multilepton Group. Electrohiggs TWIKI. https://twiki.cern.ch/twiki/bin/viewauth/CMS/Electrohiggs, 2013.

[17] Jean Iliopoulous. Introduction to the STANDARD MODEL of the Electro-Weak Interactions. http://arxiv.org/abs/1305.6779, 2013.

[18] Vardan Khachatryan et al. Searches for electroweak production of charginos, neutralinos, and sleptons decaying to leptons and W, Z, and Higgs bosons in pp collisions at 8 TeV. 2014.

[19] Stephen P. Martin. A Supersymmetry Primer. http://arxiv.org/abs/hep-ph/9709356, 2011.

[20] Pich, Antonio. The Standard Model of Electroweak Interactions. http://arxiv.org/abs/1201.0537, 2012.

[21] A L Read. Modified frequentist analysis of search results (the CL_s method). (CERN-OPEN-2000-205), 2000.

[22] Shomer, Assaf. A pedagogical explanation for the non-renormalizability of gravity. http://arxiv.org/abs/0709.3555v2, 2007.

Appendix A

A.1 Supplementary Plots

A.1.1 1d Overlay Plots

In chapters 7-8, I presented 1d curves for combination of the analyses that search for the presence of new physics within the scope of the Higgsino NLSP model. It is illuminating to see how each analysis contributes separately, both for expected and observed contours, to get a better idea what areas of higgsino mass range is being reached by which analysis. The body of the thesis attempts to explain this textually to avoid confusion and overlapping ideas. It is now appropriate to present some plots with supplementary material.

I begin this section with a reproduction of the results of the full combination for the pure hh topology. In figure 10.1, we see the same plot as in figure 7.5, but with the 1d expected contours for the 6 individual analyses overlayed. Now it is clear that the 4b analysis is what is contributing the most to the combined expected limit for higgsino masses > 175 GeV. The line ends abruptly at 175 GeV due to lack of sensitivity below this mass point. For points between 130 and 175 GeV, we can see that the multilepton analysis is the most sensitive, followed by $\gamma\gamma$bb, and finally $\gamma\gamma$ + lepton, all three of which help bring the expected limit at 130 GeV from 4 pb down to about 1.5 pb. multileptons, however, is the second largest contributor for all higgsino masses.

Next, we turn to the hZ topology. Shown in figure A.1 is a very busy plot, with all 6 analysis making a presence. This would correspond to the horizontal slice of y = 0.5 in the money plot in figure 8.6. Note that this plot, therefore, has more than just hZ events in it. We see that multileptons sets the best expected limit up until around 270 GeV, where the 2b2l and 2l2j analyses become on equal footing with multileptons for all higher higgsino masses. Amazingly, the 4b analysis also makes contributions for large higgsino masses! This could be because the 3b signal sample is still part of the datacards for 4b, and we could have a tau lepton coming from a Z being tagged as a b-jet. For the entire mass range, the two di-photon analysis are comparable to one another. The jaggedness of the grey contour is coming from the electron channel of the di-photon analysis.

To round off the 1d expected overlay curves, we have the ZZ topology pictured in figure A.3.

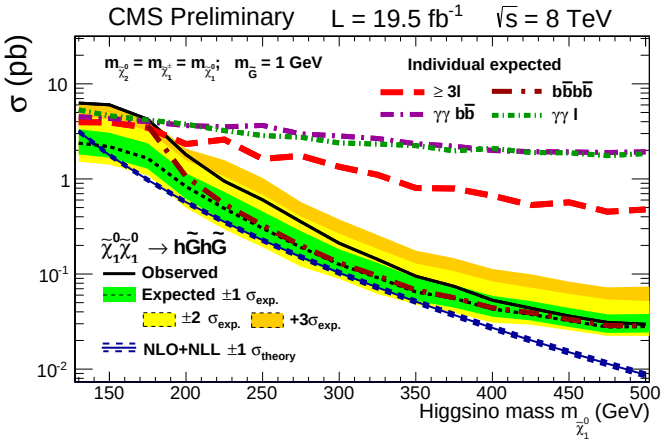

Figure A.1: 95% C.L. Exclusion of the Higgsino Mass Range in the hh Topology using the full combination. Expected curves of individual analyses are overlayed (9).

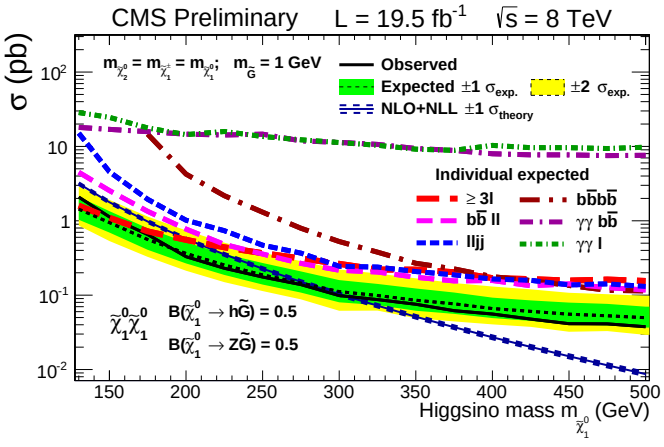

Figure A.2: 95% C.L. Exclusion of the Higgsino Mass Range in the hZ Topology using the full combination. Expected curves of individual analyses are overlayed (9).

We do not expect any contributions from any other analyses besides multileptons and 2l2j. For low higgsino mass, multileptons sets the stronger limit, and for masses beyond around 240 GeV, the roles are reversed slightly (remember this is a log scale). This is because the branching ratio of Z to jets is larger than Z to leptons, and for very boosted Z bosons, high p_T jets will be reconstructed better than if they were coming from lower values of the higgsino mass. The signal, always favoring Z decaying to jets, will dominate over the leptonic signal, if all objects are properly reconstructed.

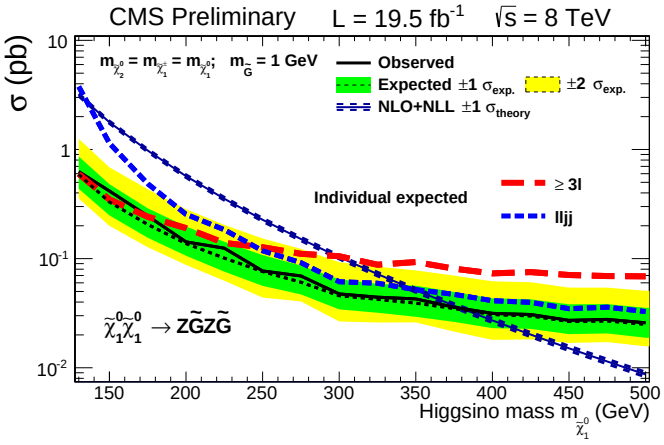

Figure A.3: 95% C.L. Exclusion of the Higgsino Mass Range in the ZZ Topology using the full combination. Expected curves of individual analyses are overlayed (9).

A.1.2 2d Overlay Plots

In addition to the 1d overlay plots, we can try to understand which analysis is contributing the most or least in the 2d contour with variable branching fraction. Instead of plotting each contour as we did in the last section, I will plot an N-1 style contour, where 5 out of the 6 analysis are in one expected contour. The reason for this is that not every analysis has sensitivity at all values of the branching ratio (as in the case of 4b and the di-photon channels, for example, which don't cross the theory curve). Thus, not all individual contours will make an appearance in an overlay. Using the N-1 style, we can see exactly how the expected contours would change if we were to remove one of the analysis.

As the name suggests in the legend, the black dashed curve is the expected contour for the full combination, exactly like in figure 8.6. The label ≥ 3 is the multileptons portion, $2l + X$ is equivalent to the 2b2l and 2l2j analyses, and $2\gamma + X$ refers to the di-photon analyses. So, for instance, the magenta curve is the result of taking the multileptons analysis out of the limit. This is by far the largest drop in the excludion plane. It really illustrates the importance of the multileptons. Removing 4b and the di-photon analyses affects the area closest to the hh topology, as expected.

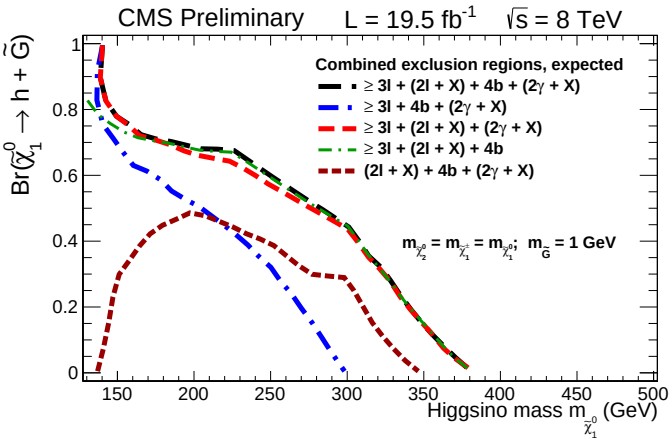

Figure A.4: 95% C.L. N-1 Expected exclusion of the Higgsino Mass Range and varying branching fraction using the full combination. Overlayed are the expected contours for a subset of the analyses; this demonstrates the individual strengths of each analysis (9).

This is the area these analyses are most sensitive to. Removing the 2l + X analyses (cyan curve) is also a huge loss, not so much near the hh topology, but for the BR = 0.5 and especially the ZZ topology.

The final plot of this section is the observed contours overlayed on the full combination plot of figure A.5.

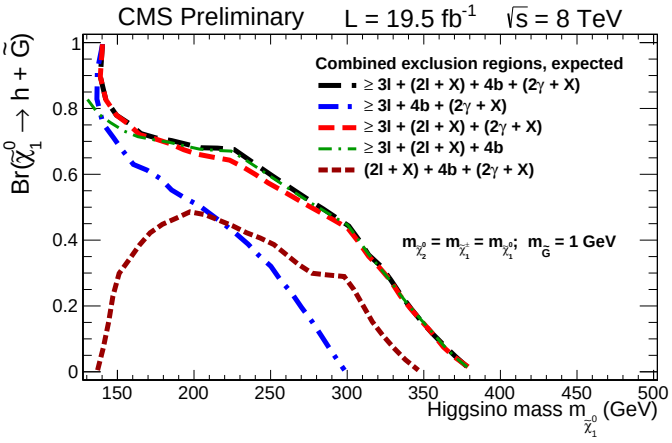

Figure A.5: 95% C.L. N-1 Observed exclusion of the Higgsino Mass Range and varying branching fraction using the full combination. Overlayed are the observed contours for a subset of the analyses; this demonstrates the individual strengths of each analysis (9).

This plot has the same "N-1" presentation as figure A.4, and same legend and color style as well. One thing that jumps out immediately from this plot, is that with multileptons removed, a significant portion of the parameter space is lost, even though the multilepton limit has the +2.57 σ excess for mass points in the hh topology. Similarly, not including the 2l + X analysis removes

about the same area of parameter space as removing multileptons.

The final plot of this section is a sensitivity plot for all the analyses. It takes a point in the (mass,BF) plane, and fills in the square with the analysis that has the lowest expected r-value. Only four of the six analyses make an appearance on this plot, which is why we have the N-1 plots to show how the analyses that are not the most sensitive in any area of the plane can also influence the total contribution. The 4b analysis, for instance, shows heavily in this plot, but its power is not done justice in the N-1 plot.

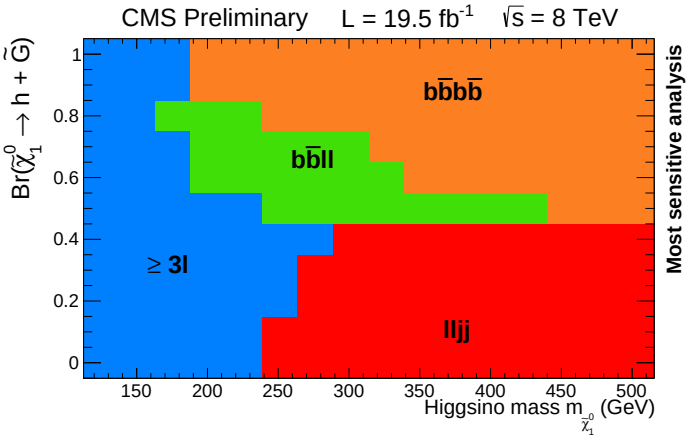

Figure A.6: Sensitivity plot based on the lowest expected r-value of each analyses (9).

Appendix B

B.1 Systematic Uncertainties

This chapter is devoted to something that is notoriously difficult to measure in an experiment, systematic uncertainties. I will go analysis by analysis and explain how each one handles this issue. I have avoided talking about it during the bulk of the review of the other analyses to give the reader the big picture without interrupting the flow. This chapter can really be skipped by the reader if so inclined. As alluded to in section 7.1.1, for the combination, the jet-energy scale, ISR, and luminosity are the only systematics correlated across the analyses. Everything else is treated as independent nuisance parameters.

B.1.1 Multi-leptons

As described in chapter 4, there are three data-driven methods that are employed to determine backgrounds that do not come from simulation. They are the f_t vs f_{sb} method, the $R_{d_{xy}}$ method, and the asymmetric photon conversion estimation. For the f_t vs f_{sb}, which is the fake rate of jets faking hadronic taus, we study data samples that are triggered on jets and di-leptons. Then, based on how the f_t vs f_{sb} distribution changes from sample to sample, we apply a conservative 30% systematic uncertainty for the method. For the $R_{d_{xy}}$, which is the fake rate of light-flavored jets faking isolated leptons, we observe how the rate changes from an e^+e^- to a $\mu^+\mu^-$ triggered data sample. We use this as a measure of the systematic. More details on the systematics can be found in (7). Finally, for the asymmetric photon conversion rate, a 50% uncertainty is applied because we use the assumption that virtual photons follow the same spectrum as real photons.

For the simulation backgrounds, i.e. the VV and $t\bar{t}$ backgrounds, the simulation and signal efficiencies rely heavily on trigger, lepton identification, and lepton isolation efficiencies. Therefore, the systematics of these three cuts will be important. For the trigger systematic, a value of 5% is applied. Additionally, since the lepton isolation and ID efficiencies are a function of p_T, the systematic error in a particular channel depends on the lepton p_T as well. For a lepton with $p_T >$ 20 GeV, a 1.5% systematic is applied. There are other values that affect the efficiency of the signal and simulation. Values like jet-energy scale (JES), b-tagging, MET, and luminosity systematics are

Source	
Jet energy scale	5-10%
Jet energy resolution	2-4%
Pileup modeling	4%
Trigger efficiency	1-5%
b-jet tagging efficiency	5-10%
Lepton identification and isolation	5%
ISR modeling	1%
Parton distribution functions	1%
Luminosity	2.6%

Figure B.1: Systematic uncertainties along with their typical size and correlation information (9).

important. There are uncertainties on the theoretical cross section as well, but for the WZ and ZZ samples, which are scaled to the data, this is a non issue. Again for more details, see (3).

Figure B.1 shows a table that describes all the systematic uncertainty values used in the analyses.

B.1.2 4b

Since this analysis relies heavily on the ratio of signal to sideband regions of $t\bar{t}$ simulation to estimate the backgrounds, we primarily focus on two types of uncertainty. In the first case, we define take the ratio of SIG/SB for the 4b, 3b, and 2b samples separately. Then we define the value R as a double ratio. For instance, the value SIG/SB in the 4b sample divided by the value SIG/SB in the 2b sample corresponds to this R definition. We calculate this double ratio, R, both for the 4b and 3b samples in the way just described. We also take the statistical uncertainty on every value of R obtained. For a given sample, we take the larger of the two, either the double ratio R, or the statistical uncertainty, and apply this as their systematic uncertainty. This is done for each S_{MET} bin as well. The typical value is quoted as 25%.

The second systematic tries to account for the difference in the ratio SIG/SB and the difference in background rates between $t\bar{t}$ simulation and QCD multijets data samples. This is done for each S_{MET} bin and for all three samples again. We find that the QCD fraction of events varies by 6% amongst the bins, and then allow for as much as a 20% systematic for the corresponding $t\bar{t}$.

These systematics are treated as uncorrelated, which means LandS treats them as separate parameters that should be added in quadrature (10).

B.1.3 $\gamma\gamma$ + X

The background here is estimated cleverly with the Higgs S_T variable for the X = bb, and m_T variable for the X = lepton. As described in the Other Analysis chapter, the analyses use two side

band regions, and average the values of the variables in the regions. Half of the difference between the two values obtained in the sidebands is what is treated as the systematic uncertainty for each analysis. There is also a 13% systematic assigned for the SM Higgs simulation due to cross section uncertainties.

B.1.4 2l + X

To end this section, the 2b2l analysis has systematics added in quadrature based upon how the Z+jets sample matches with the γ+jets sample by changing selection requirements, and how $t\bar{t}$ impacts the Z+jets events. More details on this can be found in (5). For the 2l2j analysis, recall that for the flavor symmetric background, a factor was derived from simulation. The systematic defined on this is the difference between the scale factor derived from simulation versus the one derived from data.

Appendix C

C.1 Tag and Probe

We use the standard Tag and Probe method to estimate the isolation and identification efficiencies for the leptons in our analysis. I will describe the method for muons, and refer the reader to (3) for the electron cuts. We also tried, for the 2012 analysis, using a twist on the method to estimate the tau isolation efficiency, which I will talk about briefly later.

The idea is very simple. If we can find a pair of lepton candidates, where one lepton has very strict requirements on it, and the other has minimal requirements on it, that form a Z-peak invariant mass, then we can be sure that the lepton that had the minimal requirements is, most likely, a lepton. However, because there are so few requirements for this "minimal" lepton, we can use it to test out the efficiencies of various cuts without worrying about the efficiencies of other cuts, as would be the case for a stricter lepton.

We divide the two types of leptons into what are called "tag" leptons, and "probe" leptons. The tagged leptons have the strict requirements. Tagged muons must pass the following criteria:

- $p_T > 20$ GeV
- $|\eta| < 2.1$
- must be a global muon
- must be a tracker muon
- must be "prompt" and "tight"
- $I_{rel} < 0.15$
- $D_{xy} < 0.02cm$

For probe muons, we have a much looser criteria:

- $p_T > 5$ GeV
- $|\eta| < 2.1$

- must be a global muon

By definition, all tagged muons are also probe muons, but not the other way around. However, if something satisfies the tagged requirement, it is labeled as a tag and a tag only. We are careful to identify in each event, how many tags we have, and how many probes we have. We form the invariant mass of opposite sign same flavor muon pairs in every event, where one muon is a tag muon and one is a probe. We also restrict the pairs by using each tag only once, and each probe once per tag. We do not cut on the Z-mass window yet, as we need to estimate the background under the Z-peak by using the side-bands outside the Z window. Some of the di-muon pairs will land in the Z window, and some in the side-bands as a result.

We form a two dimensional histogram of the probe muon p_T versus M_{ll} for each tag and probe muon pair. We then project onto the M_{ll} axis all the pairs that have a probe within a particular p_T range. We do this for a p_T range from 0 to 120 with 4 GeV wide bins. This range division produces 30 invariant mass plots of the tag and probe muon pairs, with each plot having probe muons within one of the 30 p_T bins. A typical plot of this type appears in figure C.1.

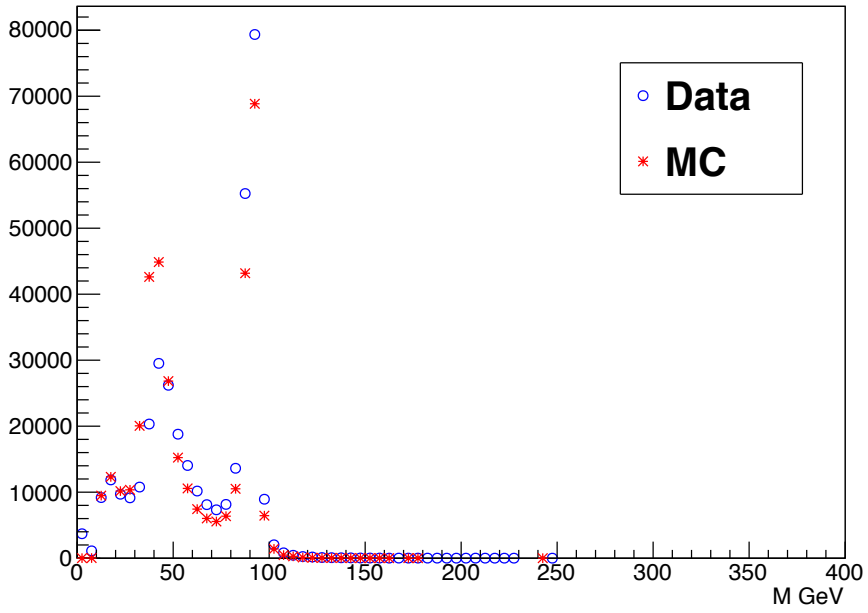

Figure C.1: Typical invariant mass of tag and probe lepton pairs used for effiency calculations (3).

For each invariant mass plot, we fit the events outside the Z window, which is the side-band region, to a 5th order polynomial. This fit extends through the Z window, but does not fit for it. For the events within the Z window, or the signal region, we fit a gaussian on top of the 5th order polynomial within the Z window. The final step is to subtract the side-band fit within the Z window from the signal region fit. This number corresponds to the number of probe muons in a particular

p_T range that are most likely real muons, as they form a Z boson invariant mass with its tagged partner.

Now we wish to test the efficiency of cuts using these probe muons. We use these probe muons, again, because there were minimal restrictions on the objects, and therefore we can test the maximum efficiency of a particular cut. We simply repeat the procedure as described above, only we add the requirement that the object pass an additional cut to be considered a probe muon. For example, to test the efficiency of the isolation cut, we would require the probe muons to additionally satisfy the $I_{rel} < 0.15$ cut. Continuing through the procedure would yield the number of probe muons that pass the isolation cut. Finally, we form the ratio of the number of probe muons that pass the isolation cut to the number of probe muons that did not require the isolation cut. This ratio is the efficiency of the isolation cut for the p_T range of interest.

The ratio is done for simulation and data events for all 30 p_T bins. Additionally, we classify the type of events based on there location in η (barrel or endcap), the number of jets (zero, one, two, and $\geq$ three), and the number of vertices (one to five, six to ten, 11 to 15, 15 to 20, and $\geq$ 20).

We also take the ratio of the efficiencies of data versus simulation for all p_T bins. This ratio is used to scale the simulation to the data values. A sum of two error functions is used to fit the resulting ratio, depicted in figure C.2

Finally, we use a similar method to measure the tau isolation efficiency. There is a caveat with using the tag and probe method for tau leptons, however, because taus decay promptly to leptons or hadrons and missing energy from neutrinos and neutral pions. It is often difficult to reconstruct a Z peak from a di-tau event due to detector misreconstruction of the missing energy. One way to get around this is to use muon candidates that also pass tau discrimants as proxies. Once we have our tau proxies, we use the tag and probe method, and test tau isolation cuts. An example can be seen in figure C.3:

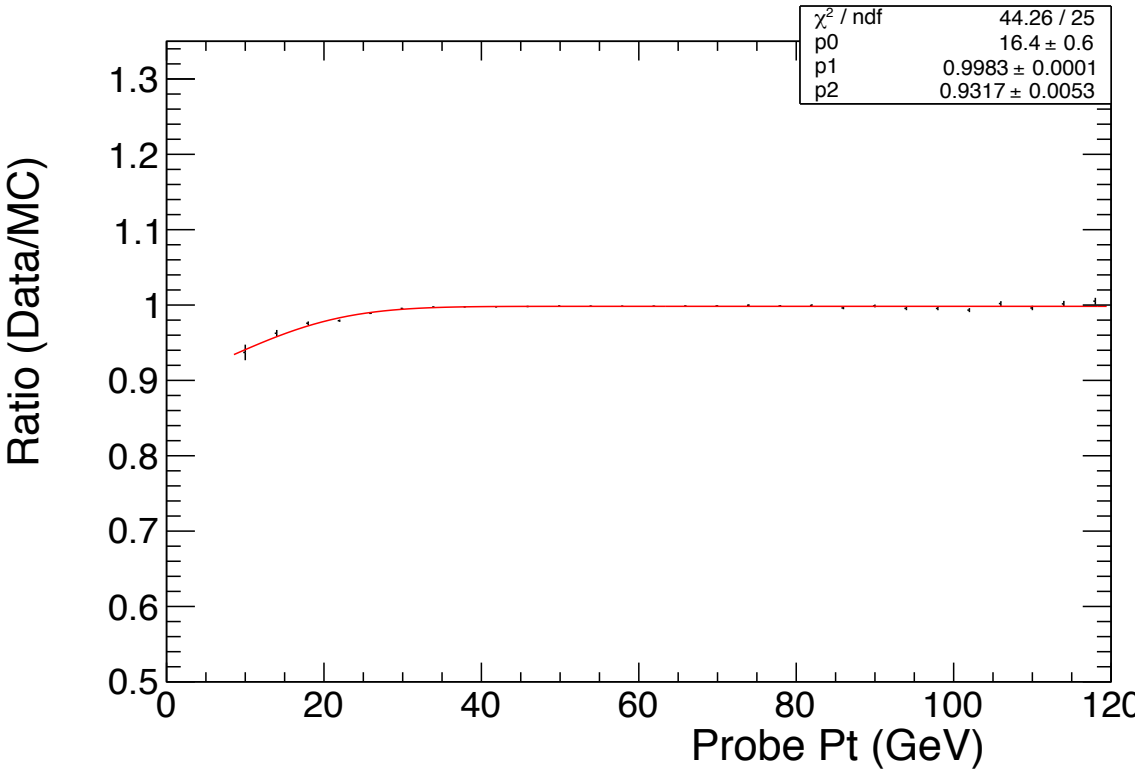

Figure C.2: Isolation efficiency ratio of data to simulation as a function of lepton p_T. Red curve is modeled with an error function (3).

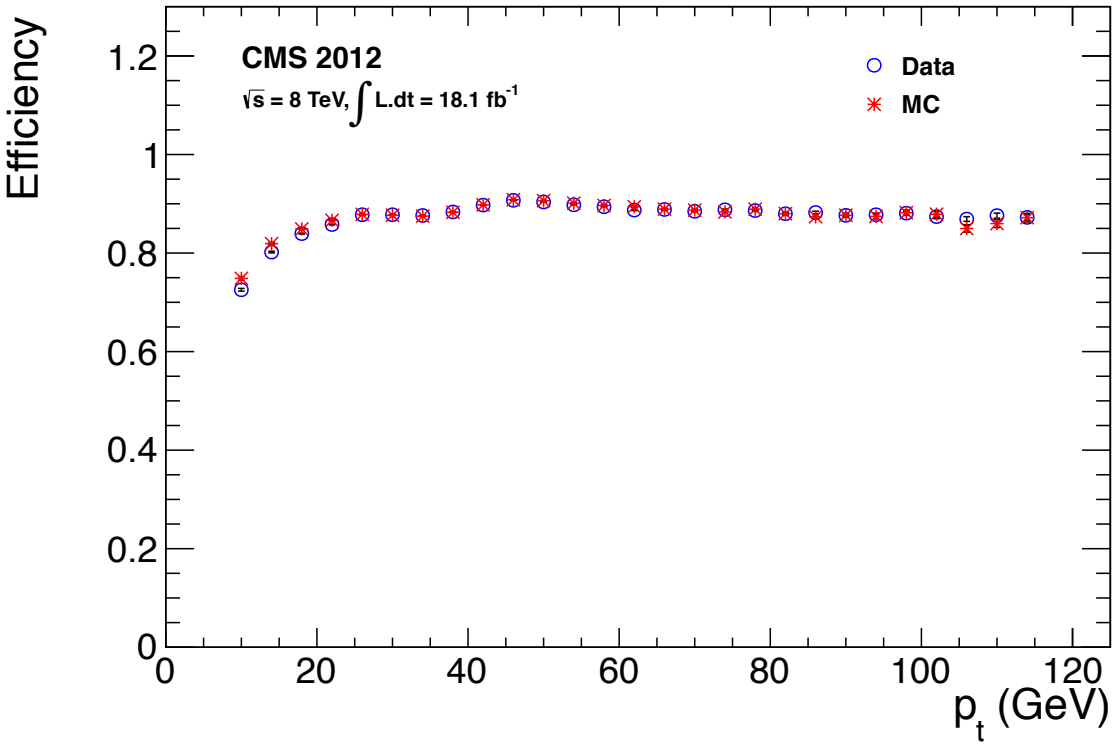

Figure C.3: Isolation efficiency plot for tau leptons using the method described above (3).